INFORMATION TO USERS

This reproduction was made from a copy of a manuscript sent to us for publication and microfilming. While the most advanced technology has been used to photograph and reproduce this manuscript, the quality of the reproduction is heavily dependent upon the quality of the material submitted. Pages in any manuscript may have indistinct print. In all cases the best available copy has been filmed.

The following explanation of techniques is provided to help clarify notations which may appear on this reproduction.

1. Manuscripts may not always be complete. When it is not possible to obtain missing pages, a note appears to indicate this.

2. When copyrighted materials are removed from the manuscript, a note appears to indicate this.

3. Oversize materials (maps, drawings, and charts) are photographed by sectioning the original, beginning at the upper left hand corner and continuing from left to right in equal sections with small overlaps. Each oversize page is also filmed as one exposure and is available, for an additional charge, as a standard 35mm slide or in black and white paper format.*

4. Most photographs reproduce acceptably on positive microfilm or microfiche but lack clarity on xerographic copies made from the microfilm. For an additional charge, all photographs are available in black and white standard 35mm slide format.*

***For more information about black and white slides or enlarged paper reproductions, please contact the Dissertations Customer Services Department.**

Zhang, Guo-Ping

STEADY AND TRANSIENT, MULTI-DIMENSIONAL SOLUTIONS FOR MELTING OR FREEZING AROUND A BURIED TUBE IN A SEMI-INFINITE MEDIUM

City University of New York PH.D. 1985

STEADY AND TRANSIENT, MULTI-DIMENSIONAL SOLUTIONS FOR MELTING OR FREEZING AROUND A BURIED TUBE IN SEMI-INFINITE MEDIUM

by

GUO-PING ZHANG

A dissertation submitted to the Graduate Faculty in Engineering in partial fulfillment of the requirements for the degree of Doctor of Philosophy, The City University of New York.

1985

This manuscript has been read and accepted for the Graduate Faculty in Engineering in satisfaction of the dissertation requirement for the degree of Doctor of Philosophy.

7/17/85
date

Latif Menashi Jiji, Chairman of Examining Committee

8/19/85
date

Paul Kamel, Executive Officer

Latif Menashi Jiji, Ph.D., Chairman

Sheldon Weinbaum, Ph.D., Co-Chairman

Jacoques Benveniste, Ph.D.

Ali Sadegh, Ph.D.

Supervisory Committee

The City University of New York

Abstract

STEADY AND TRANSIENT, MULTI-DIMENSIONAL SOLUTIONS
FOR MELTING OR FREEZING
AROUND A BURIED TUBE IN A SEMI-INFINITE MEDIUM

by

Guo-Ping Zhang

Advisers: Professor Latif M. Jiji
Professor Sheldon Weinbaum

This thesis examines melting or freezing around a buried fluid-carrying tube in a semi-infinite region. Of particular interest is the behavior of the phase change interface and the time variation of the axial temperature distribution in the fluid. Steady state and transient three-dimensional solutions are presented which account for the thermal interaction between a moving fluid and a phase change material having a free surface in the vicinity of the tube. The peripheral variation in the tube surface temperature is neglected and axial variation is left unspecified and is determined by the thermal interaction with the surrounding two-phase medium. Axial conduction is negelcted throughout the system.

Different solution methods based on the quasi-steady approximation are used depending on whether the phase change front commences at the tube wall or the plane free surface.

In the former case, a so-called apparent free surface method is developed for a corresponding two-dimensional problem using a locally two-dimensional conformal mapping technique. The approximate analytic solution agrees very

well with existing numerical results. The method is extended to include the axial thermal interaction and the three-dimensional solution reveals an important fact which has not been described in the previous two-dimensional studies. The long time required for the isotherms and thaw boundary above the tube to approach equilibrium is not controlled by the conduction process in this region but by the much slower variation in tube wall temperature.

A more general numerical method, the boundary integral technique, is employed for the second type of problem where the interface is generated at the free surface. Since the omission of the sensible heat can significantly influence the interface shape in this case, an artificial movable bottom boundary is used in the contour integral to reduce these effects. The solutions are presented for two-dimensional problems; however, the extension to three-dimensions is straightforward and follows in the same manner as when phase change starts at the tube wall.

The final equilibrium for both cases is identical. A new closed-form approximate analytic solution is obtained to describe the three-dimensional asymptotic state.

To

Father Mei-Dao Zhang

Mother Pei-Jun Li

ACKNOWLEDGEMENT

I would like to take this opportunity to thank Professor Latif M. Jiji and Professor Sheldon Weinbaum for their support and valuable guidance during the course of this research.

I am grateful to Dean Paul Karmel for handling administrative details in such a warm and friendly manner.

Most of all, I would like to thank my wife, Zi-Ming, for her encouragement and assistance during the years of this endeavor.

This research was supported by the National Science Foundation, Grant No. MEA 8209034.

TABLE OF CONTENTS

	Page
LIST OF TABLES AND FIGURES	ix
LIST OF SYMBOLES	xii
INTRODUCTION	1
CHAPTER I. GENERAL DESCRIPTION AND THE STEADY STATE PROBLEM	8
I.1. GENERAL DESCRIPTION	9
I.2. STEADY STATE THREE-DIMENSIONAL SOLUTION	11
I.2.1. FORMULATION	12
I.2.2. SOLUTION	14
I.2.3. RESULTS	18
REMARKS	19
CHAPTER II. TRANSIENT TWO-DIMENSIONAL SOLUTION FOR PHASE CHANGE COMMENCING AT THE TUBE WALL	25
II.1. THE SIMPLIFIED QUASI-STEADY APPROXIMATION	26
II.2. ANALYSIS	29
II.3. FORMULATION	40
II.3.1. THE UPPER PORTION	41
II.3.2. THE LOWER PORTION	42
II.3.3. INTERFACE SHAPE CONSTRUCTION	45
II.4. SOLUTION PROCEDURE	48
II.5. RESULTS AND DISCUSSION	50
REMARKS	53
CHAPTER III. THREE-DIMENSIONAL SOLUTION FOR PHASE CHANGE COMMENCING AT THE FREE SURFACE	58

III.1. SOLUTIONS FOR AXISYMMETRIC PROBLEMS 59
III.2. ANALYSIS AND FORMULATION 60
III.2.1. HEAT FLUX AT THE TUBE SURFACE 64
III.2.2. SOLUTION NEAR THE TUBE WALL 70
III.3. SOLUTION PROCEDURE 73
III.4. RESULTS AND DISCUSSION 74
REMARKS 77
CHAPTER IV. TWO-DIMENSIONAL SOLUTION FOR PHASE CHANGE COMMENCING AT THE FREE SURFACE 87
IV.1. ONE-DIMENSIONAL SOLUTIONS 90
IV.2. BOUNDARY INTEGRAL METHOD 93
IV.3. FLOATING BOTTOM TECHNIQUE 94
IV.4. FORMULATION 98
IV.5. NUMERICAL PROCEDURE 101
IV.6. RESULTS 103
IV.7. DISCUSSION 109
REMARKS 116
CONCLUDING REMARKS 118
APPENDIX A 124
APPENDIX B 127
APPENDIX C 130
APPENDIX D 134
APPENDIX E 138
APPENDIX F 141
NOTES 147
BIBLIOGRAPHY 149

LIST OF TABLES AND FIGURES

TABLE		Page
1.	VALUES OF λ, $\overline{\Delta Y}_i$, $\overline{\Delta \ell}_c$ FOR GIVEN St_1 AND θ_a IN WATER	92
2.	DATA FOR TWO REPRESENTATIVE CASES SHOWN IN FIGURES 25 (a,b,c)	104

FIGURE		
1.	CONFIGURATION AND COORDINATE SYSTEM	6
2.	INSTANTANEOUS PROFILES OF INTERFACE IN THE PLANE NORMAL TO TUBE AXIS WHEN (a) PHASE CHANGE STARTING AT THE TUBE WALL, AND (b) PHASE CHANGE STARTING AT THE FREE SURFACE	7
3.	TWO-DIMENSIONAL QUASI-STEADY PROBLEM IN THE PHYSICAL AND TRANSFORMED PLANES	16
4.	AXIAL VARIATION OF FLUID TEMPERATURE	21
5.	AXIAL VARIATION OF INTERFACE RADIUS	22
6.	AXIAL VARIATION OF INTERFACE DEPTH BELOW PLANAR SURFACE	23
7.	SOLUTION LIMITS	24
8.	COMPARISON OF PREVIOUS QUASI-STEADY THEORIES WITH NUMERICAL SOLUTION FOR INTERFACE POSITION	30
9.	RATIO OF INSTANTANEOUS RATE OF GROWTH OF TOP TO BOTTOM POINTS OF INTERFACE	34
10.	QUASI-STEADY SOLUTION TO INTERFACE MOTION IN THE COMPLEX PLANE OF TOP AND BOTTOM POINTS	35
11.	COMPARISON BETWEEN PREVIOUS QUASI-STEADY SOLUTIONS TO THAW DEPTH PENETRATION BELOW TUBE FOR $\theta_a = 1$, $h_o = 1.5$	38
12.	SCHEMATIC DIAGRAM SHOWING MAPPING OF BOUNDARY VALUE PROBLEM WITH APPARENT FREE SURFACE INTO COMPLEX PLANE WITH APPARENT CIRCLES R'_{ib} AND R'_{ob}	43

13.	COMPARISON BETWEEN NUMERICAL, PREVIOUS AND PRESENT QUASI-STEADY SOLUTIONS TO THAW DEPTH PENETRATION BELOW TUBE FOR $\theta_a = 50.49$, $h_o = 1.5$	54
14.	COMPARISON BETWEEN NUMERICAL, PREVIOUS AND PRESENT QUASI-STEADY SOLUTIONS FOR INTERFACE POSITION	55
15.	INTERFACE RADIUS OF CURVATURE OF TOP AND BOTTOM POINTS AS A FUNCTION OF TIME USING PRESENT THEORY FOR $\theta_a = 7.09$, $h_o = 4$	56
16.	THAW DEPTH PENETRATION BELOW AND ABOVE TUBE USING PRESENT THEORY FOR $\theta_a = .5, 1, 5$ AND $h_o = 2$	57
17.	CONFIGURATION AND COORDINATE SYSTEM FOR PHASE CHANGE COMMENCING AT THE TUBE WALL	62
18.	SCHEMATIC DIAGRAM SHOWING THE MODIFIED INTERFACE SHAPE, AND MAPPING OF HEAT FLUX LINE PASSING THROUGH POINT e	65
19(a).	AXIAL VARIATION OF THAW DEPTH PENETRATION ABOVE AND BELOW TUBE CENTER FOR $\theta_{ao} = 50.49$, $h_o = 1.5$	79
19(b).	AXIAL VARIATION OF THAW DEPTH PENETRATION ABOVE AND BELOW TUBE CENTER FOR $\theta_{ao} = 7.09$, $h_o = 4.0$	80
20(a).	AXIAL VARIATION OF HEAT FLUX AT TOP AND BOTTOM POINTS OF TUBE SURFACE FOR $\theta_{ao} = 50.49$, $h_o = 1.5$	81
20(b).	AXIAL VARIATION OF HEAT FLUX AT TOP AND BOTTOM POINTS OF TUBE SURFACE FOR $\theta_{ao} = 7.09$, $h_o = 4.0$	82
21(a).	FLUID AXIAL TEMPERATURE DISTRIBUTION FOR $\theta_{ao} = 50.49$, $h_o = 1.5$	83
21(b).	FLUID AXIAL TEMPERATURE DISTRIBUTION FOR $\theta_{ao} = 7.09$, $h_o = 4.0$	84
22(a).	INTERFACE PROFILE FOR $\theta_{ao} = 50.49$, $h_o = 1.5$	83
22(b).	INTERFACE PROFILE FOR $\theta_{ao} = 7.09$, $h_o = 4.0$	86
23.	CONFIGURATION AND COORDINATE SYSTEM FOR FREEZING COMMENCING AT THE FREE SURFACE	89
24.	SCHEMATIC DIAGRAM SHOWING (a) ARTIFICIAL	

	DOMAINS FOR LINE INTEGRAL (VI.4), AND (b) NODE DISTRIBUTION IN BOUNDARY ELEMENT METHOD	95
25(a).	INTERFACE PROFILE AT SELECTED TIMES FOR CASE I OF TABLE 2	105
25(b).	INTERFACE PROFILE AT SELECTED TIMES FOR CASE II OF TABLE 2	106
25(c).	COMPARISON OF INTERFACE PROFILES USING THE FLOATING BOTTOM TECHNIQUE AND A FIXED BOTTOM H_b = 100a FOR CASE 2 IN TABLE 2	108
26.	COMPARISON OF ONE-DIMENSIONAL SOLUTIONS CORRESPONDING TO CASES I AND II OF TABLE 2	110
27.	SCHEMATIC DIAGRAM SHOWING (a) LATERAL DISTURBANCE SCALE DUE TO WALL TEMPERATURE OF TUBE, AND (b) TRANSIENT EFFECTS OF THE NEGLECT OF THE SENSIBLE HEAT ON INTERFACE PORFILE	114
28.	GEOMETRICAL SKETCH OF POINT e (REFER TO FIGURE 18(a))	126
29.	SCHEMATIC DIAGRAM SHOWING DETERMINATION FOR δ	133
30.	SCHEMATIC DIAGRAM SHOWING DETERMINATION OF POSITION OF FLOATING BOTTOM BOUNDARY	140

LIST OF SYMBOLES

a	tube radius
A_{jK}	coefficient, equation (F3a)
a_j	j = 1,2,3, coefficients in equation (II.15)
b_j	j = 1,2,3, coefficients in equation (III.6)
b'_j	j = 1,2,3, coefficients in equation (III.13)
B_{jK}	coefficient, equation (F3b)
$C_a, C_{1,2}$	specific heat of fluid and PCM in zones 1 and 2, respectively
$C(\bar{t}^*)$	refer to equation (III.19-b)
d	dimensionless distance in Fig.28
d_{ia}	dimensionless distance of interface along $\phi = \pi/2$ measured from the top of the tube, $= h_o - (h_{ia} - r_{ia}) - 1$
d_{ib}	dimensionless distance of interface along $\phi = -\pi/2$ measured from the bottom of the tube, $= (h_{ib} + r_{ib}) - h_o - 1$
d'_{ia}	$= d_{ia} + 1$, Fig.19
d'_{ib}	$= d_{ib} + 1$, Fig.19
h_a	heat transfer coefficient of the fluid in the tube
h_i	dimensionless position below the free surface of center of interface circle, $= \tilde{h}_i/a$, Fig.1
h_{ia}	dimensionless position below the free surface of center of interface circle passing through point a, $= \tilde{h}_{ia}/a$, Fig.28
h_{ib}	dimensionless position below the free surface of center of interface circle passing through point b,

	$= \tilde{h}_{ib}/a$, Fig.12
h^*_{ib}	refer to equation (II.17)
h_{iS}	dimensionless steady state position below the free surface of center of interface circle, $= \tilde{h}_{iS}/a$,
h_o	dimensionless tube burial depth, $= \tilde{h}_o/a$, Fig.1
i	imaginary unit, $i^2 = -1$
$K_a, K_{1,2}$	heat conductivities of fluid and PCM in zones 1 and 2, respectively
ℓ	characteristic tube length
ℓ_c	lateral thermal disturbance scale, Fig.27(a)
L	latent heat of PCM
n	dimensionless normal coordinate at interface, $= \tilde{n}/a$
$n_{1,2}$	dimensionless normal coordinates pointing outward zones 1 and 2, respectively, Fig.24
$N_{1,2}$	element numbers on boundaries of regions 1 and 2, respectively, equations (VI.16,17)
PCM	phase change material
Pe*	modified Peclet number,
	$= (K_a/K_2)Pe = (K_a/K_2)(\rho_a C_a \bar{u} a/K_a)$
Pr	prandtl number, $= C_a \mu/K_a$
q_c	$= \partial\theta_2/\partial r$ evaluated at top point c on the tube, equation (III.5-a)
q_d	$= \partial\theta_2/\partial r$ evaluated at bottom point d on the tube, equation (III.10)
q_g	$= \partial\theta_2/\partial r$ evaluated at point g on the tube, equation (III.5-b)
q^*_g	refer to equations (III.8,9)

r dimensionless cylindrical coordinate with origin at $y = -h_i$, $= \tilde{r}/a$, Fig.1

r_i dimensionless interface radius, $= \tilde{r}_i/a$, Fig.1

r_i dimensionless interface radius of circle passing through point a, $= \tilde{r}_{ia}/a$, Fig.12

r_{ib} dimensionless interface radius of circle passing through point b, $= \tilde{r}_{ib}/a$, Fig.12

r^*_{ib} radius of local curvature of the modified interface at point b, equation (II.16)

r_{ibo} match position when $r_{ib} = r_{ibo}$ in formulae (B1) and (B5)

r_{is} dimensionless steady state interface radius, $= \tilde{r}_{is}/a$ equation (B2)

r_p dimensionless radial distance of the interface measured from the tube center, $= \tilde{r}_p/a$, Fig.12, equation (II.15)

r_{po} refer to equation (III.19-b)

r_t dimensionless cylindrical coordinate with origin at the tube center, $= \tilde{r}_t/a$, Fig.12

R dimensionless cylindrical coordinate, Fig.3

R^* dimensionless cylindrical coordinate, Fig.12

Re Reynolds number, $= \rho_a a\bar{u}/\mu$

R_i dimensionless interface radius, Fig.3

R_{ia} dimensionless interface radius of circle passing through point a', Fig.18

R_{ib} refer to equation (II.9)

R^*_{ib} dimensionless interface radius of circle passing

	through point b', Fig.12
R_o	dimensionless free surface radius, Fig.3
R'_{ob}	dimensionless apparent free surface radius, Fig.12
S_p	$= r_p^2$
S_{po}	$= r_{po}^2$
S_{poz}	refer to equation (D9)
St_1	Stefan number, $= C_1 (T_f - T_o)/L$
St_2	Stefan number, $= C_2 (T_a - T_f)/L$
t	time
t_{c1}	characteristic time, $= a^2/\bar{\alpha}_1 St_1$
t_{c2}	characteristic time, $= a^2/\bar{\alpha}_2 St_2$
t_d	$= 1/\bar{\alpha}_2 St_2$
t^*	dimensionless time, $= t/t_{c2}$
$\bar{t}^*$	dimensionless time, $= t^*/\bar{\theta}_a$, equation (III.2a)
t^{**}	dimensionless time, $= t/t_{c1}$
$T_{1,2}$	temperatures of zones 1 and 2, respectively
T_a	tube surface temperature
T_{ao}	tube surface temperature at entrance
T_f	freezing temperature
T_o	free surface temperature
$\bar{u}$	fluid velocity
U	fundamental singular solution, equation (VI.5)
u,v	Cartesian coordinates in the complex plane
$\vec{v}$	interface velocity
W	conformal transformation = u+iv, equation (I.11)
W^*	conformal transformation = u'+iv'
x,y,z	dimensionless Cartesian coordinates, $x = \tilde{x}/a$,

$y = \tilde{y}/a$, $z = \tilde{z}/a$, Fig.1

y_{ia} dimensionless position below the free surface of the top point of interface, $= h_{ia} - r_{ia}$

y_{ib} dimensionless position below the free surface of the bottom point of interface, $= h_{ib} + r_{ib}$

y_{iN} Neumann solution for freezing depth penetration, equation (VI.1)

y_{iS} Stefan solution for freezing depth penetration, equation (VI.2)

Z complex variable $= x+iy$

z_{max} dimesionless distance along tube where $r_i = 1$

α cylindrical coordinate in complex plane

$\alpha_{1,2}$ thermal diffusivities of zone 1 and 2, respectively

β transformation variable, $= (\ln R_{ia})^2$, equation (II.12)

γ constant in equation (B1)

δ dimensionless position of the apparent free surface measured from the real free surface

ζ transformation variable, $= \tilde{y}/(4\bar{\alpha}_1 t)^{1/2}$, see equation (VI.1)

θ_1 dimensionless temperature of zone 1, $= (T_1 - T_f)/(T_0 - T_f)$

θ_2 dimensionless temperature of zone 2, $= (T_2 - T_f)/(T_a - T_f)$

θ_a dimensionless tube temperature, $= K_2(T_a - T_f)/K_1(T_f - T_0)$

$\bar{\theta}_a$ dimensionless tube temperature, $= (T_a - T_f)/(T_{a0} - T_f)$, equation (III.1-a)

θ_{ao}	dimensionless tube entrance temperature, $= K_2(T_{ao}-T_f)/K_1(T_f-T_o)$, equation (I.9)
λ	constant in equation (VI.1-a)
μ	viscosity of fluid
ξ, η	dummy variables, equation (VI.4)
ρ	PCM density
ρ_a	fluid density
σ	ratio of rate of growth of interface at top and bottom positions, equation (II.7)
τ	transformation variable, $= \int_o^{\bar{t}^*} \theta_a(z, \bar{t}^*)\, d\bar{t}^*$
ϕ	cylindrical coordinate, Fig.1

SUPERSCRIPT

$\sim$	dimensional quantity
I,II	zone 1 (solid) and zone 2 (liquid)
(o)	short time

INTRODUCTION

Many important problems in conduction heat transfer involve phase change. These problems are characterized by a moving phase boundary that divides the relevant field into two regions. The unknown motion of the boundary, which is to be determined as part of the solution, gives rise to an inherent nonlinearity in the mathematical treatment.

Phase change is encountered in practical problems when the temperature of a system involving water or other liquids attains or varies across the freezing value. However, since the well-known Neumann solution for solidification in a semi-infinite medium was obtained over a century ago in terms of a similarity transformation, there are few other exact solutions in the sense of Neumann's. Self-similarity is known to be valid under severe restrictions which preclude all systems involving a characteristic length, such as would occur if there were a finite domain or if both phases coexisted initially, as well as most practical problems.

Due to the mathematical difficulties introduced by the nonlinearity, most of the standard mathematical techniques are not applicable to melting or freezing problems. Significant efforts have been extended toward the development of numerical techniques and approximate analytical methods, especially in the past two decades.

In recent years, melting or freezing outside fluid carrying tubes has received extensive attention because of the important engineering applications in solar energy storage systems, pipeline transportation in permafrost regions and

cryosurgery. The type of buried tube problems that are the subject of the present thesis feature three aspects: (i) a moving phase front in the phase change medium (PCM) outside the tube; (ii) the presence of a plane free surface; and (iii) the axial thermal interaction between the fluid carried in the tube and the surrounding PCM. These factors result in a mathematically complicated three-dimensional, two-domain problem with a moving interface. In an attempt to reduce this complexity, investigators have introduced a variety of two-dimensional problems which have been treated using different approximations. A commonly used simplification invoked in the previous studies is the uncoupling of the fluid domain from the PCM by specifying appropriate boundary conditions on the tube surface. The thermal interaction with axial variation between the fluid inside the tube and the external PCM has been investigated only very recently. These newly addressed studies have been limited to a tube surrounded by an infinite PCM which is initially at the phase change temperature. All the related research to date has been devoted to two-dimensional mathematical treatments.

The system considered in the present studies is a semi-infinite PCM with a fluid carrying tube embedded in the vicinity of a free surface (Figures 1,2). In addition to the presence of the free surface, the PCM is initially not at the freezing temperature. A melting (or freezing) front in the PCM can be initiated by a sudden change in temperature

of either the inlet fluid or the free surface. The initial interface shape corresponding to the former case is a circular cylinder whereas that of the latter is a planar surface. The interface profiles in the plane normal to the tube axis are sketched for each case in Figures 2(a,b). Different solution techniques are applied for each problem because of the different behaviors of the phase front arising from the corresponding initial conditions. In addition, an approximate analytic solution for the asymptotic equilibrium state, which is identical for both cases, is included in the present research.

Since the same basic geometry is considered in these problems which are treated in separate chapters, the general description of the subject, including the fundamental assumptions and coordinate system, is stated in the first subsection of Chapter I. Additional information specific to the individual problems will be given in each chapter. The second part of Chapter I demonstrates the solution for the three-dimensional steady state problem. Chapters II and III deal with the two-dimensional and three-dimensional problems, respectively, when the phase change starts at the tube wall. In contrast to all previous analytical studies, a new approximate analytical solution method that is capable of determining a moving non-circular phase front is developed in Chapter II and later extended to three dimensions in Chapter III. In Chapter IV, the problem with a planar interface generated at the free surface, for which no rele-

vant work has been found, is treated by a boundary integral method. This numerical technique has not previously been applied in heat transfer problems with a moving phase change boundary. Although the present solution is for the two-dimensional case, the technique is also applicable to three-dimensional problems. In each chapter, the relevant research will be briefly reviewed.

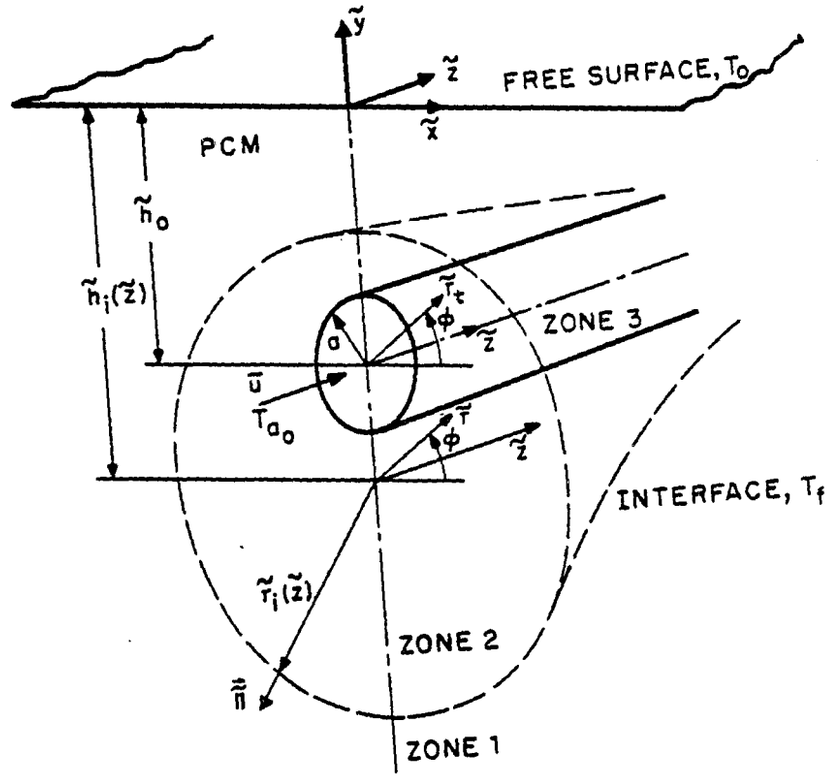

FIGURE 1. CONFIGURATION AND COORDINATE SYSTEM

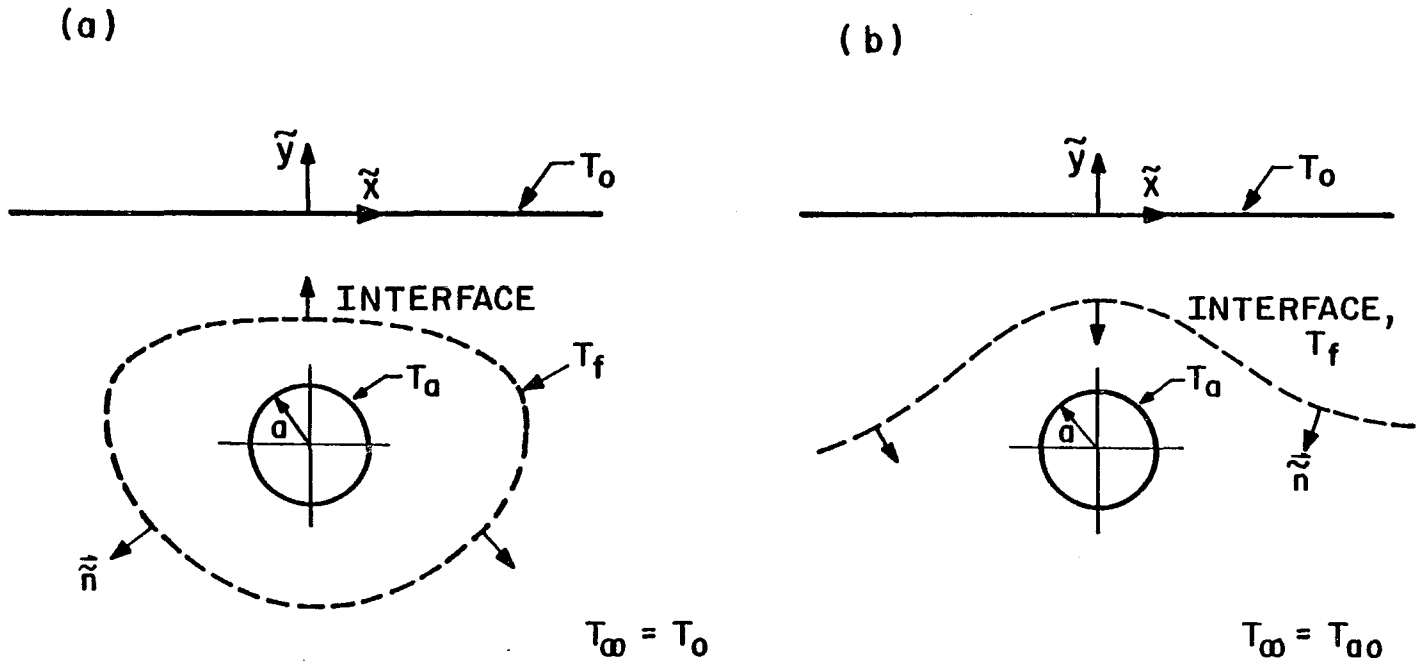

FIGURE 2. INSTANTANEOUS PROFILES OF INTERFACE IN THE PLANE NORMAL TO TUBE AXIS WHEN (a) PHASE CHANGE STARTING AT THE TUBE WALL, AND (b) PHASE CHANGE STARTING AT THE FREE SURFACE

CHAPTER I

GENERAL DESCRIPTION

AND

THE STEADY STATE SOLUTION

I.1 GENERAL DISCRIPTION

The system under consideration is shown in Figure 1. The free surface of the semi-infinite PCM, $\tilde{y} = o$, is maintained at a uniform temperature T_o which is below the freezing point T_f of the PCM. A thin walled tube of radius a is buried in the PCM at a distance $\tilde{h}_o$ below the planar surface $\tilde{y} = 0$. Fluid enters the tube at $\tilde{z} = o$ with an average velocity $\bar{u}$ and a uniform temperature T_{ao} where $T_{ao} > T_f$. The phase change may commence at either the tube wall or the free surface depending on whether the initial temperature of the PCM is at T_o or T_{ao}. Because of the interaction between the fluid and PCM temperature fields, a solid-liquid interface moves in the PCM in a three-dimensional manner while the temperature of fluid, T_a, varies with time and its axial position along the tube. Of particular interest is the shape of the interface and variation of the fluid temperature in the axial direction in both steady and unsteady situations.

Although the problem is described in terms of a liquid phase outside the tube and a solid phase adjacent to the free surface, i.e. $T_o < T_f < T_{ao}$, the mathematical formulation and solution are basically the same for the corresponding case of $T_o > T_f > T_{ao}$ where the solid phase is outside the tube.

The mathematical models proposed in the research are based on two major assumptions:

(A) Since the depth $(\tilde{h}_o + a)$ is small compared to the tube length, and the Peclet number $Pe = PrRe = \rho_a C_a \bar{u} a / K_a$ of

the fluid flowing in the tube is large in most practical problems, the axial properties of the phase change are slowly varying and result from gradual bulk temperature changes in the fluid as it flows downstream and loses heat to the PCM. Therefore, the heat conduction in the axial direction $\tilde{z}$ is neglected throughout the system.

(B) The sensible heat $C\Delta T$, where C is the specific heat and ΔT is the imposed temperature difference, is small in comparison with the latent heat L, i.e. the Stefan number $St = C\Delta T/L << 1$; and the temperature variation with time at the tube wall is slowly varying compared to the transit time for the fluid in the tube. Under these conditions, the quasi-steady approximation is justified and the variation of the whole system is characterized by a relatively large time scale $(\tilde{h}_o+a)^2/\bar{\alpha}\,St$ describing the quasi-steady motion of the interface, where $\bar{\alpha}$ is the thermal diffusivity.

The additional assumptions are listed as follows:

(a) No change in density takes place during phase transformation.

(b) Thermal properties of the PCM in solid and liquid phases and the fluid in the tube are constant but different in each phase.

(c) Change of phase occurs at a distinct temperature, T_f.

(d) Fluid flow rate in the tube is constant and its bulk velocity is given by the average value, $\bar{u}$. Implied in this approximation is the assumption that solidification

of the fluid does not occur.

(e) Fluid temperature is uniform across the tube and represents an average value. This bulk temperature varies with axial position along the tube and with time. This is a reasonable approximation for turbulent flow.

(f) The thermal resistance of the convection boundary layer and the tube wall are negligible (large Biot number) and thus the surface temperature is assumed to be the same as the fluid bulk temperature. The extension of the theory to include an insulating layer or finite thermal resistance in the fluid is straightforward and is described in the work of previous investigators [1-3].

(g) Free convection due to buoyancy forces in the surrounding PCM can be neglected. This is a good approximation when the PCM is a component of a matrix such as tissue or ground material.

(h) Viscous dissipation is negligible. This is true for low Eckert number flows.

I.2 STEADY STATE THREE-DIMENSIONAL SOLUTION

Even in the steady state case, there is no existing three-dimensional solution involving freezing around an embedded tube with axial interaction. All foregoing time dependent solutions with axial thermal interaction have no steady state since the surrounding PCM is infinite and initially at phase change temperature. The present analysis

(refer to Figure 1) will account for the effects of the planar free surface, thermal interaction between the PCM and the fluid, and axial variation throughout the system. The available steady state solution to the corresponding two-dimensional buried tube problem is used in a surprisingly simple scheme to obtain a closed-form analytic solution. The solution neglects axial conduction and peripheral variation in the surface temperature of the tube.

I.2.1 FORMULATION

Three zones are identified in the system under consideration in Figure 1. In zones 1 and 2, the PCM is in the solid and liquid phases, respectively. In zone 3, the fluid in the tube interacts thermally with the PCM in zone 2.

Two coordinate systems are used to describe the problem mathematically. A Cartesian system $(\tilde{x},\tilde{y},\tilde{z})$ with the origin on the surface of the PCM and a cylindrical system $(\tilde{r}_t,\Phi,\tilde{z})$ with its origin at the center of the tube, $\tilde{x} = \tilde{z} = o$ and $\tilde{y} = -\tilde{h}_o$. Another set of cylindrical coordinates $(\tilde{r},\Phi,\tilde{z})$ is used to define the solid-liquid surface. Since the interface at any axial distance $\tilde{z}$ is circular with radius $\tilde{r}_i(\tilde{z})$, the origin of this system is at $\tilde{x} = \tilde{z} = o$ and $\tilde{y} = -\tilde{h}_i(\tilde{z})$, which is the center of the circle $\tilde{r}_i(\tilde{z})$ in the $\tilde{x}\tilde{y}$ plane.

To formulate the problem in dimensionless form, the following quantities are defined:

$$\theta_1 = (T_1 - T_f)/(T_o - T_f), \qquad \theta_2 = (T_2 - T_f)/(T_a - T_f)$$

$$\theta_a = K_2(T_a - T_f)/K_1(T_f - T_0), \qquad x = \tilde{x}/a$$
$$y = \tilde{y}/a, \quad z = \tilde{z}/a, \quad r = \tilde{r}/a, \quad r_t = \tilde{r}_t/a$$
$$h_i = \tilde{h}_i/a, \quad r_i = \tilde{r}_i/a, \quad h_o = \tilde{h}_o/a, \quad \vec{n} = \tilde{\vec{n}}/a$$

where K is the conductivity of the PCM and the subscripts 1,2 denote zones 1 and 2, respectively. The definition of θ_2 in terms of the variable fluid temperature is chosen to simplify the interface boundary condition. Note that the normal vector $\vec{n}$ defined on the interface has also been made dimensionless.

Based on the aforementioned assumptions, except assumption (B) which applies only in transient cases, the dimensionless heat conduction equations in the two zones of the PCM are given by

$$\frac{\partial^2\theta_1}{\partial x^2} + \frac{\partial^2\theta_1}{\partial y^2} = 0 \qquad \text{(I.1)}$$

and

$$\frac{\partial^2\theta_2}{\partial x^2} + \frac{\partial^2\theta_2}{\partial y^2} = 0 \qquad \text{(I.2)}$$

Conservation of energy in zone 3 gives:

$$\frac{\pi Pe^*}{\theta_a}\frac{d\theta_a}{dz} = \int_0^{2\pi} \frac{\partial\theta_2(1,\phi,z)}{\partial r_t}\, d\phi \qquad \text{(I.3)}$$

where Pe* is a modified Peclet number defined as

$$Pe^* = \frac{\rho_a C_a \bar{u} a}{K_a}\frac{K_a}{K_2} = \frac{K_a}{K_2} Pe \qquad \text{(I.3-a)}$$

and Pe is the fluid Peclet number. θ_a appears in the denominator on the left hand side of equation (I.3) owing to the

definition of θ_2. The boundary conditions are:

$$\theta_1(X, 0, z) = \theta_1(X, -\infty, z) = \theta_1(\infty, Y, z) = 1 \quad , \tag{I.4}$$

$$\frac{\partial \theta_1(0, Y, z)}{\partial X} = 0 \quad , \tag{I.5}$$

$$\theta_1(r_i, \Phi, z) = \theta_2(r_i, \Phi, z) = 0 \quad , \tag{I.6}$$

$$\theta_2(1, \Phi, z) = 1 \quad , \tag{I.7}$$

$$\frac{\partial \theta_2(0, Y, z)}{\partial X} = 0 \quad , \tag{I.8}$$

$$\theta_a(0) = K_2(T_{a0} - T_f)/K_1(T_f - T_0) \equiv \theta_{a0} \quad , \tag{I.9}$$

Conservation of energy at the interface gives:

$$\frac{1}{\theta_a(z)} \frac{\partial \theta_1(r_i, \Phi, z)}{\partial n} + \frac{\partial \theta_2(r_i, \Phi, z)}{\partial n} = 0 \quad , \tag{I.10}$$

where n is the normal dimensionless coordinate at the interface.

I.2.2 SOLUTION

The governing equations for θ_1 and θ_2, equations (I.1,2) and the associated eight boundary conditions (I.4-8) are recognized to represent a two-dimensional problem and can be solved in terms of the unknown function $r_i(z)$. The three-dimensional character of the problem is attributed to $\theta_a(z)$ which causes r_i to vary with axial distance z. Once a solution for θ_1 and θ_2 is obtained in terms of $r_i(z)$, the energy

equation (I.3) and the interface equation (I.10) can be used to solve for $\theta_a(z)$ and $r_i(z)$. Solutions to the steady state two-dimensional problem have been obtained using a source-sink method [4] or conformal mapping technique [4,5]. The latter will now be used to construct the solution to the three-dimensional problem. The semi-infinite region surrounding the tube in the physical Z-plane is transformed to an annular region in the complex W-plane (Figure 3) using the bicircular transformation:

$$W = \frac{R_0 Z + (R_0 h_0 - 1) i}{(R_0 - h_0) + Z i} \quad , \tag{I.11}$$

where

$$Z = x + iy = r e^{i\phi} - i h_i \quad , \tag{I.11-a}$$

$$W = u + iv = R e^{i\alpha} \tag{I.11-b}$$

and

$$R_0 = h_0 + (h_0^2 - 1)^{1/2} \quad , \tag{I.11-c}$$

where R and α are the cylindrical coordinates in the complex plane. The eccentric circles representing the tube surface and the interface, respectively, map into concentric circles in the complex W-plane. The planar surface y = 0 forms another concentric circle. The radius of the interface circle r_i and the location of its center $y = -h_i$ in the physical plane are related to the corresponding radius, R_i, in the complex plane through the transformation (I.11),

$$r_i = (R_0^2 - 1) R_i / (R_0^2 - R_i^2) \tag{I.12}$$

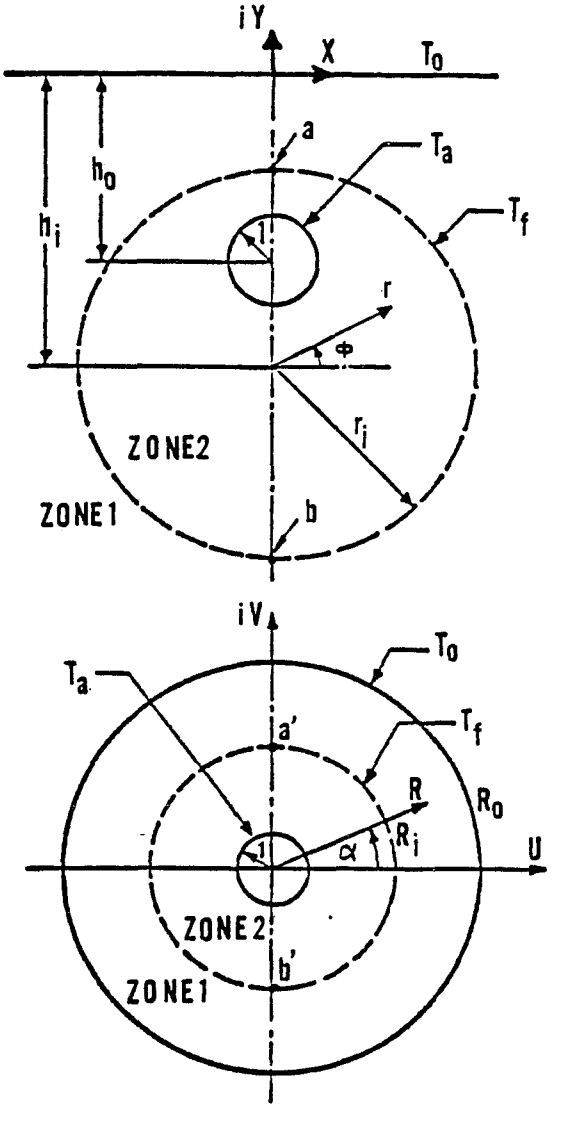

FIGURE 3. TWO-DIMENSIONAL QUASI-STEADY PROBLEM IN THE PHYSICAL AND TRANSFORMED PLANES

and

$$h_i = h_o + (R_i^2 - 1) R_o / (R_o^2 - R_i^2) \quad . \tag{I.13}$$

Transformation of equations (I.3) and (I.10) yields:

$$\frac{\pi Pe^*}{\theta_a(z)} \frac{d\theta_a(z)}{dz} = \int_0^{2\pi} \frac{\partial \theta_2(1, \alpha, z)}{\partial R} \, d\alpha \tag{I.14}$$

and

$$\frac{1}{\theta_a(z)} \frac{\partial \theta_1(R_i, \alpha, z)}{\partial R} + \frac{\partial \theta_2(R_i, \alpha, z)}{\partial R} = 0 \quad . \tag{I.15}$$

Note that a scale factor does not appear in the integrand of equation (I.14) since for a conformal transformation, R and α coordinates have been stretched by the same magnitude.

The two-dimensional solutions to equations (I.1,2) and boundary conditions (I.4-8) in the transformed W-plane are:

$$\theta_1 = \frac{\ln R / R_i}{\ln R_o / R_i} \tag{I.16}$$

and

$$\theta_2 = \frac{\ln R / R_i}{\ln 1 / R_i} \quad . \tag{I.17}$$

Substituting equations (I.16,17) into interface condition (I.15) yields a solution for R_i in terms of θ_a,

$$R_i = R_o^{\theta_a / (1 + \theta_a)} \tag{I.18}$$

Substituing equations (I.17,18) into (I.14), one obtains:

$$\frac{d\theta_a}{1 + \theta_a} = - \frac{2}{\ln R_o} \frac{dz}{Pe^*} \quad . \tag{I.19}$$

Integrating equation (I.19) and satisfying the entrance condition (I.9), one finds:

$$\frac{1+\theta_a}{1+\theta_{ao}} = \exp\left(-\frac{2}{\ln R_o}\,\frac{z}{Pe^*}\right) \qquad \text{(I.20)}$$

Equation (I.20) gives the tube temperature as a function of z in terms of the parameters θ_{ao} and R_o. With $\theta_a(z)$ determined, the radius of the solid-liquid interface surface $r_i(z)$ is obtained from equations (I.12), (I.18) and (I.20),

$$r_i(z) = \frac{(R_o^2-1)}{R_o}\;\frac{R_o^{\frac{1}{1+\theta_{ao}}\exp\left(\frac{2}{\ln R_o}\frac{z}{Pe^*}\right)}}{R_o^{\frac{2}{1+\theta_{ao}}\exp\left(\frac{2}{\ln R_o}\frac{z}{Pe^*}\right)}-1} \qquad \text{(I.21)}$$

The depth of the interface below the planar surface, $(h_i - r_i)$, is constructed from equations (I.13) and (I.21),

$$h_i - r_i = h_o - R_o\;\frac{1+R_o^{\frac{1}{1+\theta_{ao}}\exp\left(\frac{2}{\ln R_o}\frac{z}{Pe^*}\right)-2}}{1+R_o^{\frac{1}{1+\theta_{ao}}\exp\left(\frac{2}{\ln R_o}\frac{z}{Pe^*}\right)}} \qquad \text{(I.22)}$$

The solution is valid up to a maximum axial distance z_{max} where the interface intersects the tube. Noting that $\theta_a = 0$ at $z = z_{max}$, equation (I.20) gives:

$$\frac{z_{max}}{Pe^*} = \frac{1}{2}\cosh^{-1} h_o \ln(1+\theta_{ao}) \qquad \text{(I.23)}$$

Thus the region of validity, $0 < z < z_{max}$, is determined by the parameters θ_{ao} and h_o.

I.2.3 RESULTS

Examination of the closed-form analytic solution shows

that the problem is characterized by three dimensionless parameters: h_o, θ_{ao} and Pe^*. Parameter h_o describes the depth of the buried tube and θ_{ao} reflects the effects of inlet, surface and freezing temperatures. Flow conditions and fluid properties are described by the modified Peclet number, Pe^*. The effect of these parameters on the solution is presented in Figures 4-6. Fluid temperature variation in the axial direction, $\theta_a(z)$, is plotted in Figure 4 for various values of h_o. As might be expected the temperature gradient increases as the burial distance h_o is decreased. Figure 5 shows the radius of the cylindrical surface $r_i(z)$ representing the solid-liquid interface. This interface radius is seen to diminish axially. Furthermore, a decrease in h_o or θ_{ao} causes r_i to decrease at a given axial distance z. The effects of h_o and θ_{ao} on the distance between the planar free surface and the upper-most position of the interface, $(h_i - r_i)$, is presented in Figure 6.

The criterion for the regional validity of the solution is presented graphically in Figure 7. The region of validity is also seen in Figure 6.

REMARKS

The solution describes the final equilibrium state of the interface and axial temperature distribution whether the phase change starts at the tube wall or the planar surface. The relatively simple algebraic relationship between R_i and

θ_a given by equation (I.18) does not carry over to the transient situation even if one assumes that isotherms are eccentric circles as in the steady state solution. In fact, it will be shown that the circular interface profile cannot be maintained as the phase front moves into the PCM from the tube surface. The actual situation can be more easily clarified by examining the corresponding two-dimensional problem with a specified tube surface temperature to uncouple the fluid domain inside the tube.

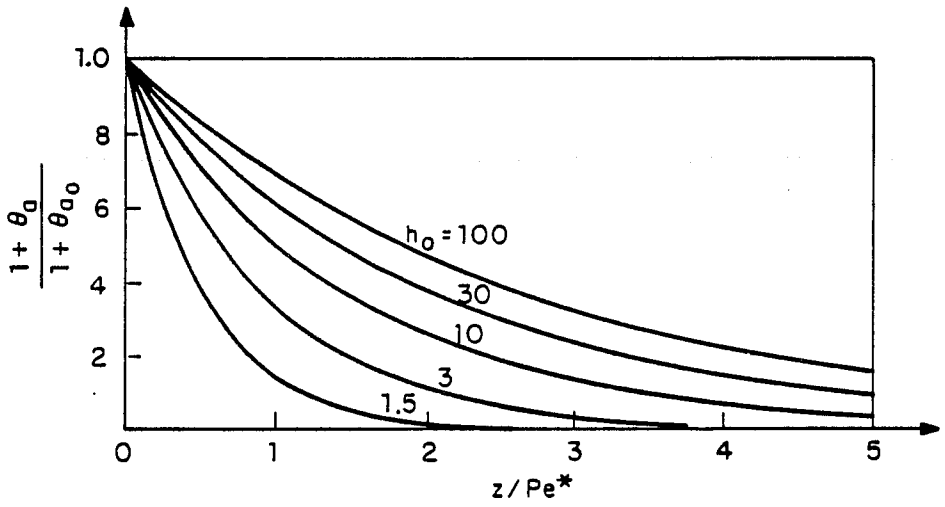

FIGURE 4. AXIAL VARIATION OF FLUID TEMPERATURE

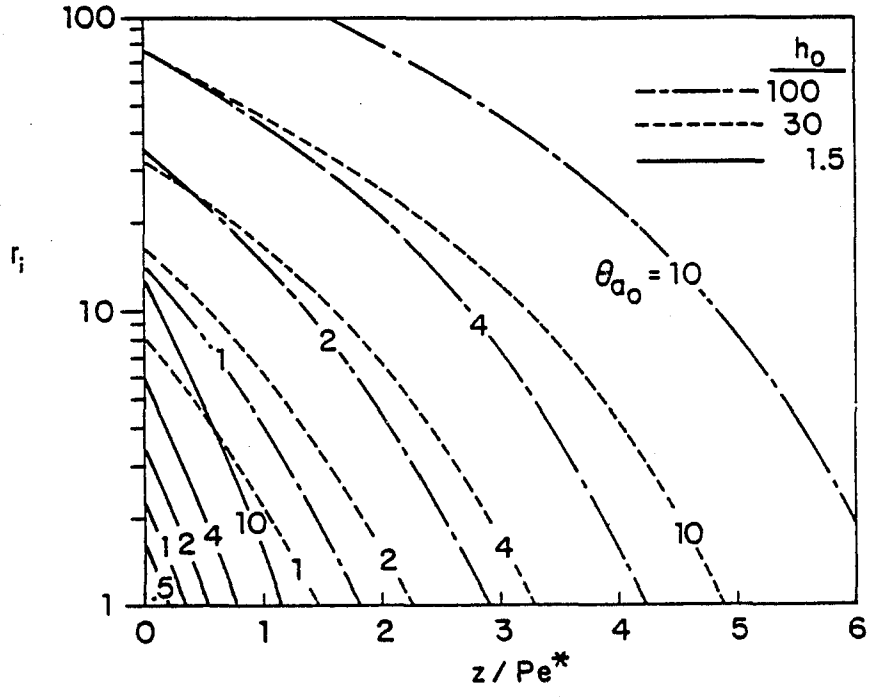

FIGURE 5. AXIAL VARIATION OF INTERFACE RADIUS

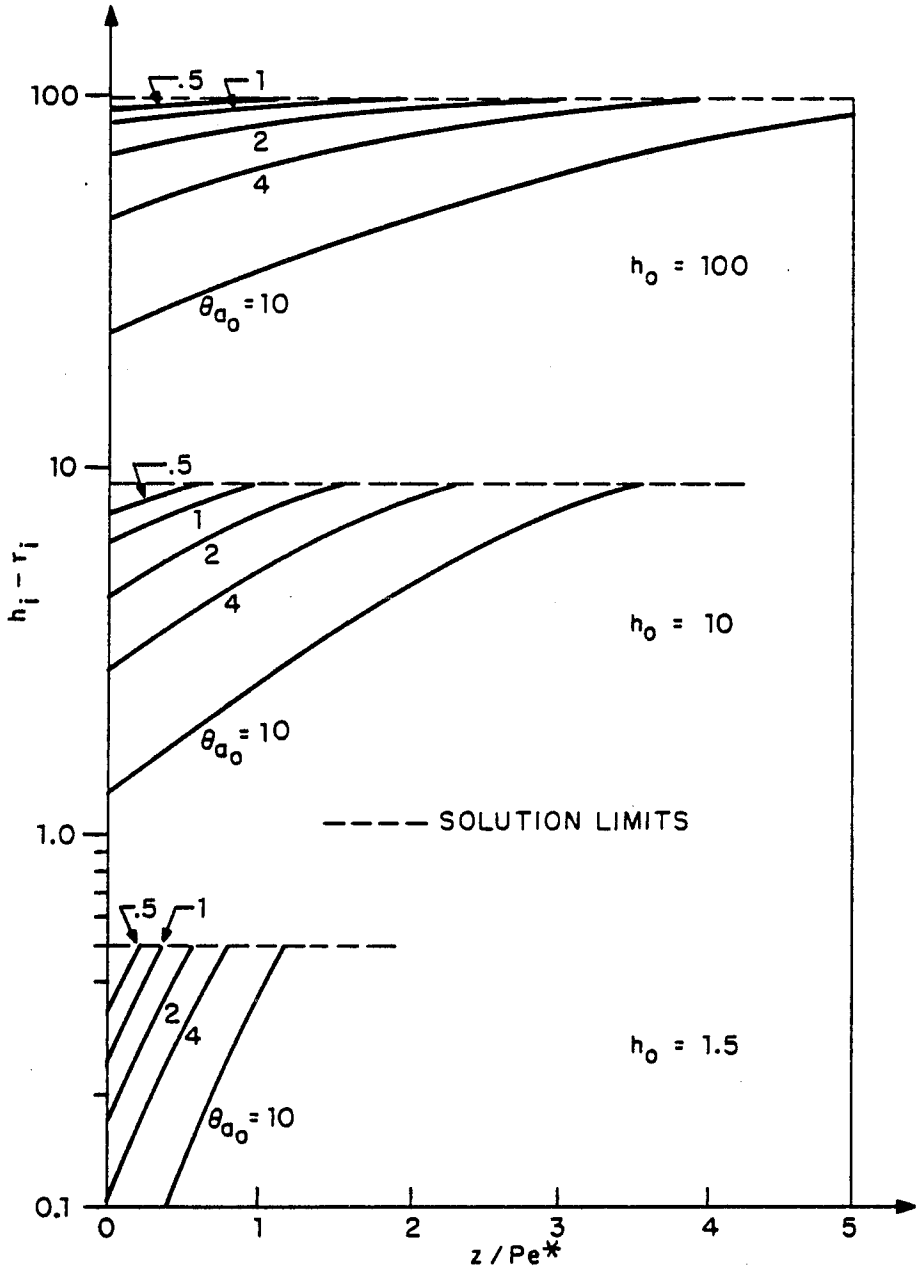

FIGURE 6. AXIAL VARIATION OF INTERFACE DEPTH BELOW PLANAR SURFACE

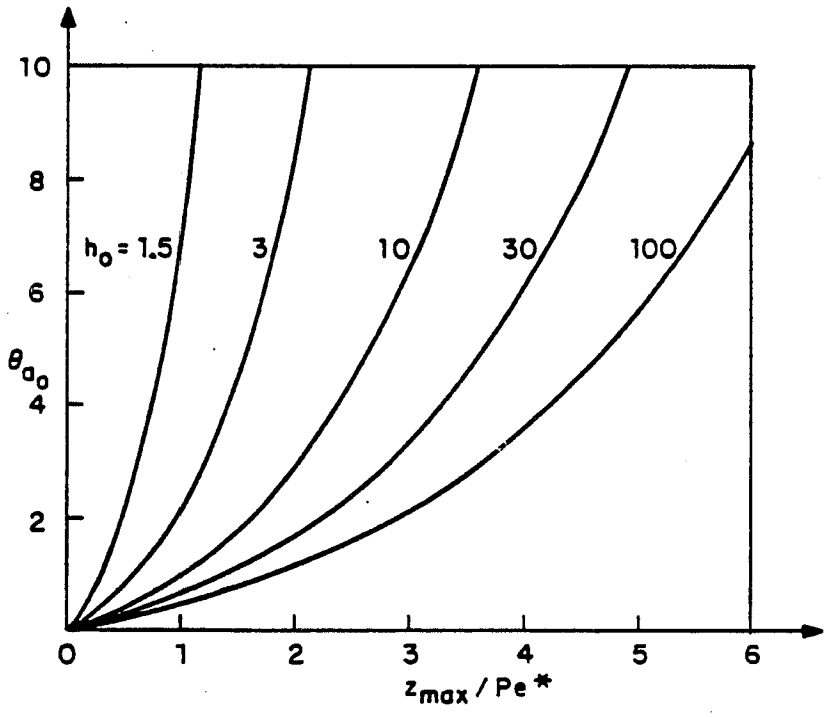

FIGURE 7. SOLUTION LIMITS

CHAPTER II

TRANSIENT TWO-DIMENSIONAL SOLUTION

FOR

PHASE CHANGE COMMENCING AT THE TUBE WALL

Of interest herein is the problem in the plane perpendicular to the tube axis as shown in Figure 2(a) and the physical Z-plane of Figure 3. The temperature of the tube wall is suddenly raised to a constant value, T_a, above T_f. A two-dimensional melting front starts at the tube surface. All notation used in the previous steady state problem will be retained unless otherwise stated. Equations (I.1,2) and boundary conditions (I.4-8) can still be used but the system now is two-dimensional and time-dependent. The new features are reflected in the motion of the interface.

There is currently no quasi-steady theoretical approach which can be used to determine the detailed shape of a moving non-circular interface without going to extensive numerical computations even for this two-dimensional case. All the previous analytic studies are based on a simplified quasi-steady approximation in which the isotherms and interface are always circular.

II.1 THE SIMPLIFIED QUASI-STEADY APPROXIMATION

Because of the widespread use of buried tubes in engineering applications, phase change problems in cylindrical geometries have been of long standing interest. However, even for the simple axisymmetric situation, there is no exact solution. Carslaw and Jaeger [6] presented an approximate analytic solution for melting or freezing outside a tube in which initial temperature is at the fusion value,

T_f, of the PCM. The radius, r_i, of the circular interface is given by

$$t^* = \frac{1}{2}\left[r_i^2 \left(\ln r_i - \frac{1}{2} \right) + \frac{1}{2} \right] \qquad \text{(II.1)}$$

The dimensionless time t^* in equation (II.1) is defined as $t^* = K_2 (T_a - T_f)\, t / \rho L a^2$. It can also be written as $t^* = t/t_{c2}$ where $t_{c2} = a^2/\bar{\alpha}_2 St_2$ is the characteristic time defined for the phase change starting at the tube wall with the Stefan number, $St_2 = C_2 (T_a - T_f)/L$. The solution is based on the quasi-steady approximation which is a widely used analytical method of great value in the mathematical simplification of phase change problems. For small Stefan number, the phase front moves relatively slowly so that the motion of the interface can be treated as moving through a sequence of quasi-steady states in which the temperature field in each phase is assumed to obey an instantaneous steady state conduction equation.

The method has been extended to the two-dimensional, embedded tube problem in the presence of a planar free surface (see Z-Plane in Figure 3) for the case where the phase change starts at the tube wall. Solutions for the penetration depth of the thaw region have been obtained for both insulated and thin walled tubes with the prescribed constant temperatures at the tube and free surfaces [1,2,7-12]. All these solutions are based on a simplified quasi-steady approximation wherein the isotherms and hence the phase front are assumed to be eccentric circles that are geometri-

cally similar to the steady state solutions obtained from pure conduction without phase change in which the interface is a circular stationary isotherm (Figure 3). The only difference among these previous investigations is in the approximation used to satisfy the interface energy equation,

$$K_1 \frac{\partial T_1}{\partial \tilde{n}} - K_2 \frac{\partial T_2}{\partial \tilde{n}} = \rho_L \vec{V} \cdot \vec{\tilde{n}} \quad , \qquad \text{(II.2)}$$

where $\vec{V}$ is the local velocity of the interface and $\vec{\tilde{n}}$ is positive directing outward region 2 as shown in Figure 2(a). In dimensionless form, equation (II.2) can be written as

$$\frac{1}{\theta_a} \frac{\partial \theta_1}{\partial n} + \frac{\partial \theta_2}{\partial n} = - \frac{dn}{dt^*} \qquad \text{(II.2-a)}$$

In the Porkhayev approximation [7], equation (II.2) is satisfied only at the bottom-most point of the circular phase front. The results show an underestimation of the thaw depth when compared with numerical solutions. Hwang [9] suggested the use of the mean value of the Porkhayev solution and the solution given by Carslaw and Jaeger [6]. As noted by Lunardini [4,10], this method is not always valid at least for deeply buried tubes. Thornton [8] used an average heat flux over the circular interface in satisfying the energy condition. Very poor agreement was found with the numerical solution for the depth of the thaw bulb, and the approximation leads to the physically unrealistic result that the more shallow the depth of the buried tube the deeper the penetration of the thaw front. Hwang [9] explained this surprising behavior by showing that the heat

flux at the top of the thaw region became progressively greater than at the bottom as the burial depth decreased, and that averaging the net heat flux over the interface would yield a large overestimation of the velocity of the bottom-most point for small burial depths. These results were carefully reviewed by Lunardini [10], and a new approximation was proposed in which only the heat flux at the bottom-most point was used to calculate the average flux that contributed to the growth of the thaw region.

A number of two-dimensional numerical solutions were carried out for various surface conditions and thermal properties by finite difference schemes [13,14] and variational finite element techniques [3,15,16]. Although numerical techniques offer great flexibility with respect to nonhomogeneity of properties and complicated boundary conditions, their expense is usually appreciable. Especially for the present three-dimensional two-domain problem, the huge storage space and long computational time required for the finite difference and finite element techniques actually rule out their practical use at least for the present time.

II.2 ANALYSIS

As sketched in Figure 2(a), the transient shape of the interface in reality is not a circle. The basic distortion of the thaw bulb from its assumed circular geometry is clearly observed in all numerical solutions obtained to date

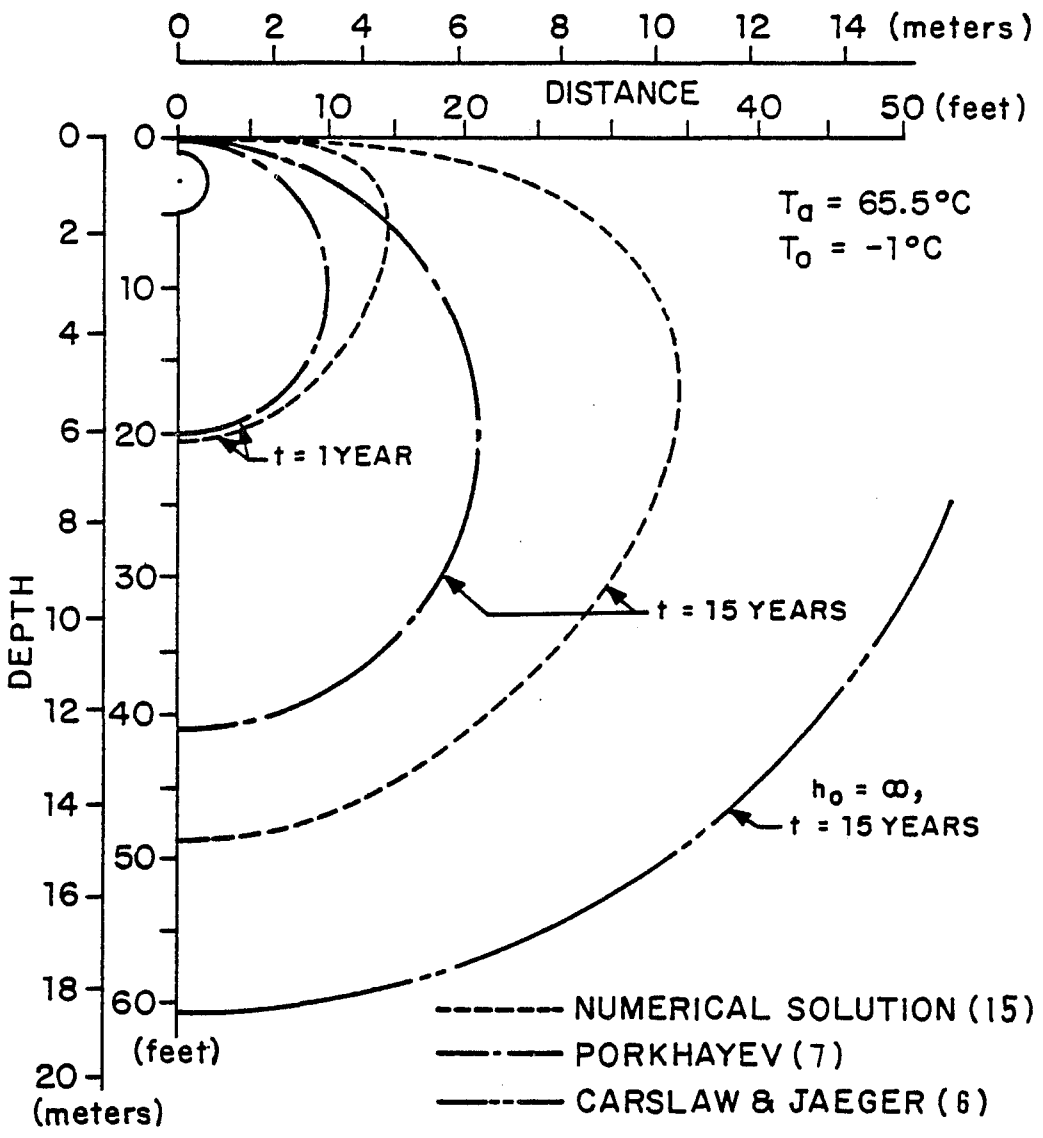

FIGURE 8. COMPARISON OF PREVIOUS QUASI-STEADY THEORIES WITH NUMERICAL SOLUTION FOR INTERFACE POSITION

and is shown in Figure 8 taken from Hwang [9]. It is convenient to examine this distortion in the complex W-plane because it is only in this plane that the interface remains a concentric circle according to the quasi-steady bicircular transformation (I.11) (Figure 3).

One can show that the actual velocity of the interface in equation (II.2) is given by

$$\vec{v} \cdot \vec{\tilde{n}} = \frac{d\tilde{n}}{dt} = a \left|\frac{dZ}{dW}\right| \frac{dR_i}{dt} \quad , \tag{II.3}$$

where |dZ/dW| is the scale factor of the transformation. Radius a appears in equation (II.3) due to the dimensional normal coordinate $n = a\tilde{n}$. The interface energy equation (II.2) hence can be transformed into the complex W-plane to give:

$$\left(K_1 \frac{\partial T_1}{\partial R} - K_2 \frac{\partial T_2}{\partial R}\right) \Big/ a \left|Z'(W)\right| = \rho L a \left|Z'(W)\right| \frac{dR_i}{dt} \quad , \tag{II.4}$$

or in dimensionless form,

$$\frac{1}{\theta_a} \frac{\partial \theta_1}{\partial R} + \frac{\partial \theta_2}{\partial R} = - \left|Z'(W)\right|^2 \frac{dR_i}{dt^*} \quad , \tag{II.4-a}$$

where |Z'(W)| = |dZ/dW| is evaluated along the interface and is given by

$$\left|Z'(W)\right| = (R_0^2 - 1) / (R_0^2 + R_i^2 + 2R_0 R_i \sin\alpha) \quad . \tag{II.5}$$

Using the steady state solution forms (I.16,17) for θ_1 and θ_2 in terms of R_i, equation (II.4-a) becomes:

$$\frac{1}{\theta_a \ln R_i/R_o} + \frac{1}{\ln R_i} = |Z'(W)|^2 \frac{dR_i}{dt^*} R_i \qquad \text{(II.6)}$$

It is evident from equations (II.5) and (II.6) that dR_i/dt varies along the interface because $|Z'(W)|$ is a function of α, and thus any assumed circular interface will immediately distort with R_i increasing at different rates along the interface in the W-plane. This rate of distortion is easily observed by comparing the instantaneous rates of growth of R_i at the top-most and bottom-most points of the interface. From equations (II.5) and (II.6), the ratio of the two rates, σ, is given by

$$\sigma \equiv \frac{dR_i(\pi/2)}{dt^*} \Big/ \frac{dR_i(-\pi/2)}{dt^*} = \frac{(R_o + R_i)^4}{(R_o - R_i)^4} . \qquad \text{(II.7)}$$

Equation (II.7) relating the growth rates of the top and bottom points of the interface in the complex plane is readily converted to the growth in radius of curvature of the thaw front in the physical plane using equation (I.12),

$$\frac{dr_i}{dt} = \frac{(R_o^2 - 1)(R_o^2 + R_i^2)}{(R_o^2 - R_i^2)^2} \frac{dR_i}{dt} . \qquad \text{(II.7-a)}$$

Since the coefficient of dR_i/dt in equation (II.7-a) is independent of angle, it follows that for isotherms corresponding to bicircular transformation, the ratio $[dr_i(\pi/2)/dt]/[dr_i(-\pi/2)/dt]$ is also given by equation (II.7). It is seen from equations (I.11-c) and (I.12) that the right hand side of equation (II.7) is only a function of the burial depth h_o and the instantaneous radius r_i of the

assumed circular interface. The plot of equation (II.7) in Figure 9 shows that the interface radius of curvature at the top-most point with $\alpha = \pi/2$ grows much more rapidly than at the bottom-most point with $\alpha = -\pi/2$ for shallow burial depths and for all burial depths when r_i is large and the interface approaches the top surface. For a specified burial depth h_0, the ratio σ is bounded from above by the maximum of R_i in the steady state, which is determined by equation (I.18). These solution limits which depend on θ_a are also shown in Figure 9 as dashed curves.

On the other hand, it can be shown that the upper and lower regions of the thaw bulb approach equilibrium at drastically different rates. Applying equations (II.5) and (II.6) at the top point with $\alpha = \pi/2$, we obtain:

$$R_{ia}\frac{\partial R_{ia}}{\partial t^*} = \frac{(R_0 + R_{ia})^4}{(R_0^2 - 1)^2}\left(\frac{1}{\theta_a \ln R_{ia}/R_0} + \frac{1}{\ln R_{ia}}\right), \qquad \text{(II.8)}$$

whereas at the bottom point with $\alpha = -\pi/2$, we have:

$$R_{ib}\frac{\partial R_{ib}}{\partial t^*} = \frac{(R_0 - R_{ib})^4}{(R_0^2 - 1)^2}\left(\frac{1}{\theta_a \ln R_{ib}/R_0} + \frac{1}{\ln R_{ib}}\right), \qquad \text{(II.9)}$$

where R_{ia} and R_{ib} are the radii of the curvatures of the interface at the top and bottom points, respectively, and t^* is the dimensionless time as defined in equation (II.1). Equation (II.8) is the Porkhayev approximation applied at the upper-most point of the thaw bulb in the complex W-plane. The time-dependent growth of R_i at the top and

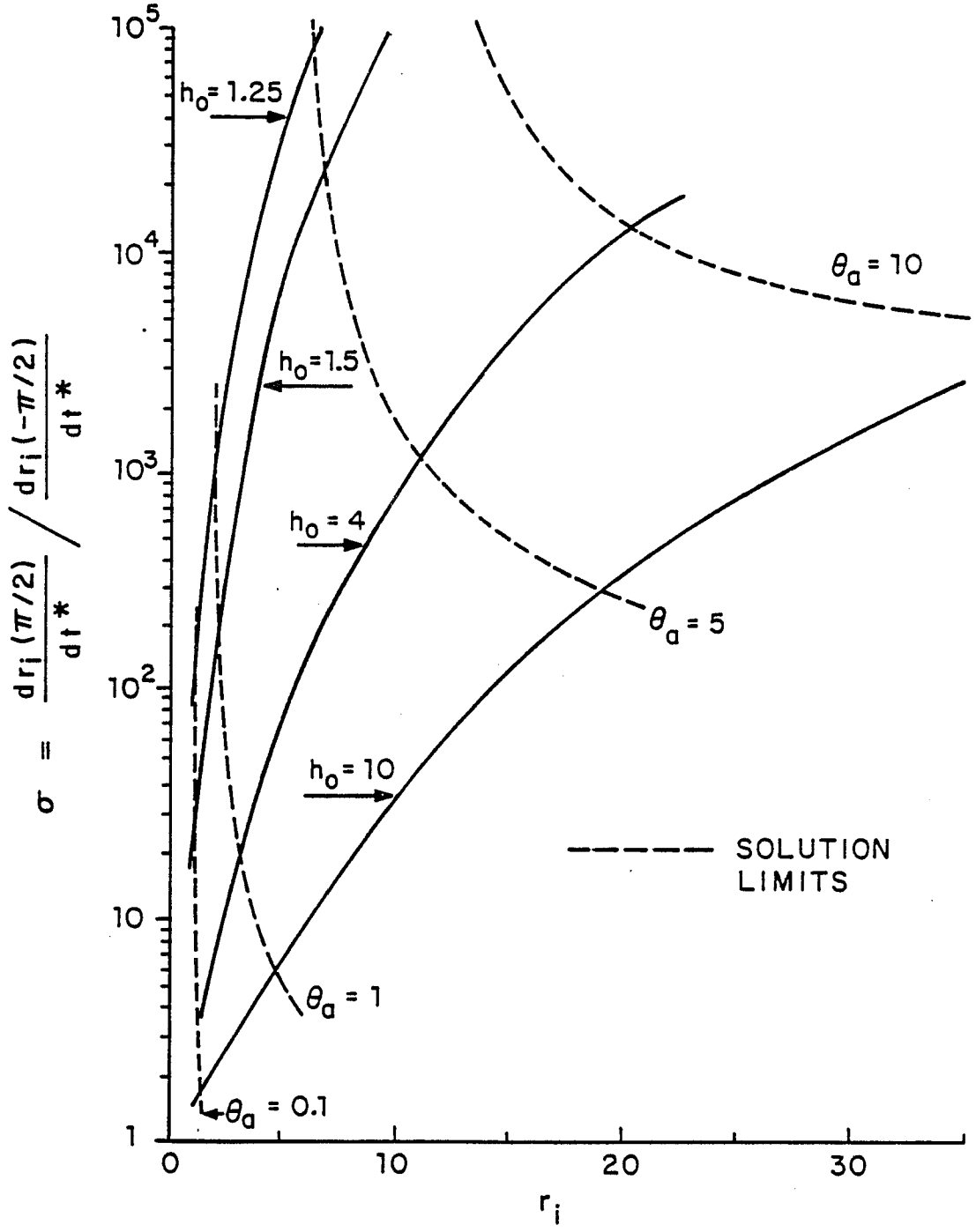

FIGURE 9. RATIO OF INSTANTANEOUS RATE OF GROWTH OF TOP TO BOTTOM POINTS OF INTERFACE

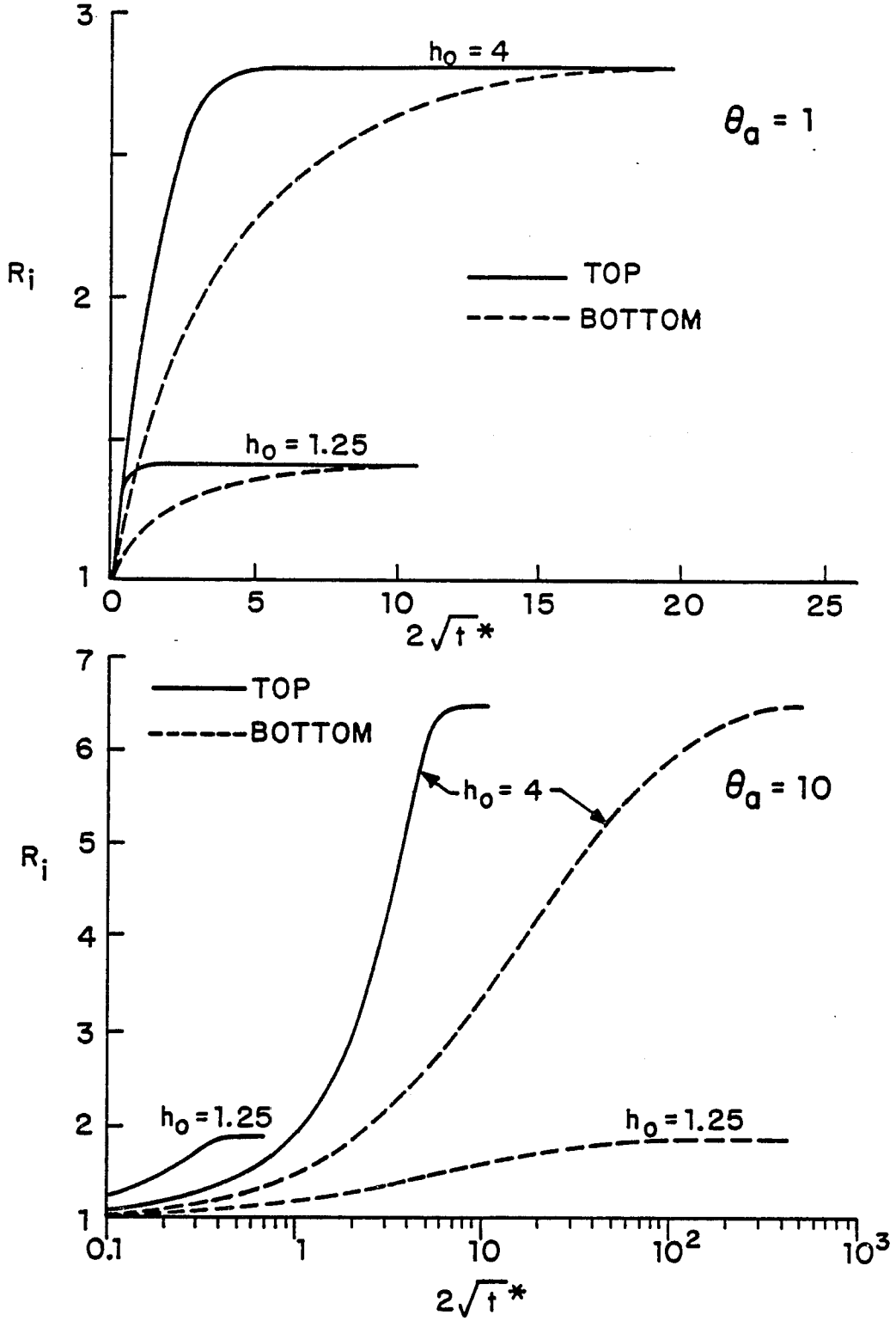

FIGURE 10. QUASI-STEADY SOLUTION TO INTERFACE MOTION IN THE COMPLEX PLANE OF TOP AND BOTTOM POINTS

bottom points are shown in Figure 10 where one can see that there is a distinct difference in behavior between $R_{ib}(t^*)$ and $R_{ia}(t^*)$. The distortion of the interface shape is significant even at early times, especially for small h_o and large θ_a. In addition, one observes that R_i develops at a much faster rate than R_{ib} and therefore that the characteristic time for the upper and lower portions of the thaw bulb to approach the asymptotic steady state (Figure 10) can differ by order of magnitude.

One notices that equation (II.9) is the Porkhayev solution in the complex W-plane. It is convenient to compare all available quasi-steady solutions mentioned in the preceding subsection in terms of the W-plane. In the Thornton approximation [8], equation (II.6) is first multiplied through by $d\alpha$ and then integrated around the circular interface. This results in

$$\int_0^{2\pi} |Z'(W)|^2 R_i \frac{dR_i}{dt^*} d\alpha = 2\pi \left(\frac{1}{\theta_a \ln R_i/R_o} + \frac{1}{\ln R_i} \right) \qquad \text{(II.10-a)}$$

The left hand side of equation (II.10-a) represents the time rate of increase of the area of the thaw bulb and is therefore simply $2\pi r_i (dr_i/dt)$. However, r_i and R_i are related by equations (I.11-c). Thus, equation (II.10-a) can be rewritten as

$$R_i \frac{dR_i}{dt^*} = \frac{(R_o^2 - R_i^2)^3}{(R_o^2-1)^2(R_o^2+R_i^2)} \left(\frac{1}{\theta_a \ln R_i/R_o} + \frac{1}{\ln R_i} \right) \qquad \text{(II.10)}$$

to give the desired expression for dR_i/dt^*. In the Lunardini approximation [10], the heat flux given by the Porkhayev approximation (II.9) is integrated around the assumed circular interface and set equal to the time rate of increase of area of the thaw region, the left hand side of equation (II.10-a). Thus, from equations (II.9,10),

$$R_i \frac{dR_i}{dt^*} = \left(\frac{R_o^2 - R_i^2}{R_o^2 - 1}\right)^2 \frac{(R_o - R_i)^2}{(R_o^2 - R_i^2)} \left(\frac{1}{\theta_a \ln R_i/R_o} + \frac{1}{\ln R_i}\right) \qquad \text{(II.11)}$$

Equations (II.1,9,10,11) provide four approximations for the growth of the thaw region beneath the tube. These results are easily converted to the penetration depth in the physical plane, $d_{ib} = (h_{ib}+r_{ib})-h_o-1$, which is defined as the distance along $\Phi = -\pi/2$ measured from the bottom point on the tube. From equations (I.8,9),

$$d_{ib} = (R_o R_i - 1)/(R_o - R_i) - 1 \qquad \text{(II.11-a)}$$

The four solutions are plotted in Figure 11 for $h_o = 1.5$ and $\theta_a = 1$ and will be used later for comparison with the numerical results and present theory. The case of $h_o = 1.5$ and $\theta_a = 1$ is selected to represent a solution where the steady state circular interface determined by equation (I.18) intersects the $x = 0$ plane roughly midway between the upper most point of the tube and the free surface. It is clear that all reasonable solutions for penetration depth, d_{ib}, must be less than the infinite burial solution given by

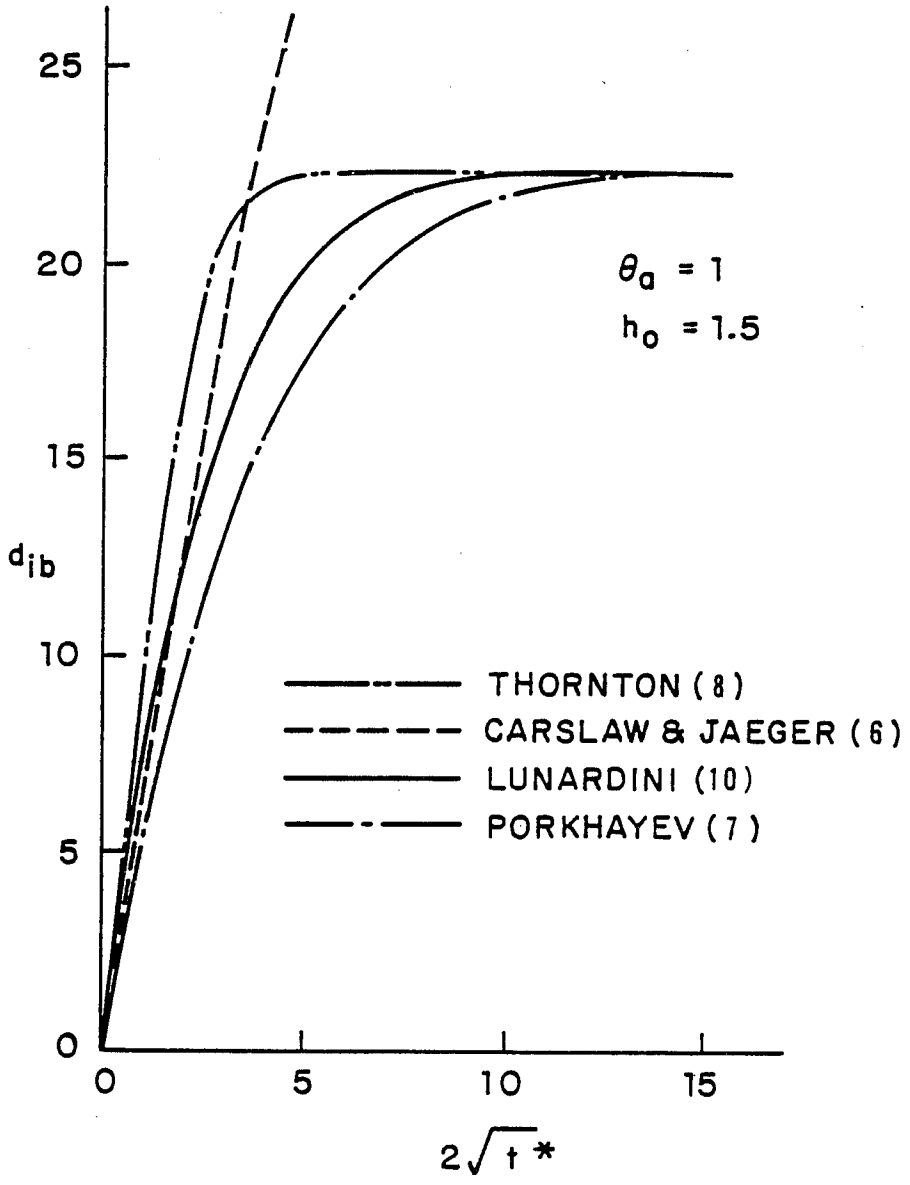

FIGURE 11. COMPARISON BETWEEN PREVIOUS QUASI-STEADY SOLUTIONS TO THAW DEPTH PENETRATION BELOW TUBE FOR $\theta_a = 1$, $h_o = 1.5$

equation (II.1). Thus, the Thornton [8] solution overestimates the thaw depth. Also, the part of the Lunardini [10] solution which is located above the Carslaw and Jaeger [6] solution up to $d_{ib} \approx 11$ is questionable. The Porkhayev [7] solution, which gives here the most conservative prediction of the penetration, always underestimates the thaw depth as will further be shown in comparison with the numerical results in subsection II.5. The infinite burial solution (II.1) is obviously not applicable since there is a free surface with a finite flux at all times. However, for short times when the thaw region is thin compared to the burial depth of the top of the tube, one can show from simple one-dimensional arguments that the gradients in the narrow thaw region must be much larger than in the solid and thus the motion of the thaw boundary is controlled almost entirely by the uniform temperature gradient at the tube wall. It is clear that here too the initial motion of the interface must correspond to concentric circles rather than the eccentric circles of the bicircular mapping whose free surface is the circle $R = R_o$ in the W-plane. The basic difficulty is that the bicircular transformation gives a very poor description of the temperature gradient at the tube wall for short times because of the non-uniform stretching of the normal coordinate which is much larger at the bottom than at the top of the tube wall. The concentric isotherms pattern, however, can be achieved using the bicircular mapping if the free surface at temperature T_o is removed and placed instead at

same fictitious large value of y. At large times, an opposite behavior is anticipated. For these times, all solutions must asymptotically approach the equilibrium steady state shape given by equation (I.18), which is a constant coordinate surface at y = 0. From the foregoing analysis, it is evident that if one is to obtain a more realistic representation of the interface geometry using the quasi-steady approximation, separate considerations are necessary at least for the regions above and below the tube. It is also confirmed by the numerical solution as shown in Figure 8 that the top and bottom portions of the interface are approximately constructed by two different circular arcs.

II.3 FORMULATION

The observations in subsection II.2 lead to a rather intriguing new quasi-steady analytic model for the thawing or freezing around a buried tube in a half space. As demonstrated in the preceding analysis, the interface evolves at vastly different rates in the upper and lower regions. This behavior suggests that the motion of the upper and lower portions of the thaw boundary at any instant may first be uncoupled and a separate analysis may be developed for each region. The formulation for each region is described in the next two subsections. The relationship between the two analyses, which is reflected in the construction of the

instantaneous interface shape, is considered in subsection II.3.3.

II.3.1 THE UPPER PORTION

The behavior of the interface at $\phi = \pi/2$ is largely independent of the temperature distribution in the lower region and is primarily controlled by the temperatures of the tube and free surfaces and the dimensionless burial depth h_o. The temperature distribution in the vicinity of the central line in this region is thus well represented by a family of steady state isotherms which are constant coordinate surfaces of the bicircular transformation. In consequence, the local curvature of the interface at $\phi = \pi/2$, can be appropriately determined by the energy balance equation (II.8). The singularity at $R_{ia} = 1$, $t^* = 0$ in equation (II.8) is removed by using the transformation, $R_{ia} = \exp(\beta^{1/2})$. The new form of equation (II.8) is given by

$$\frac{d\beta}{dt^*} = \frac{2(R_o + e^{\sqrt{\beta}})^4}{(R_o^2 - 1)^2 e^{2\sqrt{\beta}}} \left[\frac{\sqrt{\beta}}{\theta_a(\sqrt{\beta} - \ln R_o)} + 1 \right] \qquad \text{(II.12)}$$

With β or R_{ia} obtained at a given time t^*, the location of the upper portion of the interface in the physical Z-plane is determined from the geometrical relationship given by equations (I.12,13).

II.3.2 THE LOWER PORTION

The motion of the lower-most point is much more subtle since the free surface and shape of the isotherms above the tube do have a significant influence on the motion and curvature of the interface in the lower region, except for very early times when the interface is a concentric circle as in an infinite medium. The problem is not that isotherms in the vicinity of the $\phi = -\pi/2$ line can not be well approximated by a bicircular coordinate transformation, but the apparent location of the free surface for such a transformation to represent the tube wall and the interface in the lower region varies continuously from $y = \infty$ at $t^* = 0$ to $y = 0$ at $t^* = \infty$. Thus, as shown in Figure 12, at each time t^*, there is a virtual surface $y = \delta(t^*)$ such that the bicircular transformation (I.11) with R_o or h_o appropriately redefined will map the tube wall, the virtual free surface and the circle with origin $y = -h_{ib}(t^*)$ and radius $r_{ib}(t^*)$ into concentric circles in the complex W^*-plane. If $h_{ib}(t^*)$, $r_{ib}(t^*)$ and h_o are known, there is only one value of $\delta(t^*)$ which will permit these surfaces to be constant coordinate surfaces in the transformation (I.11). This transformation satisfies the identity, $h_i^2 - r_i^2 = h_o^2 - 1$ for $\delta = 0$, and hence for $\delta > 0$, the identity,

$$(h_{ib} + \delta)^2 - r_{ib}^2 = (h_o + \delta)^2 - 1 \qquad \text{(II.13)}$$

which gives:

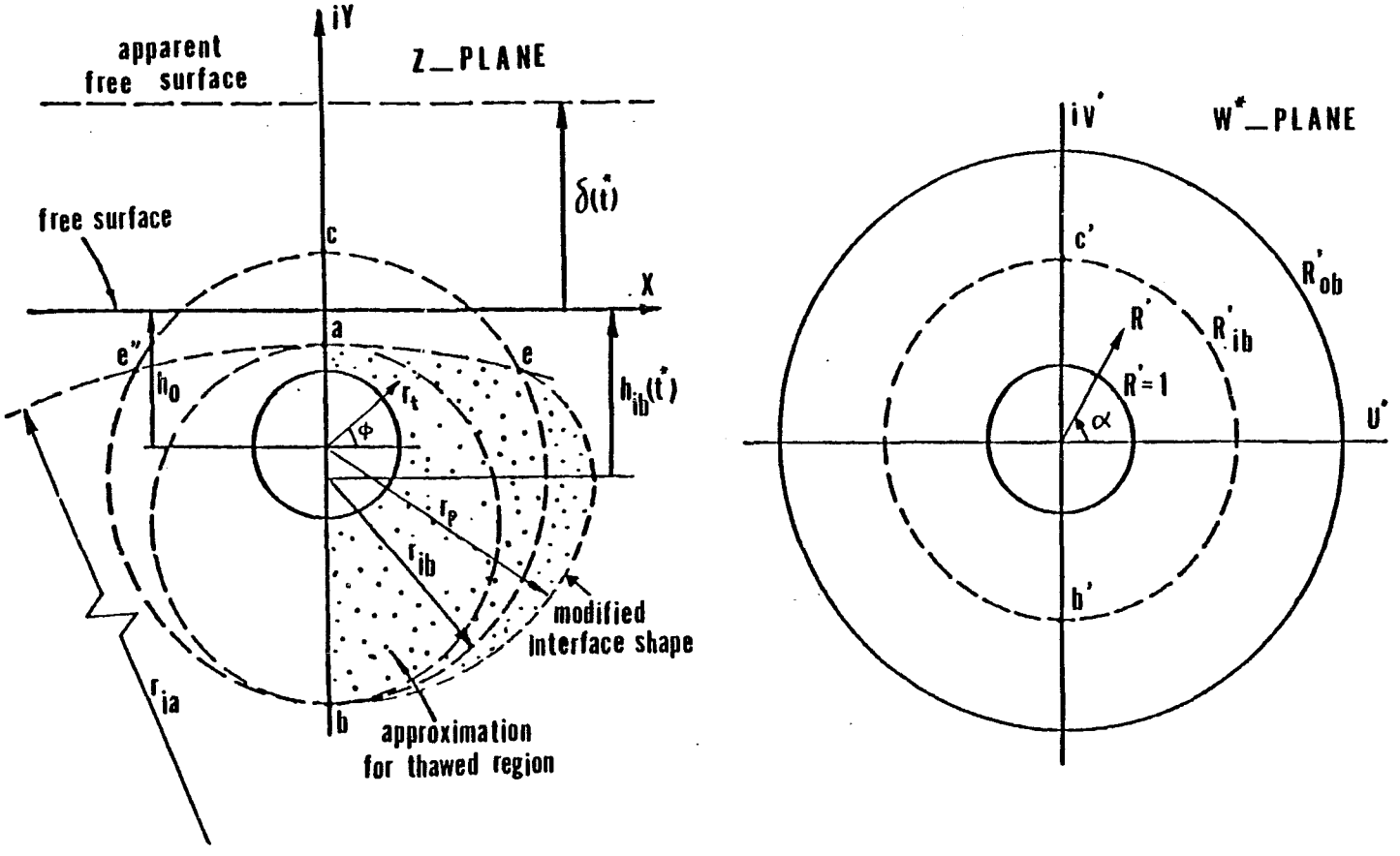

FIGURE 12. SCHEMATIC DIAGRAM SHOWING MAPPING OF BOUNDARY VALUE PROBLEM WITH APPARENT FREE SURFACE INTO COMPLEX PLANE WITH APPARENT CIRCLES R'_{ib} AND R'_{ob}

$$\delta = \frac{h_o^2 + r_{ib}^2 - h_{ib}^2 - 1}{2(h_{ib} - h_o)} \qquad \text{(II.13-a)}$$

Corresponding to r_{ib} and h_{ib} are the virtual circles R^*_{ib} and R^*_{ob} in the W*-plane. From equation (I.11c),

$$R'_{ob} = h_o + \delta + [(h_o + \delta)^2 - 1]^{1/2} \qquad \text{(II.13-b)}$$

whereas from equation (I.12),

$$R'_{ib} = \frac{1}{2r_{ib}}\left[1 - R'^2_{ob} + \sqrt{(R'^2_{ob} - 1)^2 + 4r_{ib}^2 R'^2_{ob}}\right] \qquad \text{(II.13-c)}$$

The solution for the temperature distribution in the W*-plane is given by equations (I.16,17) with R_{ib} and R_o replaced by R^*_{ib} and R^*_{ob}. Note that this solution is only intended to be accurate in the vicinity of the line with $\phi = -\pi/2$ where the curvature of the interface is given by r_{ib}.

The energy equation for the motion of the lower most interface point is of the same form as the Porkhayev formula (II.9),

$$R'_{ib}\frac{dR'_{ib}}{dt^*} = \frac{(R'_{ob} - R'_{ib})^4}{(R'_{ob} - 1)^2}\left(\frac{1}{\theta_a \ln R'_{ib}/R'_{ob}} + \frac{1}{\ln R'_{ib}}\right) \qquad \text{(II.14)}$$

The fundamental difference between the two formulae is that equation (II.14) is solved relative to the instantaneous fictitious free surface $y = \delta(t^*)$ rather than the actual free surface $y = 0$ in equation (II.9). This flexibility allows the solution for the thaw boundary near the lower

most point to undergo a continuous transition from the behavior of the Carslaw and Jaeger solution (II.1) at early times to the bicircular mapping (I.11) with $\delta = 0$ as the steady state is approached.

II.3.3 INTERFACE SHAPE CONSTRUCTION

The numerical integration of equations (II.8,14) will determine the two circles described by (r_{i_a}, h_{i_a}) and (r_{i_b}, h_{i_b}) respectively in the physical Z-plane. These circles intersect one another at points e" and e and the two arcs, $\overset{\frown}{e"ae}$ and $\overset{\frown}{e"be}$, are to be used to construct an approximation for the shape of the interface (Figure 12). As discussed earlier, the motion of the upper portion of the interface is largely independent of the temperature distribution in the lower region. The radius of curvature of the interface in the top region gradually diminishes as one proceeds from points e or e" to point b. A reasonable approximation for the shape of the lower portion of the interface between b and e is given by the polynomial:

$$r_p(\phi) = a_1 + a_2\left(\phi + \frac{\pi}{2}\right)^2 + a_3\left(\phi + \frac{\pi}{2}\right)^4 , \qquad \text{(II.15)}$$

where r_p is the local radial distance measured from the center of the tube. One requires that r_p satisfy the following conditions:

$$r_p\left(-\frac{\pi}{2}\right) = r_{i_b} + h_{i_b} - h_o , \qquad \text{(II.15-a)}$$

$$\frac{d r_p(-\frac{\pi}{2})}{d\phi} = 0 \quad . \tag{II.15-b}$$

$$r_p(\phi_e) = r_e \quad , \tag{II.15-c}$$

$$\frac{d r_p(\phi_e)}{d\phi} = C_e \quad . \tag{II.15-d}$$

Here, r_e and ϕ_e are the cylindrical coordinates of point e and C_e is the derivative $dr_p/d\phi$ evaluated at point e along the circle of radius r_{ia}. The location of point e is easily determined from the geometry (see Appendix A) as

$$x_e = \left\{ r_{ib}^2 - \left[\frac{r_{ia}^2 - (h_{ia} - h_{ib})^2 - r_{ib}^2}{2(h_{ia} - h_{ib})} \right]^2 \right\}^{1/2} \tag{II.15-e}$$

and

$$y_e = -h_{ib} + \frac{r_{ia}^2 - (h_{ia} - h_{ib})^2 - r_{ib}^2}{2(h_{ia} - h_{ib})} \quad . \tag{II.15-f}$$

As a function of r_{ia}, h_{ia}, r_{ib} and h_{ib} which are all known, r_e and ϕ_e can be calculated by

$$r_e = \sqrt{x_e^2 + (y_e + h_o)^2} \tag{II.15-g}$$

$$\phi_e = \tan^{-1} \frac{y_e + h_o}{x_e} \tag{II.15-h}$$

To evaluate C_e, one may first formulate the circle r_{ia} in the polar coordinates (r_t, ϕ) shown in Figure 12 to give:

$$f(r_t, \phi) \equiv (r_t \cos\phi)^2 + (h_{ia} - h_o + r_t \sin\phi)^2 - r_{ia}^2 = 0 \quad .$$

Using the relationship, $dr_t/d\phi = -(\partial f/\partial \phi)/(\partial f/\partial r_t)$, one then obtains:

$$C_e = \frac{(1 - r_e)\sin\phi_e - (h_{ia} - h_o)}{r_e + (h_{ia} - h_o)\sin\phi_e} \; r_e \cos\phi_e \quad . \qquad \text{(II.15-i)}$$

The coefficients a_1, a_2 and a_3 in equation (II.15) can finally be determined from boundary conditions (II.15-a-d), in which equation (II.15-b) is automatically satisfied,

$$a_1 = h_{ib} + r_{ib} - h_o \qquad \text{(II.15-j)}$$

$$a_2 = \frac{2(r_e + h_o - h_{ib} - r_{ib})}{(\phi_e + \frac{\pi}{2})^2} - \frac{C_e}{2(\phi_e + \frac{\pi}{2})} \qquad \text{(II.15-k)}$$

and

$$a_3 = \left[C_e - \frac{2(r_e + h_o - h_{ib} - r_{ib})}{(\phi_e + \frac{\pi}{2})} \right] \Big/ 2(\phi_e + \frac{\pi}{2})^3 \quad . \qquad \text{(II.15-l)}$$

It will be seen that equation (II.15) with boundary conditions (II.15-a-d) provides a very good approximation to the actual interface shape in the lower region predicted by the numerical solutions. The local curvature at point b of the modified interface shape, equation (II.15), can then be obtained from

$$r'_{ib} = \left| \frac{a_1^3}{a_1^2 - 2a_1 a_2} \right| \quad . \qquad \text{(II.16)}$$

using the standard formula for curvature in the polar coordinates. The position of its center, $y = -h'_{ib}$, is then calculated from

$$h'_{ib} = h_{ib} + r_{ib} - r'_{ib} \qquad \text{(II.17)}$$

To integrate equation (II,14), one needs an independent relation to determine δ or R^*_{ob}. Two methods are presented in the paper. A reasonable functional form for $\delta(t^*)$ was assumed in the earlier work [17], which was required to match with an approximate analytic solution at early times (Appendix B). Although the solution did show good agreement with the numerical results, this method is difficult to extend to three dimensions where the axial interaction takes place and is a complicated function of the axial position z as well as time. In the present study, a new method is used in terms of a numerical scheme to calculate the value of $\delta(z,t^*)$ at each time step for any given location using the knowledge of the instantaneous shape of the interface equation (II.15) as shown in Figure 12 and described in Appendix C. From equation (II.13-a), one may recognize that there is a unique relationship between δ and the local curvature of the interface at the bottom-most point b if the thaw depth is found. Thus, it is reasonable to use the modified radius of curvature, r^*_{ib}, given by equation (II.16) to calculate $\delta(t^*)$. This is:

$$\delta(t^*) = \frac{h_o^2 + r'^2_{ib} - h'^2_{ib} - 1}{2(h'_{ib} - h_o)} \qquad \text{(II.18)}$$

where h^*_{ib} is given by equation (II.14).

II.4 SOLUTION PROCEDURE

With R_{ia} and R'_{ib} or r_{ia}, r_{ib}, h_{ia} and h_{ib} known at time t^*, one may use equations (II.15-h-j) and (II.16,17) to determine $\delta(t^*)$ or R'_{ob} with equation (II.13-b), and then by employing equations (II.8,14) obtain the new values of $R_{ia}(t^* + \Delta t^*)$ and $R'_{ib}(t^* + \Delta t^*)$, respectively. In integrating equation (II.14), the apparent free surface is held fixed, that is R'_{ob} or δ is evaluated at time t^*. This is equivalent to using a local quasi-stationary approximation in which at each instant in time, the tube wall and the apparent free surface are treated as fixed coordinates in an instantaneous bicircular transformation $W^*(Z)$.

For early times, as stated previously, the location of the bottom-most point b of the interface (see Figure 12) may be directly determined by the Carslaw and Jaeger solution, equation (II.1). The principal difference between the Carslaw and Jaeger solution and the present solution is that there is a slight change in the penetration distance upward and downward from the tube surface due to the small non-uniform heat flux in region 1 caused by the free surface when θ_a is finite. It can be shown that the slight eccentricity of the interface is accompanied by a same order difference in curvature. The real radius of curvature at the bottom-most point is smaller than the Carslaw and Jaeger solution. In the calculations, the interface is approximated by a slightly eccentric circle passing through points a and b in Figure 12. The radius and the center of this circle, which can be determined geometrically in terms of r_{ia}, h_{ia}, h_o and

tne Carslaw and Jaeger solution for r_{ib}, can then be used in equation (II.18) to predict δ (refer to Appendix B). It is obvious that the value of δ for short times is much greater than h_o and the precise location of the apparent free surface does not significantly affect the prediction of point b since this is well approximated by the Carslaw and Jaeger solution.

II.5 RESULTS AND DISCUSSION

In Figure 13, the solution for the penetration depth of the lower-most point of the thaw boundary is plotted for the case, $\theta_a = 50.49$ and $h_o = 1.5$, corresponding to the Hwang et al [15] finite difference solution, and compared with the foregoing four solutions, equations (II.1,9-10). While the present and Lunardini's solutions agree well with the numerical solution and represent an improvement over the Porkhayev and Thornton approximations, this agreement must be viewed cautiously, especially when St_2 is not small, since the sensible heat has been neglected and this omission cannot rigorously be analyzed due to the complexity of the interface geometry. To avoid the added approximation and uncertainty associated with the effective latent heat based on a planar interface [4] used by several previous investigators [8,10], all data presented herein are calculated using the real latent heat.

The large θ_a provides a close comparison with the infi-

nite burial solution (II.1) and also a convenient illustration of an important shortcoming of existing solutions based on the bicircular transformation. The key features illustrated by Figure 13 (refer to Figure 11 as well) are that (i) the Porkhayev solution always underestimates the depth of penetration and lags the infinite burial deptn solution especially at small burial depths, (ii) the Thornton solution substantially overestimates the depth of penetration except at very large burial depths and (iii) the Lunardini solution gives good agreement with the numerical results but is unreasonable up to $2\sqrt{t^*} \approx 20$ or $t^* \approx 100$ when it is larger than the Carslaw and Jaeger solution. Perhaps the most important observation for Figure 13 is that the Carslaw and Jaeger solution for infinite burial depth (II.1) provides the best agreement with the numerical solution until $2\sqrt{t^*} \approx 10$ or $t^* \approx 25$. It is evident that the presence of the free surface has almost no effect on the motion of the bottom-most point of the thaw region until this time. It can be anticipated that for smaller θ_a, this time limit would be shorter because of the stronger influence of the free surface temperature.

The results of the present approximation for the shape of the entire interface are compared in Figures 14(a,b) with the Porkhayev and Lunardini approximations and the numerical solutions of Gold [14] and Hwang et al [15] at (a) $h_0 = 1.5$, $\theta_a = 50.49$ and (b) $h_0 = 4.0$ and $\theta_a = 7.09$. A very good agreement is observed almost everywhere. The fundamental

notion that the upper and lower portions of the thaw boundary approach their final equilibrium on different time scales is well illustrated.

The results for very early and very late times are not easily seen in Figure 14 because of the huge difference in time scales for the development of the upper and lower regions when $h_o = 1.5$. The latter behavior is more easily seen in Figure 15 where the growth of r_{ia} and r_{ib} as a function of time have been plotted for $\theta_a = 7.09$ and $h_o = 4.0$. Even for this moderate burial depth, the non-circular distortion of the thaw boundary is very substantial.

In Figure 16, the dimensionless growth of the top and bottom points of the thaw boundary for $h_o = 2$ and representative values of θ_a: 0.5, 1.0 and 5.0 shows the role of θ_a. For large values of θ_a, the final thaw radius is large and it takes a longer time to reach the steady state equilibrium position for both top and bottom thaw boundary points. In general, the difference in time for the two portions to achieve the steady state grows as θ_a increases.

The foregoing results show that the distortion of the thaw region from a circular shape is a complicated function of both h_o and θ_a. The difficulty in using the steady state bicircular transformation, however, is more subtle than just the assumed circular interface geometry. At short times when the phase front is close to being circular, the growth rates of the top and bottom boundary points are in fact very nearly equal, whereas the bicircular mapping leads to a

highly asymmetric heat flux at small burial depths due to the non-equal stretching of the length coordinates, $|Z'(W)|$, at the top and bottom of the tube. Thus, if one is to retain the mathematical simplification afforded by the bicircular mapping, the free surface must be relocated at some large distance to equalize the stretching of line segments above and below the tube. As time progresses, the isotherms in the lower region do develop as nearly eccentric circles except that this apparent free surface gradually shifts downward approaching the actual free surface as t approaches infinity.

REMARKS

Thus far, the key equation (II.2-a) at the interface surface has been solved relatively easily for two cases: (i) the steady state where equation (II.2-a) reduces to equation (I.10), and (ii) the two-dimensional transient approximation where θ_a is constant and equation (II.2-a) is treated separately by equations (II.8) and (II.14), which are solved numerically for R_{ia} and R^*_{ib} as a function of time. For the three-dimensional case where $\theta_a = f(z,t^*)$, the interface equation must be solved simultaneously with the energy equation for the fluid inside the tube due to the thermal interaction between the PCM and fluid domains.

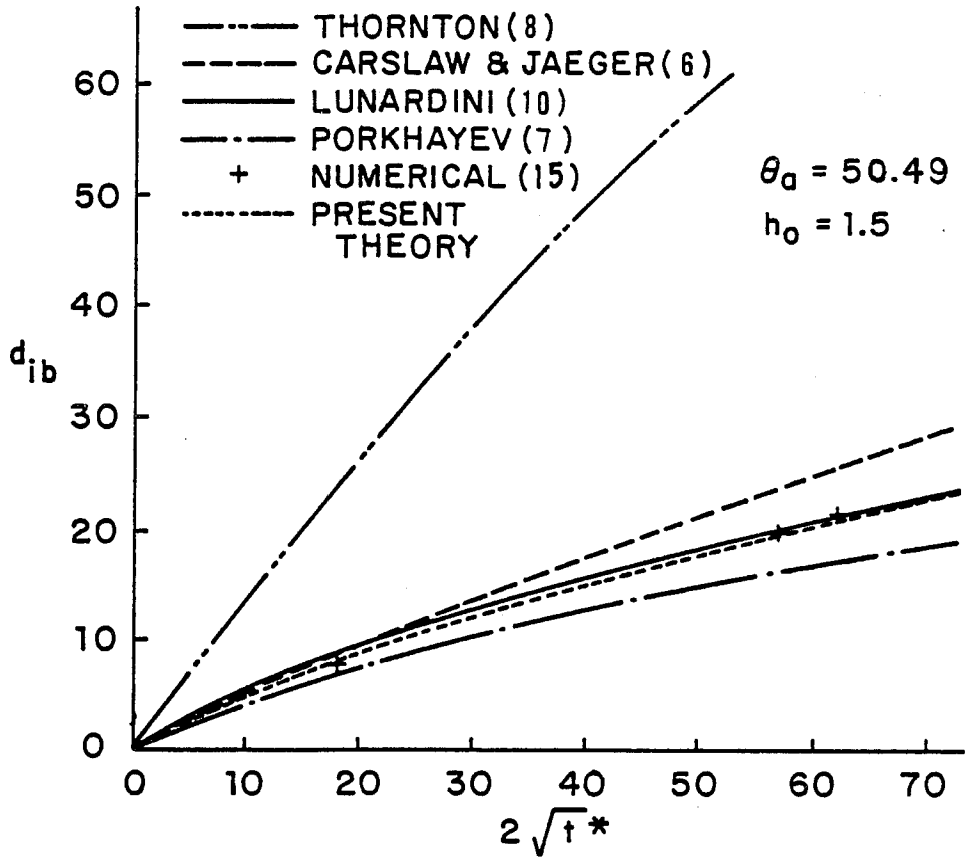

FIGURE 13. COMPARISON BETWEEN NUMERICAL, PREVIOUS AND PRESENT QUASI-STEADY SOLUTIONS TO THAW DEPTH PENETRATION BELOW TUBE FOR $\theta_a = 50.49$, $h_o = 1.5$

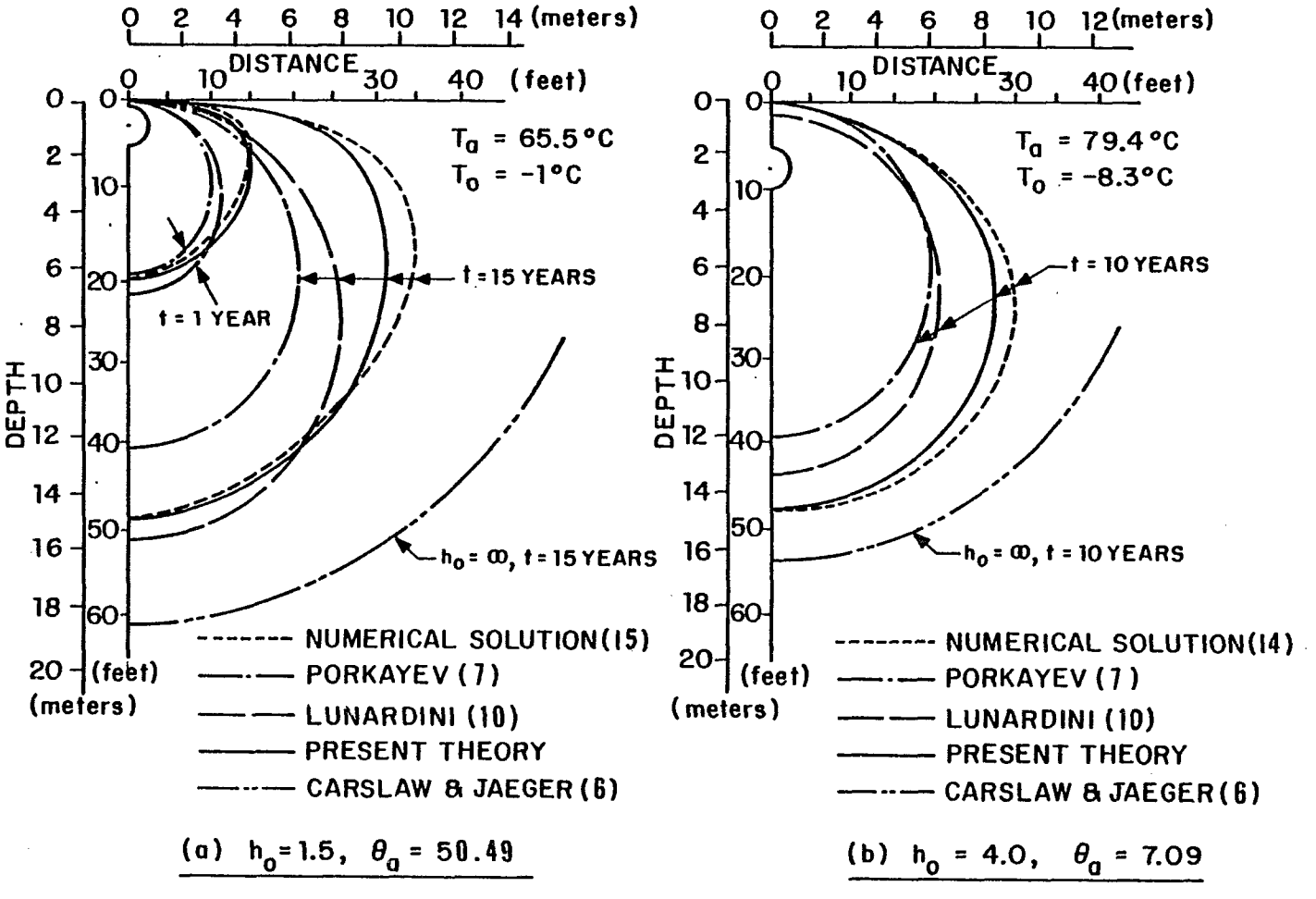

FIGURE 14. COMPARISON BETWEEN NUMERICAL, PREVIOUS AND PRESENT QUASI-STEADY SOLUTIONS FOR INTERFACE POSITION

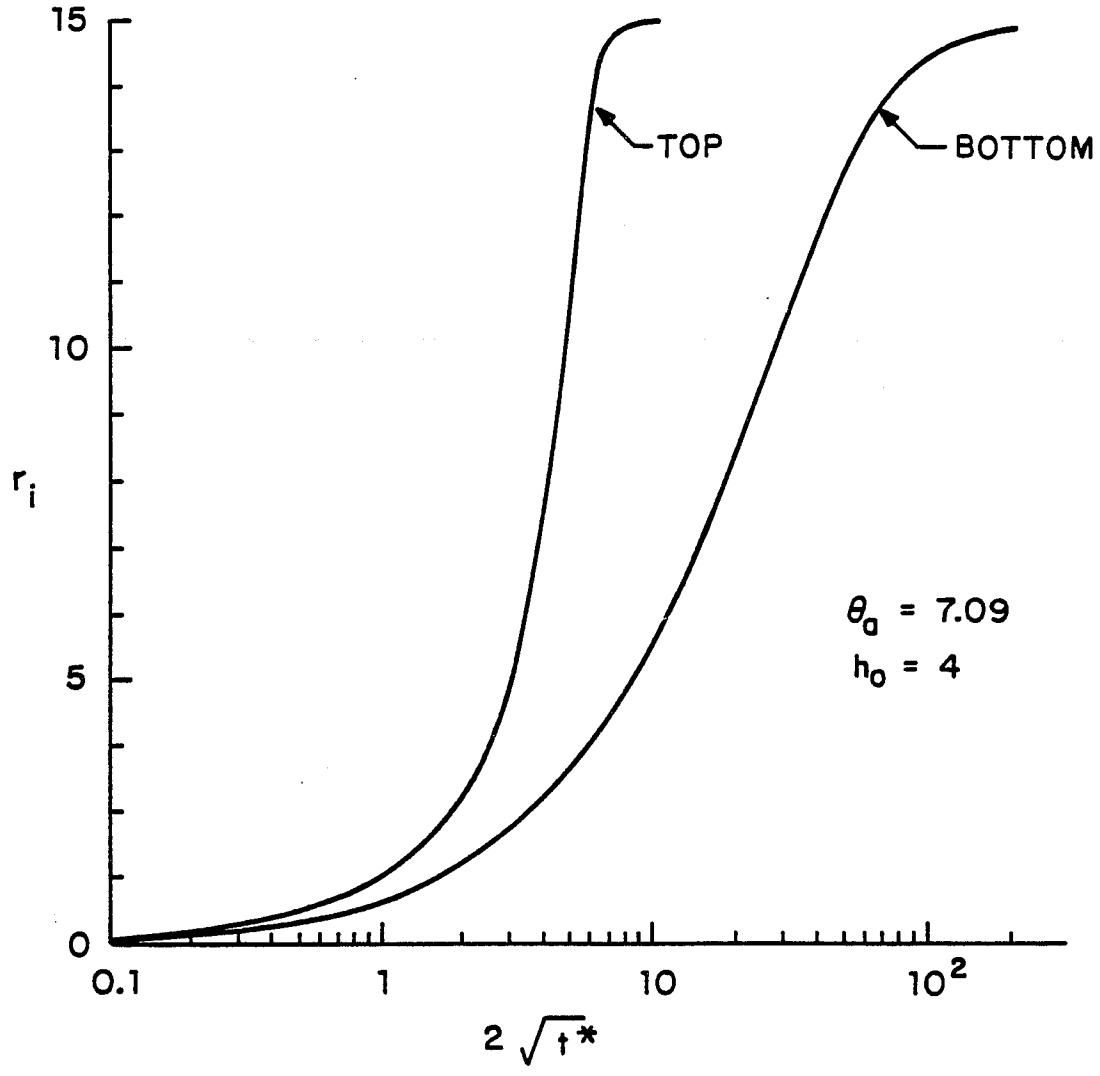

FIGURE 15. INTERFACE RADIUS OF CURVATURE OF TOP AND BOTTOM POINTS AS A FUNCTION OF TIME USING PRESENT THEORY FOR θ_a = 7.09, h_o = 4

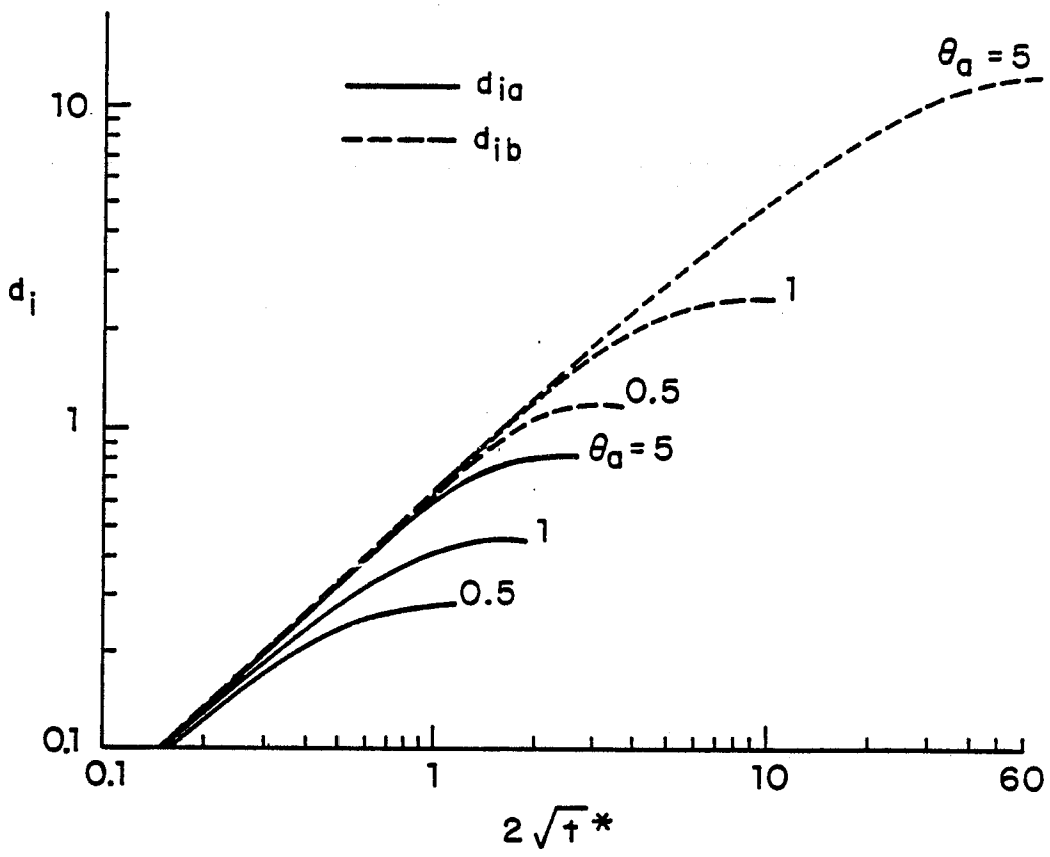

FIGURE 16. THAW DEPTH PENETRATION BELOW AND ABOVE TUBE USING PRESENT THEORY FOR θ_a = .5, 1, 5 AND h_o = 2

CHAPTER III

THE THREE-DIMENSIONAL SOLUTION

FOR

PHASE CHANGE COMMENCING AT THE TUBE WALL

In this chapter, the two-dimensional solution method is extended to determine the three-dimensional motion of the interface and the time variation of the axial temperature distribution in the fluid for freezing starting at the tube surface. Due to the singularities of the differential equations along the tube surface, an axisymmetric analytic solution is provided for the region near the tube wall. Solutions are presented for several representative flow geometries and initial conditions. The results reveal some important factors in the interface behavior attributed to the fluid-PCM interaction.

In the following subsection, some of the important existing axisymmetric solutions for phase change around a buried tube coupled with the axial fluid domain are briefly reviewed.

III.1 SOLUTIONS FOR THE AXISYMMETRICAL PROBLEM

It is only recently that embedded tube problems involving axial thermal interaction have been addressed. All the investigations to date have focused on axisymmetric geometries where the surrounding PCM is infinite in the radial direction and initially at the phase change temperature [18-22]. The numerical solutions have accounted for axial conduction and the finite heat capacity of the PCM [18,19]. In Sparrow and Hsu [19], a short time quasi-steady analytic solution for freezing is also presented in which a linear

radial temperature profile is assumed in the solid region. Good agreement with the numerical solutions is obtained provided that the frozen layer is less than 20-30 % of the tube radius. Most recently, Shamsunder [21] has obtained a simple elegant analytic solution to the same quasi-steady problem but has extended the analysis to long times by including the logarithmic radial conduction profile in the solid phase. The remarkable accuracy of this quasi-steady solution (error is less than 0.2 % for small Stefan number for all the numerical solutions shown in [19]) convincingly justifies the neglect of axial conduction and the use of the quasi-steady approximation. Since the PCM is infinite, all these solutions with axial thermal interaction have no steady state.

III.2 ANALYSIS AND FORMULATION

The new two-dimensional quasi-steady analytic model established in the preceding chapter also allows for the time dependent boundary conditions on the tube wall and the plane surface with the principal restriction that the characteristic time scale of the temperature variations in the boundary conditions be much larger than the thermal diffusion time, $(\tilde{h}_o+a)^2 / \bar{\alpha}_2 St_2$, required for quasi-steady conditions to be satisfied in both the thaw and solid regions. These conditions are often valid in the three-dimensional axial flow interaction problems described in the Introduc-

tion where the temperature of the fluid in the tube flow varies with time and distance along the tube axis.

In contrast to the two-dimensional model, the temperature of the tube surface T_a, now becomes a function of the axial position as well as time while the interface moves outward from the tube with a three-dimensional configuration due to the axial thermal interaction. The two coordinate systems $(\tilde{x},\tilde{y},\tilde{z})$ and $(\tilde{r}_t,\Phi,\tilde{z})$ defined in subsection I.2.1 are retained in Figure 17 where the radial distance $\tilde{r}_p(\phi,\tilde{z},t)$ is used to describe the instantaneous position of the interface in the tube centered coordinate system. Two additional dimensionless variables are defined to include the axial effects,

$$\bar{\theta}_a = (T_a - T_f)/(T_{ao} - T_f) = \theta_a / \theta_{ao} \qquad \text{(III.1-a)}$$

and

$$\bar{t}^* = K_2 (T_{ao} - T_f) t / \rho L a^2 = t^* / \bar{\theta}_a \,, \qquad \text{(III.1-b)}$$

where $T_{ao} > T_f$ is the inlet temperature of the fluid at $\tilde{z} = 0$. The dimensionless time t* defined in the two-dimensional problem must be changed to $\bar{t}^*$ in the three-dimensional case because the wall temperature, T_a, is no longer a constant. Based on the the assumptions listed in chapter I, equations (I.1,2) and boundary conditions (I.4-9) are still valid in the present problem except the temperature fields, $\theta_{1,2}(x,y,z,t^*)$, in both regions here are time-dependent in the three-dimensional space. The energy conservation at the

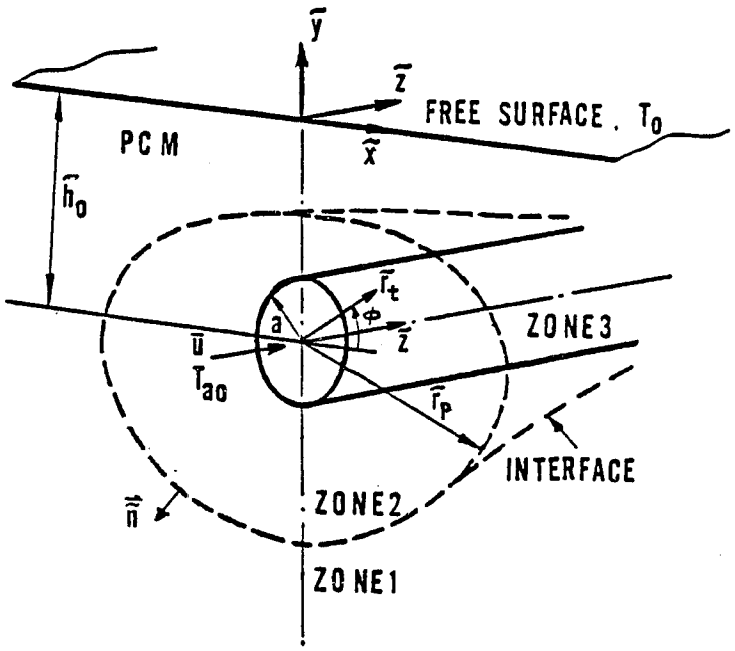

FIGURE 17. CONFIGURATION AND COORDINATE SYSTEM FOR PHASE CHANGE COMMENCING AT THE TUBE WALL

interface is written as

$$\frac{1}{\theta_a(z,\bar{t}^*)}\frac{\partial\theta_1(r_t,\Phi,z,\bar{t}^*)}{\partial n}+\frac{\partial\theta_2(r_t,\Phi,z,\bar{t}^*)}{\partial n}=-\frac{1}{\bar{\theta}_a(z,\bar{t}^*)}\frac{\partial n}{\partial \bar{t}^*} \qquad \text{(III.2)}$$

Equation (III.2) with new dimensionless variables $\bar{\theta}_a(z,\bar{t}^*)$ and $\bar{t}^*$ reduces to equation (II.2-a) when θ_a is constant. Since interface curvature in the axial direction is neglected (consistent with the negligible axial heat conduction), vector $\vec{n}$ is assumed to be in the xy plane only.

The axial thermal interaction is mostly reflected in the energy conservation equation in the fluid, which is given by

$$\frac{\rho_e^*}{\bar{\theta}_a}\frac{\partial\bar{\theta}_a}{\partial z}=\frac{2}{\pi}\int_{-\frac{\pi}{2}}^{\frac{\pi}{2}}\frac{\partial\theta_2(1,\alpha,z,\bar{t}^*)}{\partial R}\,d\alpha \qquad \text{(III.3)}$$

where the transient term, $\partial\bar{\theta}_a/\partial\bar{t}^*$, does not appear in the left hand side of equation (III.3) because the characteristic time of convection in the fluid, $\ell/\bar{u}$, where ℓ is the characteristic length of the tube, is assumed small in comparison with $a^2/\bar{\alpha}_2 St_2$. Equation (III.3) is of the same form as equation (I.3) where $\theta_a=\bar{\theta}_a\theta_{ao}$ and θ_{ao} is constant and can be integrated using a finite difference scheme because the time variable does not appear explicitly. To proceed with the numerical calculation, one must first evaluate the integral on the right hand side of the equation for any specified position along the tube axis.

III.2.1 HEAT FLUX AT THE TUBE SURFACE

The integrand in equation (III.3) actually represents the heat flux at the tube surface in the complex W-plane. It can be shown that by virtue of the good approximation shape of the interface, which has been determined by equation (II.15) for any given time in terms of r_{ia}, h_{ia}, r_{ib} and h_{ib}, the heat flux can also be well approximated by an analytical form as a function of α. The geometrical relationship due to the mapping W(Z) given in Figure 3 is represented in Figure 18 where point g is the intersection of the tube wall and the heat flux line passing point e. One can easily find point g through point e in terms of the bicircular mapping where its image, point g', satisfies $R_{g'} = 1$ and $\alpha_{g'} = \alpha_{e'}$. From the geometrical relationship shown in Figure 18, $\alpha_{e'}$ can be determined by (see Appendix A)

$$\alpha_{e'} = \frac{-R_o x_e^2 + [R_o - (h_o + y_e)][R_o(h_o + y_e) - 1]}{x_e(R_o^2 - 1)} \qquad \text{(III.4-a)}$$

where x_e and y_e given by equations (II.15-e,f) are the location of point e in the physical Z-plane. Since $d\Phi = |Z'(W)|d\alpha$ along the tube surface, Φ_g can be calculated from $\alpha_{e'}$ by the integral

$$\Phi_g + \frac{\pi}{2} = \int_{-\frac{\pi}{2}}^{\alpha_{g'}} |Z'(W)|\, d\alpha = \int_{-\frac{\pi}{2}}^{\alpha_{e'}} \frac{R_o^2 - 1}{R_o^2 + 1 - 2R_o \sin\alpha}\, d\alpha$$

With $|Z'(W)|$ given by equation (II.5) and $R_i = 1$, the integration gives:

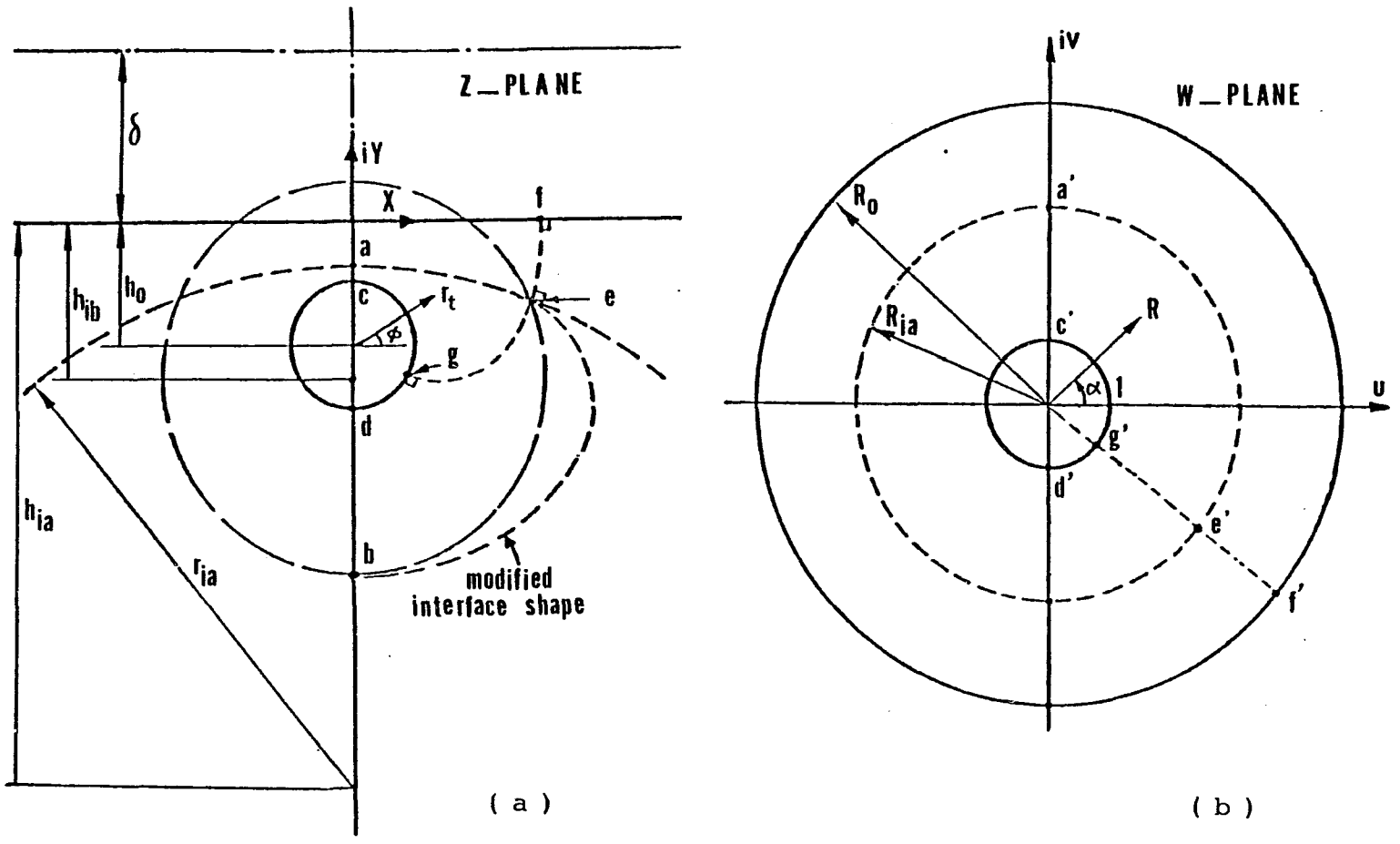

FIGURE 18. SCHEMATIC DIAGRAM SHOWING (a) THE MODIFIED INTERFACE SHAPE, AND (b) MAPPING OF HEAT FLUX LINE PASSING THROUGH POINT e

$$\phi_g = -\frac{\pi}{2} + \frac{2(R_o^2-1)}{R_o^2+1}\left[\tan^{-1}\frac{\tan\alpha_e'/2 + \frac{2R_o}{R_o^2+1}}{1-\left(\frac{2R_o}{R_o^2+1}\right)^2} + \tan^{-1}\frac{(R_o-1)^2}{R_o^2-1}\right] \qquad \text{(III.4-b)}$$

Once α_e' or ϕ_g is determined, the heat flow rate through the tube wall is evaluated separately along the segments of arc $\widehat{cg}$ and $\widehat{gd}$. Using equation (I.17), the heat flux through the upper portion of the tube wall in the complex W-plane is obtained by

$$\frac{\partial\theta_2(1,\alpha)}{\partial R} = -\frac{1}{\ln R_{ia}} \qquad (\text{along } \widehat{c'g'}) \qquad \text{(III.4)}$$

Note that the right hand side of equation (III.4) is not a function of α. Using the scale factor, the heat flux in the physical Z-plane can be easily evaluated by

$$\frac{\partial\theta_2(1,\phi)}{\partial r_t} = \frac{1}{|Z'(w)|}\frac{\partial\theta_2(1,\alpha)}{\partial R} = -\frac{R_o^2+1+2R_o\sin\alpha}{R_o^2-1}\cdot\frac{1}{\ln R_{ia}} \qquad (\text{on } \widehat{cg}). \qquad \text{(III.5)}$$

This is valid at the tube wall, where becomes a function of α only. Applying equation (III.5) at $\phi = \pi/2$, one obtains:

$$q_c = -\frac{1}{\ln R_{ia}}\,\frac{(R_o+1)^2}{R_o^2-1} \qquad \text{(III.5-a)}$$

Similarly, the heat flux at point g is given by

$$q_g = -\frac{1}{\ln R_{ia}}\left(\frac{R_o^2+1+2R_o\sin\alpha_g'}{R_o^2-1}\right) \qquad \text{(III.5-b)}$$

For the lower portion of the tube, $\widehat{dg}$, the heat flux in the physical Z-plane is approximated by the polynomial:

$$\frac{\partial\theta_3(1,\phi)}{\partial r_t} = b_1 + b_2\left(\phi+\frac{\pi}{2}\right)^2 + b_3\left(\phi+\frac{\pi}{2}\right)^4 \qquad \text{(III.6)}$$

where b_1, b_2 and b_3 are chosen to satisfy the following boundary conditions:

$$\frac{\partial \theta_2(1,-\pi/2)}{\partial r_t} = q_d \,, \qquad \text{(III.7-a)}$$

$$\frac{\partial^2 \theta_2(1,-\pi/2)}{\partial r_t \, \partial \phi} = 0 \,, \qquad \text{(III.7-b)}$$

$$\frac{\partial \theta_2(1,\phi_g)}{\partial r_t} = q_g \,, \qquad \text{(III.7-c)}$$

$$\frac{\partial^2 \theta_2(1,\phi_g)}{\partial r_t \, \partial \phi} = q_g' \qquad \text{(III.7-d)}$$

q_g and q_g' here are respectively the values of the heat flux and its derivative with respect to Φ at point g. While q_g in equation (III.7-b) is simply calculated from equation (III.5), the value of q_g' can be determined in terms of the transformation (I.11) where $\partial\theta_2(1,\alpha)/\partial R$ is constant along the upper surface of the tube, $\widehat{c'g'}$, (Figure 18). Using the scale factor, one can replace the differences $d\Phi$ and dr in the physical plane with $|Z'(W)|d\alpha$ and $|Z'(W)|dR$, respectively. Note that this replacement is valid in the (r,Φ,z) coordinates as defined in subsection I.2.1 and can be used in the tube centered coordinates (r_t,Φ,z) only at the surface of the tube. With these relations, q_g' can be written as

$$q_g' = \frac{\partial^2 \theta_2(1,\phi_g)}{\partial r_t \partial \phi} = \frac{1}{|Z'(w)|}\frac{\partial}{\partial \alpha}\left[\frac{\partial \theta_2(1,\alpha)}{\partial R}\frac{1}{|Z'(w)|}\right] \qquad \text{(III.8)}$$

With $|Z'(W)|$ or equation (II.5) evaluated at $R_i = 1$ and equation (III.4), one obtains:

$$q_g' = -\frac{1}{\ln R_{ia}}\frac{2R_0(R_0^2+1+2R_0\sin\alpha_{e'})}{(R_0^2-1)^2}\cos\alpha_{e'} \qquad \text{(III.9)}$$

q_d, which has the value $-1/\ln R_{ib}'$ in the complex W*-plane, is given by

$$q_d = \frac{1}{|Z'(W^*)|}\frac{\partial \theta_2(1,-\pi/2)}{\partial R} = -\frac{1}{\ln R_{ib}'}\frac{R_{ob}'-1}{R_{ob}'+1} \qquad \text{(III.10)}$$

where $|Z'(W^*)|$ is the scale factor of the transformation $W^*(Z)$ evaluated at $\alpha = -\pi/2$ on the tube surface. The formulae for local heat flux in the physical plane, equations (III.5-a,10) are used later to calculate q_c and q_d as shown in Figure 18. The coefficients b_1, b_2 and b_3 in equation (III.6) can easily be obtained from the boundary conditions (III.7a-d).

$$b_1 = q_d \,, \qquad \text{(III.11-a)}$$

$$b_2 = -\frac{q_g'}{2(\alpha_{g'}+\frac{\pi}{2})} - \frac{2(q_g'+q_d)}{(\alpha_{g'}+\frac{\pi}{2})^2} \qquad \text{(III.11-b)}$$

and

$$b_3 = \frac{q_g'(\alpha_{g'}+\frac{\pi}{2}) - 2(q_g'+q_d)}{2(\alpha_{g'}+\frac{\pi}{2})^4} \qquad \text{(III.11-c)}$$

Boundary condition (III.7-b) is automatically satisfied.

Finally, the integrated heat flux per unit axial length at the tube wall is given by

$$2\int_{-\frac{\pi}{2}}^{\frac{\pi}{2}} \frac{\partial \theta_2(1,\alpha)}{\partial R}\, d\alpha = 2\left[\int_{-\frac{\pi}{2}}^{\phi_g} \frac{\partial \theta_2(1,\phi)}{\partial r_t}\, d\phi - \int_{\alpha_{e'}}^{\frac{\pi}{2}} \frac{\partial \theta_2(1,\alpha)}{\partial R}\, d\alpha\right]$$

$$= 2\left[b_1'(\phi_g+\tfrac{\pi}{2}) + \frac{b_3'}{2}(\phi_g+\tfrac{\pi}{2})^3 + \frac{b_5'}{5}(\phi_g+\tfrac{\pi}{2})^5\right] - \frac{2}{\ln R_{ia}}\left(\frac{\pi}{2}-\alpha_{e'}\right) \qquad \text{(III.12)}$$

Note that the heat flow rate is the same for the physical and complex planes because the scale factor does not appear in the integral form. If the shape of the interface described by r_{ia}, h_{ia}, r_{ib} and h_{ib} (or R_{ia}, R_{ib}^* and R_{ob}^*) is known at each cross-section on the tube axis, the integral on the right hand side of equation (III.3) can be evaluated from equation (III.12). Thus the dimensionless fluid temperature, $\bar{\theta}_a(z,\bar{t}^*)$, can be determined by integrating equation (III.3) using a finite difference procedure.

A simpler but less accurate estimation of the flow rate can be obtained by using a lower order polynomial in place of equation (III.6) in the integral of equation (III.3). A suitable approximation is the parabola:

$$\frac{\partial \theta_2(1,\phi)}{\partial r_t} = b_1' + b_2'(\phi-\tfrac{\pi}{2}) + b_3'(\phi-\tfrac{\pi}{2})^2 \qquad \text{(III.13)}$$

which satisfies the boundary conditions:

$$\frac{\partial \theta_2(1,\pi/2)}{\partial r_t} = q_c \qquad \text{(III.13-a)}$$

$$\frac{\partial \theta_2(1,-\pi/2)}{\partial r_t} = q_d \qquad \text{(III.13-b)}$$

$$\frac{\partial^2 \theta_2(1,\pi/2)}{\partial r_t \partial \phi} = 0 \quad . \qquad \text{(III.13-c)}$$

It results in a simple expression for the heat flow rate,

$$2\int_{-\frac{\pi}{2}}^{\frac{\pi}{2}} \frac{\partial \theta_2(1,\phi)}{\partial r_t} d\phi = 2\pi\left(\frac{2}{3} q_c + \frac{1}{3} q_d\right) \quad . \qquad \text{(III.14)}$$

Equation (III.14) shows that the average heat flux at the tube wall can be approximated by $(2q_c+q_d)/3$.

It can be anticipated that equations (III.5) and (III.6) provide a good approximation of the angular distribution of the heat flux at the tube wall. This is because the quasi-steady state heat flux is uniquely related to the instantaneous interface geometry and that the formulation is based on a much improved analytical approximation for the interface configuration which has been confirmed by comparison with numerical results (see Figure 14). To solve equation (III.3) for the axial temperature distribution, however, one may use either equation (III.12) or (III.14). The latter was used in the present computation. Since the difference in heat flow rate, ΔQ, calculated by these two equations is small compared to the absolute value of Q, no significant error will be introduced by using equation (III.14).

III.2.2 SOLUTION IN THE REGION NEAR THE TUBE WALL

The right hand side of equation (III.3) and also equations (II.8,14) become singular as the interface intersects the tube surface, so an analytical solution has been developed for short times and also for all times in the region

near the tube wall where the interface is in the vicinity of the tube surface.

It is noted that the shape of the interface is nearly symmetric in the vicinity of the tube surface and therefore the energy equation for the fluid in the tube and the moving interface condition can be approximated by

$$\frac{Pe^*}{\bar{\theta}_a}\frac{\partial \bar{\theta}_a}{\partial z} = 2\,\frac{\partial \theta_2(1, z, \bar{t}^*)}{\partial r_t} \qquad \text{(III.16)}$$

and

$$\frac{\partial r_p}{\bar{\theta}_a\,\partial \bar{t}^*} = -\frac{\partial \theta_2(r_p, z, \bar{t}^*)}{\partial r_t} \qquad \text{(III.17)}$$

where the heat flux in region 1 is neglected in approximating the moving interface, equation (III.2). This approximation is valid provided that the interface is much closer to the tube wall than the free surface and consequently the normal temperature gradient outward at the interface will be much smaller than at the tube wall. Defining $S_p = r_p^2$ and substituting $\theta_2 = \ell n(r_t/r_p)/\ell n(1/r_p)$, which follows from the steady state solution, in equations (III.16,17), one obtains:

$$\frac{Pe^*}{\bar{\theta}_a}\frac{\partial \bar{\theta}_a}{\partial z} = -\frac{4}{\ell n\, S_p} \qquad \text{(III.16-a)}$$

and

$$\frac{\partial S_p}{\bar{\theta}_a\,\partial \bar{t}^*} = \frac{4}{\ell n\, S_p} \qquad \text{(III.17-a)}$$

By introducing a new variable $\tau(z,\bar{t}^*) = \int_0^{\bar{t}^*} \bar{\theta}_a(z,\bar{t}^*)\,d\bar{t}^*$, one can show that equation (III.17-a) has a solution of the same

form as that of the Carslaw and Jaeger solution (II.1), and thus that S_p is a function of τ only. Equations (III.16-a,17-a) when combined field:

$$Pe^* \frac{\partial \ln \bar{\theta}_a}{\partial z} = - \frac{dS_p}{d\tau} \qquad \text{(III.18)}$$

Since $dS_p/d\tau = (\partial S_p/\partial z)/(\partial \tau/\partial z)$, where $(\partial \tau/\partial z)$ can be expressed in terms of S_p by using the definition of τ and equations (III.16-a,17-a), one can relate $(\partial \ln \bar{\theta}_a/\partial z)$ and $(\partial S_p/\partial z)$ using equation (III.18). This results in

$$\frac{\partial \ln \bar{\theta}_a}{\partial z} = \frac{\partial S_p}{\partial z} \frac{1}{(S_p - 1)} \qquad \text{(III.19)}$$

which when integrated gives:

$$\frac{\bar{\theta}_a}{S_p - 1} = e^{C(\bar{t}^*)} \qquad \text{(III.19-a)}$$

By applying the inlet boundary condition at $z = 0$, $\bar{\theta}_a = 1$, in the Carslaw and Jaeger solution (II.1), one can show that $C(\bar{t}^*)$ in equation (III.19-a) is given by

$$C(\bar{t}^*) = - \ln [r_{po}^2(\bar{t}^*) - 1] \qquad \text{(III.19-b)}$$

where r_{po} is the radius of the interface at $z = 0$ obtained from the Carslaw and Jaeger solution (II.1). To obtain the radius of the thaw region, one can use the relationship between S_p and z from equations (III.16-a,19),

$$\frac{\partial S_p}{\partial z} = - \frac{4(S_p - 1)}{Pe^* \ln S_p} \qquad \text{(III.20)}$$

Integrating equation (III.20), one obtains:

$$\frac{z}{Pe^*} = - \frac{1}{4} \int_{r_{po}^2}^{r_p^2} \frac{\ln S_p}{S_p - 1} \, dS_p \qquad \text{(III.20-a)}$$

The integral on the right hand side of equation (III.20-a) can be evaluated by using a Taylor expansion of $\ln S_p$ at $S_p = 1$. For early times, equations (III.19-a,20-a) are used to calculate the radius of the interface $r_p(z,\bar{t}^*)$ and the temperature $\bar{\theta}_a(z,\bar{t}^*)$. A similar procedure is employed for all times to treat the tail of the interface in the vicinity of the tube wall. The short time solution just outlined is valid for all times for an infinite axisymmetric geometry which is initially at the phase change temperature. The formulae obtained herein for infinite Biot number cannot be directly derived from the Shamsunder solution [21]. Further details are shown in Appendix D.

III.3 SOLUTION PROCEDURE

The original three-dimensional problem has now been reduced to a one-dimensional finite difference procedure in which equation (III.3) is integrated at each time step after the local two-dimensional solution for equation (III.2) is obtained by using the technique described in chapter II. The procedure for calculation is summarized as follows:

(1) The calculation starts at $z = 0$ where the Carslaw and Jaeger solution (II.1) is applied as if the tube is buried at an infinite depth. At short times, one calculates the radius of the interface circle, $r_{p0} = r_p(0,\bar{t}^*)$, and then uses the approximate analytic solution for the axisymmetric case shown in subsection III.2.2 to obtain $r_p(z,\bar{t}^*)$ and $\bar{\theta}_a(z,\bar{t}^*)$

for $0 < z < z_{max}$ where z_{max} is the position at which the interface intersects the tube wall. Note that z_{max} is a function of time.

(2) Since the axial length is subdivided into finite segments, the two-dimensional solution in Chapter II is applied to the cross-section at each node. If R_{ia}, R'_{ib} and R'_{ob} are known at time $\bar{t}^*$, the new locations of the upper and lower portions of the interface at time $(\bar{t}^* + \Delta\bar{t}^*)$ are determined using equations (II.8,14), respectively. The interface shape thus can be described by r_{ia}, h_{ia} and equation (II.15). The heat flow rate at the tube surface at any position z is evaluated from equation (III.14) or equation (III.15) for the near region. Using a cubic spline to smooth the axial distribution of the heat flow rate, one may readily integrate equation (III.3) to obtain $\bar{\theta}_a(z, \bar{t}^* + \Delta\bar{t}^*)$.

Because of the use of the analytic solution in the region near the tube wall, care should be taken to preserve the continuity of the solution at all matching positions using the three different formulae for the upper and lower regions of the interface and the analytic solution in the z direction, particularly for treating the bottom region of the interface where one needs an independent relation to determine $R'_{ob}(z, \bar{t}^*)$ or $\delta(z, \bar{t}^*)$ at each time step with a numerical procedure as described in Appendix C.

III.4 RESULTS AND DISCUSSION

Figures 19-22 show some typical solutions for two representative sets of input data. The first set is for a shallow burial depth $h_o = 1.5$ and large $\theta_{ao} = 50.49$ to illustrate the strong influence of the free surface. The other set, $h_o = 4.0$ and $\theta_{ao} = 7.09$, is for a medium burial depth where the initial temperature differs significantly from the phase change temperature. These conditions are coincident with the previous two-dimensional problem at the cross-section z = 0. The dimensionless length of the tube is 0.8 for both cases. The penetration of the top and bottom points of the thaw region, $d'_{ia} = h_o - (h_{ia} - r_{ia})$ and $d'_{ib} = (h_{ib} + r_{ib}) - h_o$, as a function of axial distance and time is shown in Figures 19(a,b). In Figure 19(b), the thaw depth varies almost linearly with distance along the tube axis even after three years because of the quite deep burial depth and moderate dimensionless temperature of the fluid at the inlet of the tube. In contrast, the top and particularly the bottom of the cylindrical thaw region are obviously curved in the r_t-z plane for the first case where the influence of the free surface is important (Figure 19(a)). The interface location after 15 years is still very far from the final steady state solution since much of the heat is removed at the free surface. The asymmetry in the heat flux from the top and bottom of the tube is shown in Figures 20(a,b), where q_c and q_d determined by equations (III.5,10) denote the instantaneous heat fluxes through the top-most and bottom-most points. Since more heat leaves through the free surface in case 1,

where $q_c \sim 5q_d$, the thaw depth decreases more rapidly in the axial direction due to the shallower burial depth. This can also be observed from the variation of the fluid temperature in Figure 21(a) where the dimensionless temperature of the fluid at outlet is as low as zero for 0.05 years and less than 0.05 even after 10 years. This phenomenon is much more moderate for the deeper burial depth as seen in Figures 20(b) and 21(b). The entire thaw volume, however, not only depends on the burial depth but also on the dimensionless entrance temperature of the fluid, θ_{ao}. Figures 22(a,b) show the change in cross-sectional shape of the thaw cylinder along the axis of the tube. As might be anticipated, the departure of the interface profile from the circular shape is most apparent at the inlet of the tube and then gradually diminishes as one proceeds downwards. Also, it might be interesting for engineers to note that in the symmetry plane shown in Figures 22(a,b), the top of the thaw cylinder appears as a concave curve whereas it is convex for the bottom with respect to an observer at the tube surface.

The three-dimensional solutions presented herein expose one very important aspect which the two-dimensional studies have not been concerned with. In those studies, the tube wall temperature is assumed constant and the approach to the steady state equilibrium is uncoupled from the fluid in the tube. It is evident from Figures 20 and 21, that this steady equilibration time is actually controlled by the fluid interaction with the PCM and that the time required for the

fluid in the tube to achieve equilibrium can be large. It is nonrealistic to simply replace the wall temperature by a constant as assumed in the equivalent two-dimensional problem since the tube wall temperature itself can be far from the equilibrium value. This effect is more pronounced for the shallower burial depth since the more heat lost from the free surface the more slowly the fluid temperature approaches equilibrium. The important consequences are also shown in the local heat flux and isotherms. Therefore, the long time required for the isotherms and thaw boundary above the tube to achieve equilibrium is not a reflection of the conduction process in this region but of the much slower variation in tube wall temperature. In both cases (Figures 20(a,b)), q_c quickly approaches an initial equilibrium value after approximately 0.3 years and then slowly varies on a much larger time scale which is controlled by the fluid-PCM interaction in the lower portion of the tube. This situation is also reflected in the variation of the fluid temperature (Figures 21(a,b)). Existing two-dimensional models, which neglect the flow, can thus lead to a very misleading estimation of the motion of the interface, especially above the tube surface.

REMARKS

All calculations were performed on an IBM 4341 computer. The computational time required to predict the three-dimen-

sional interface location up to 10 years is of the order of several minutes. It is unfortunate that there are neither theoretical nor experimental results for comparison. The solution techniques in chapters II,III are developed for the case where freezing or melting starts at the tube wall and moves outward in a closed surface. This type of problem is generated from the gas or oil pipes buried in permafrost regions, where the fluid in the pipe is at temperatures well above the melting temperature of the ground, and solar energy storage systems using phase change material. In the next chapter, we will consider another aspect of the problem where the interface has a distinctly different behavior although the geometry of the system remains unchanged.

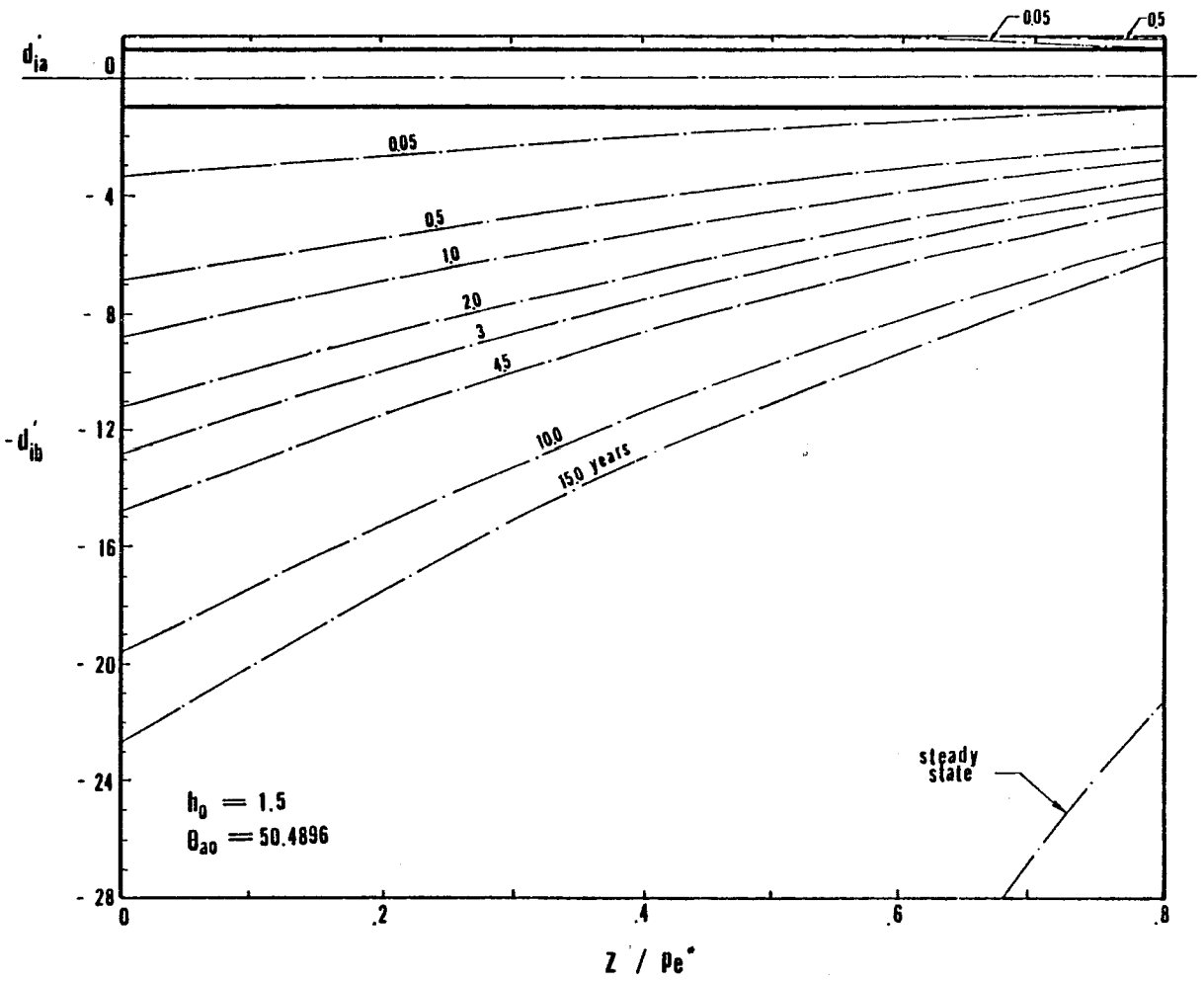

FIGURE 19(a). AXIAL VARIATION OF THAW DEPTH PENETRATION ABOVE AND BELOW TUBE CENTER FOR $\theta_{a0} = 50.49$, $h_o = 1.5$

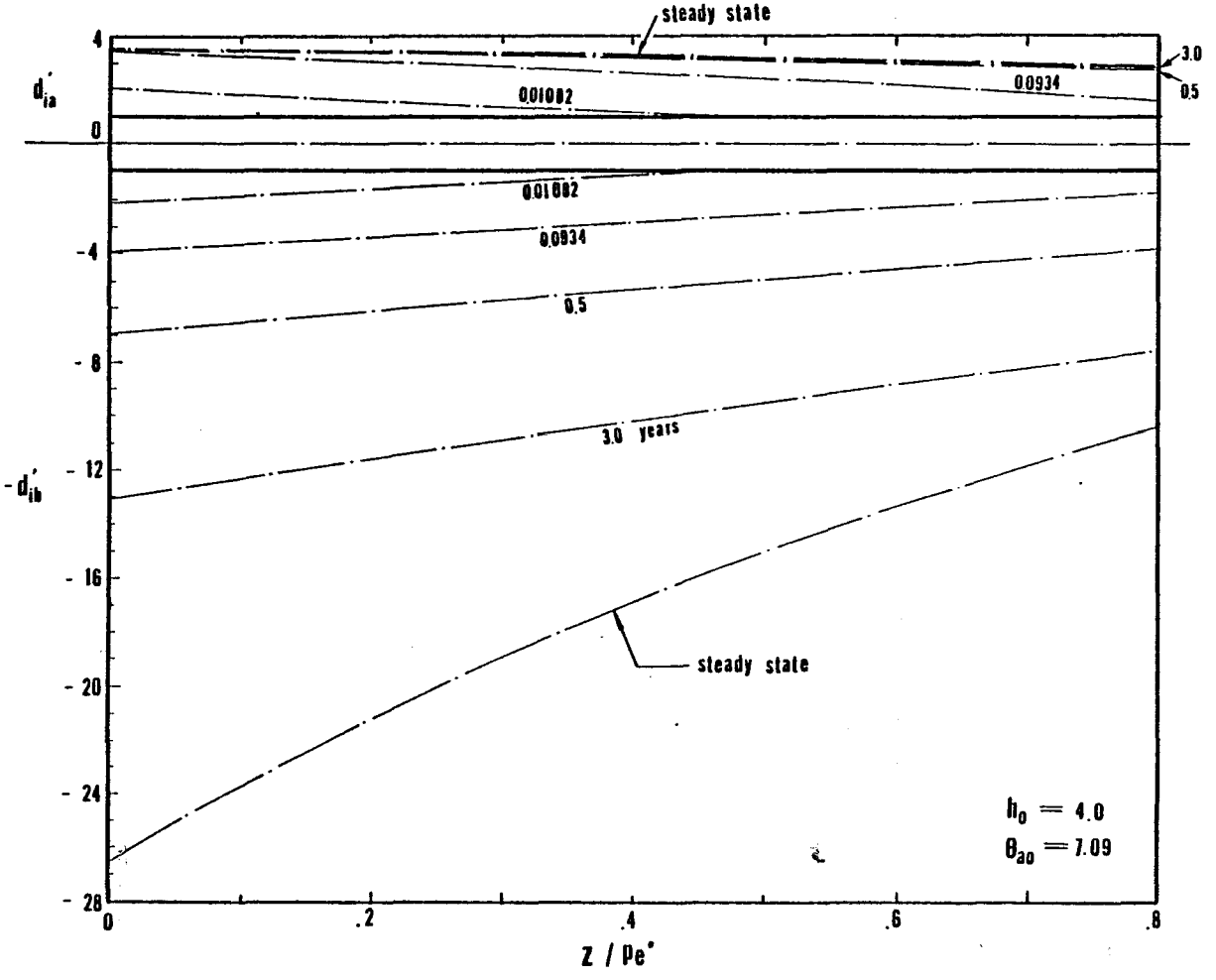

FIGURE 19(b). AXIAL VARIATION OF THAW DEPTH PENETRATION ABOVE AND BELOW TUBE CENTER FOR $\theta_{a0} = 7.09$, $h_0 = 4.0$

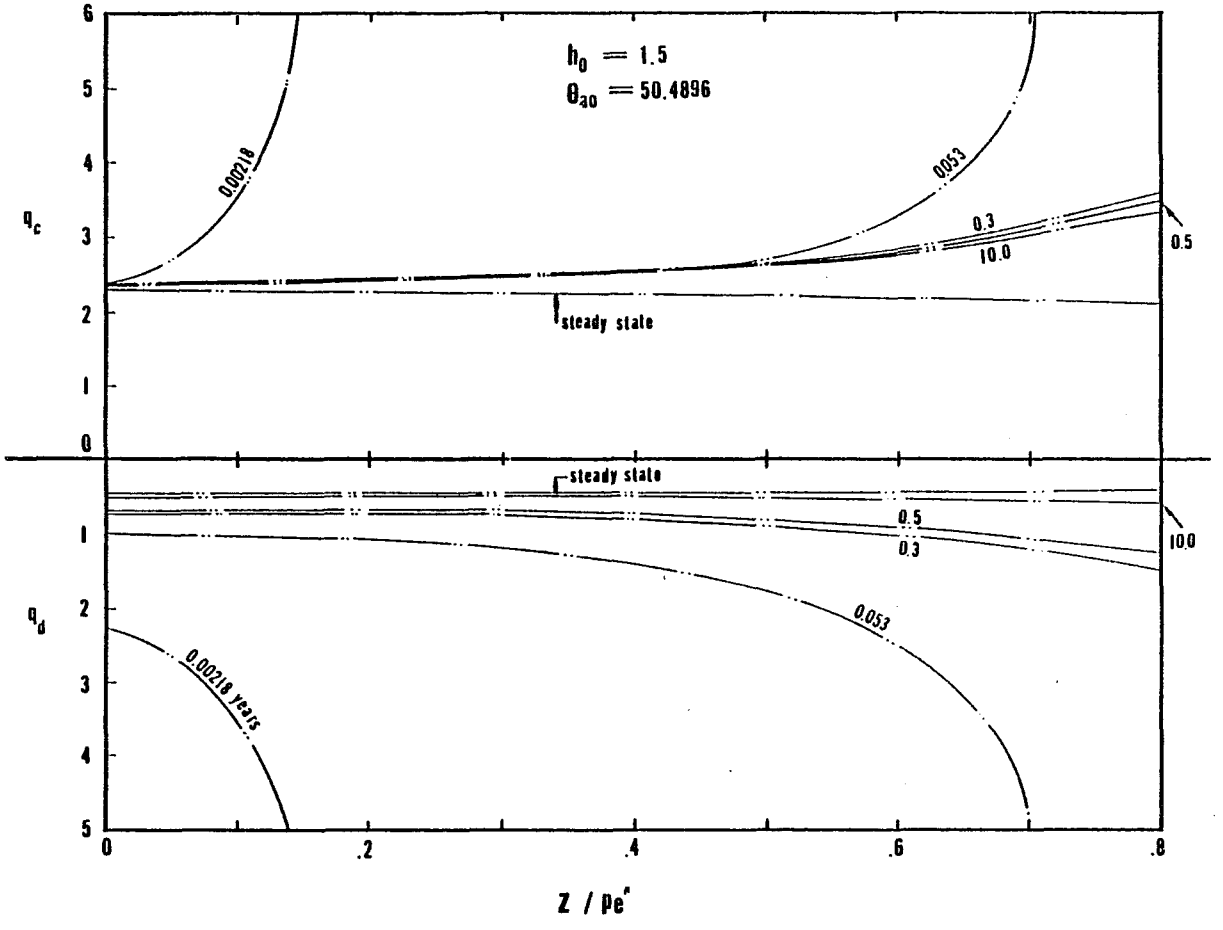

FIGURE 20(a). AXIAL VARIATION OF HEAT FLUX AT TOP AND BOTTOM POINTS OF TUBE SURFACE FOR $\theta_{a0} = 50.49$, $h_o = 1.5$

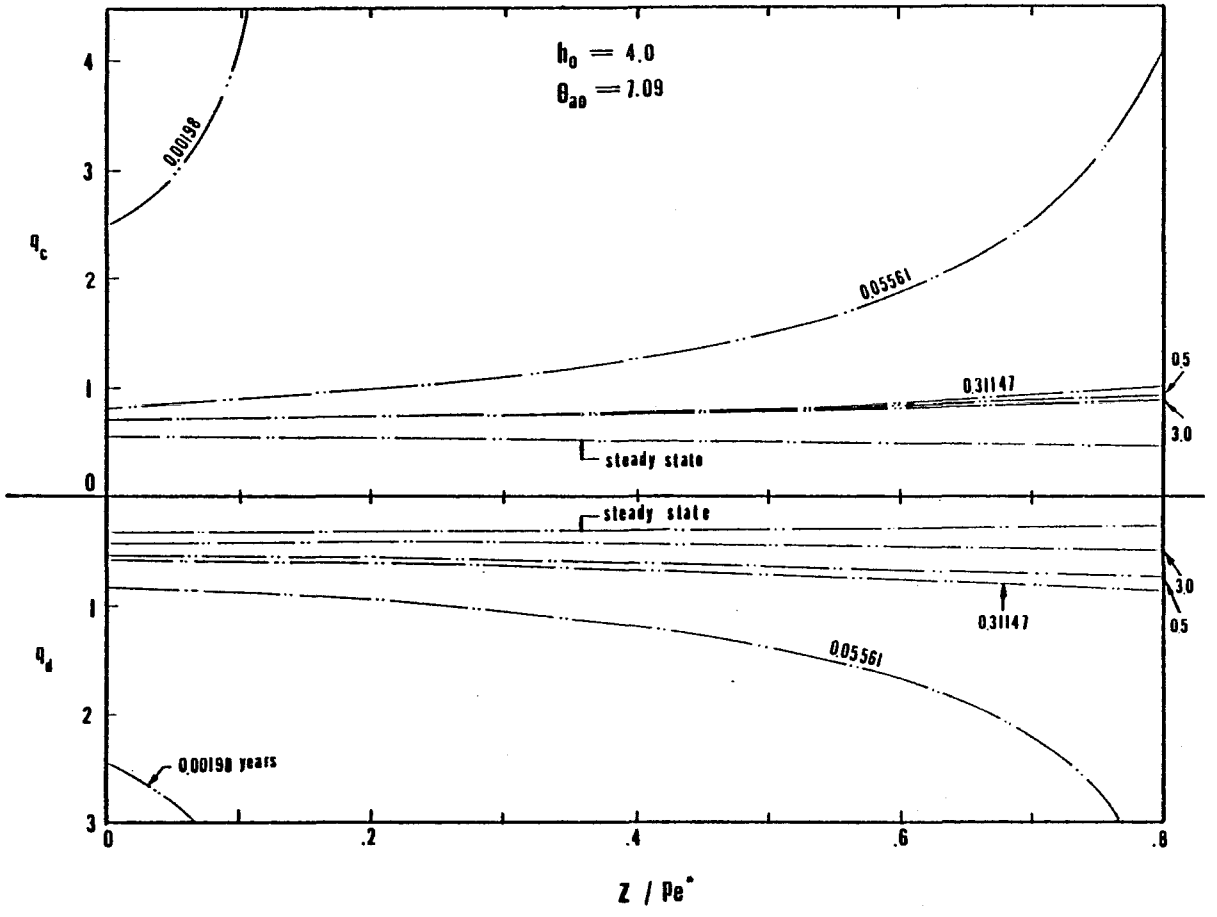

FIGURE 20(b). AXIAL VARIATION OF HEAT FLUX AT TOP AND BOTTOM POINTS OF TUBE SURFACE FOR $\theta_{ao} = 7.09$, $h_o = 4.0$

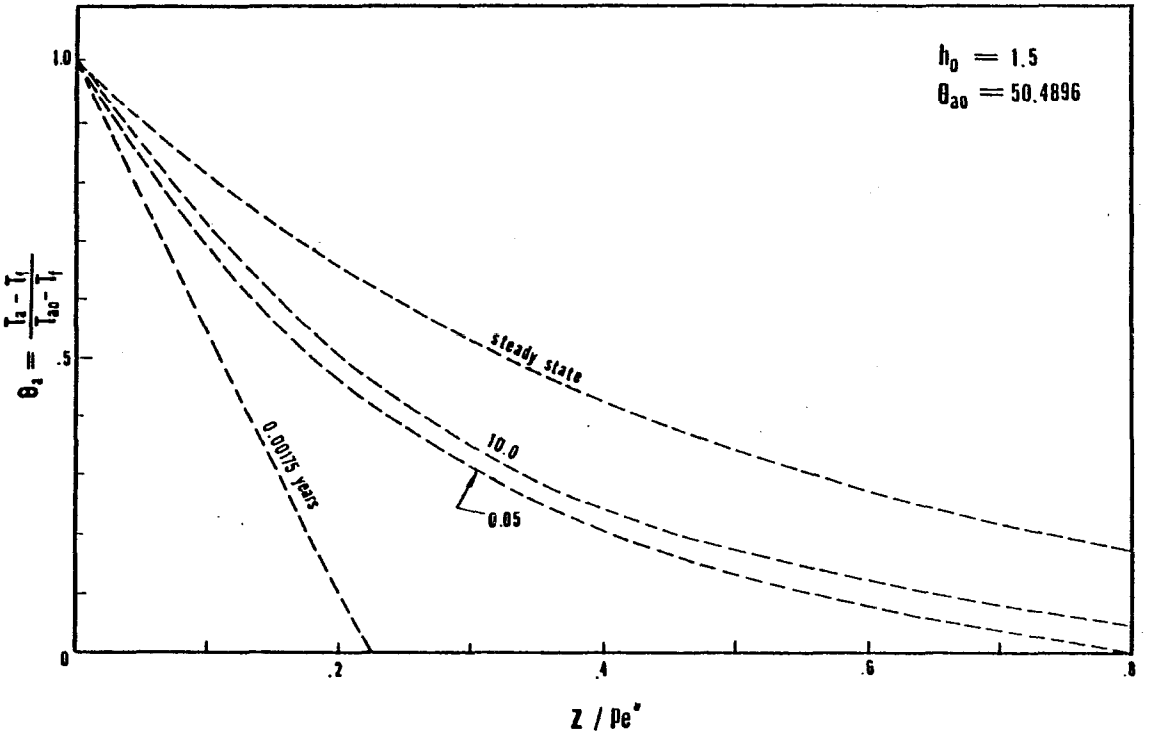

FIGURE 21(a). FLUID AXIAL TEMPERATURE DISTRIBUTION FOR θ_{ao} = 50.49, h_o = 1.5

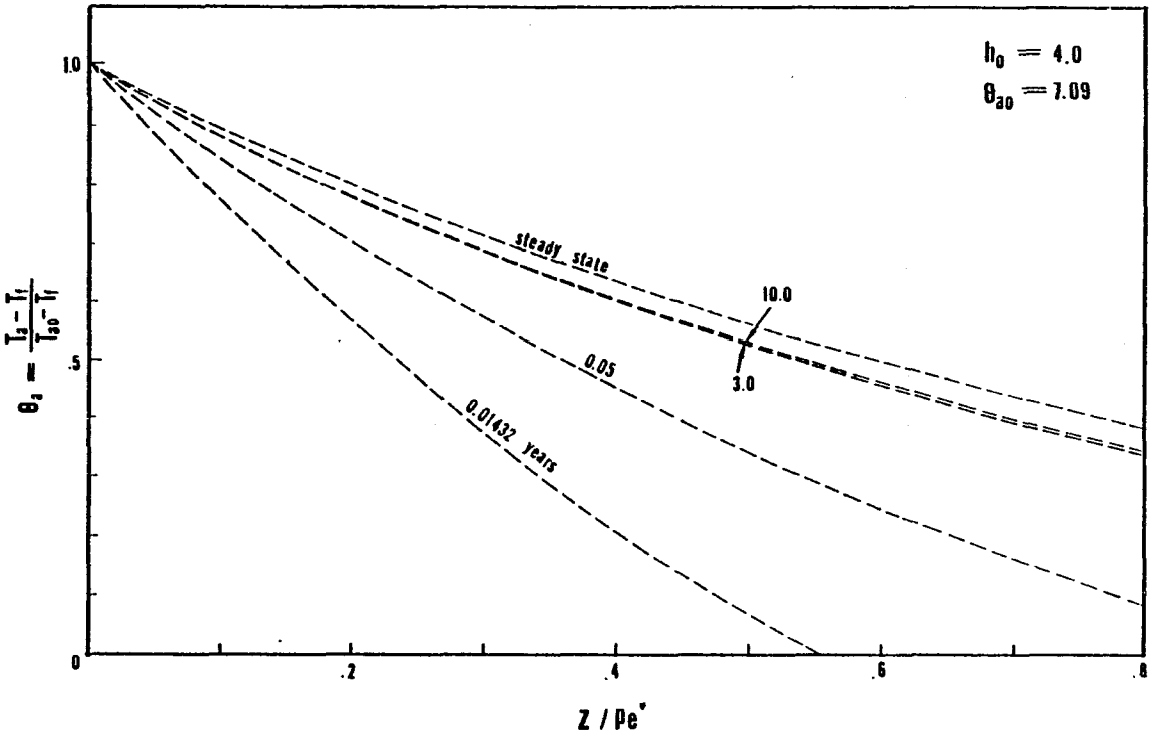

FIGURE 21(b). FLUID AXIAL TEMPERATURE DISTRIBUTION FOR $\theta_{a0} = 7.09$, $h_o = 4.0$

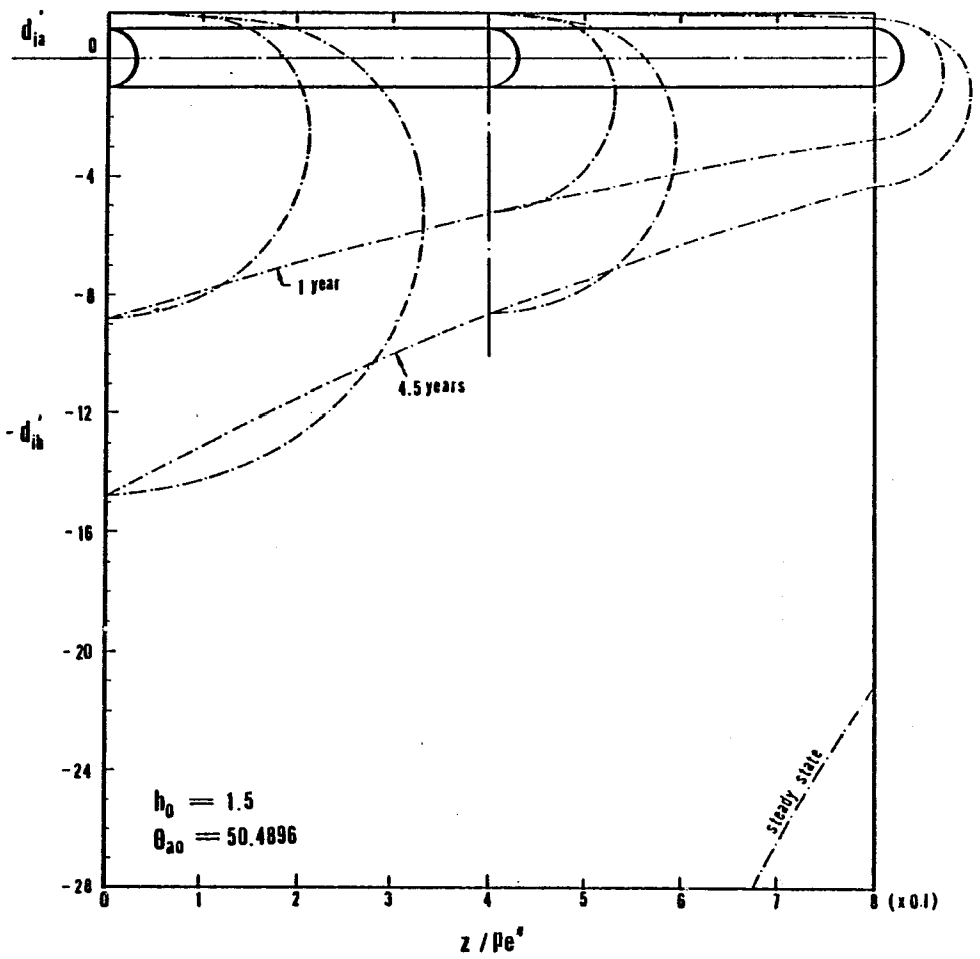

FIGURE 22(a). INTERFACE PROFILE FOR $\theta_{a0} = 50.49$, $h_o = 1.5$

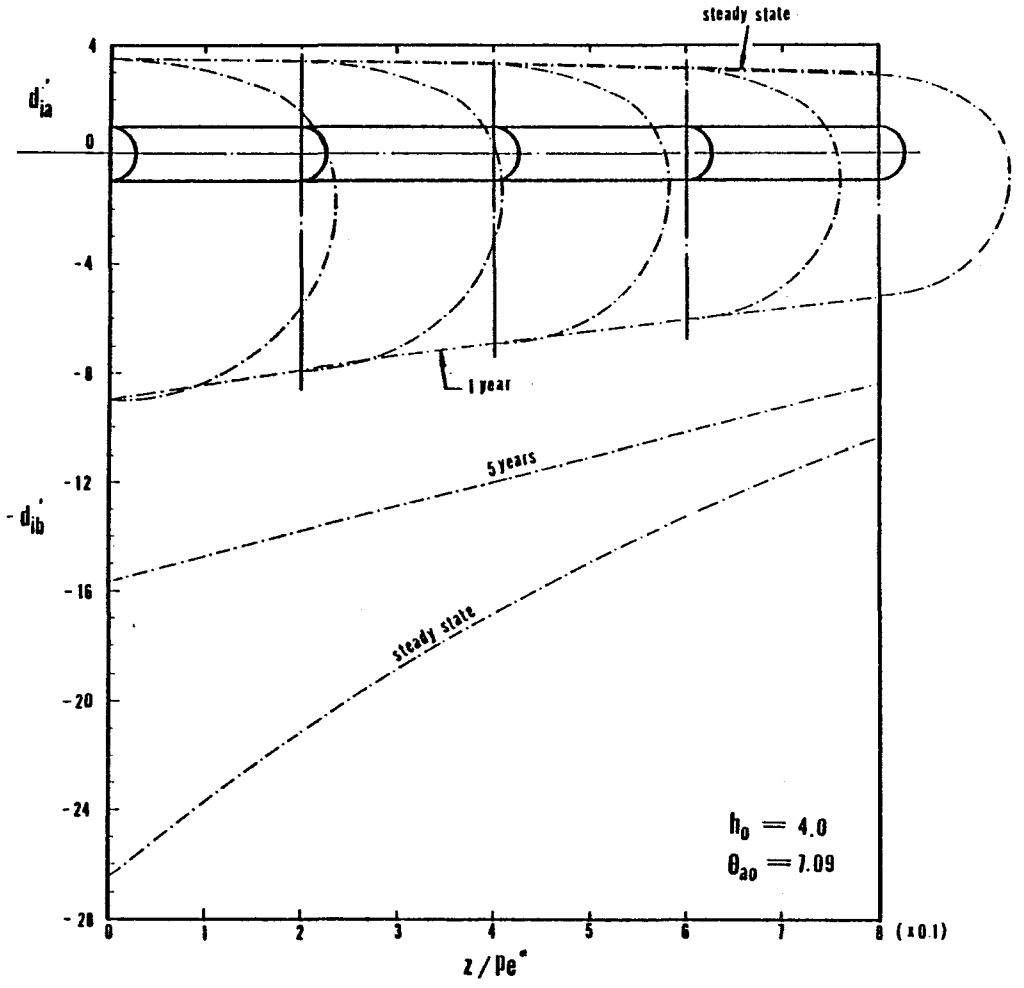

FIGURE 22(b). INTERFACE PROFILE FOR $\theta_{a0} = 7.09$, $h_o = 4.0$

CHAPTER IV

THE TWO-DIMENSIONAL SOLUTION
FOR
PHASE CHANGE COMMENCING AT THE FREE SURFACE

The transient problem with the same geometry as in chapters II,III may occur in another manner, such as in cryosurgery where the freezing front is initiated at the surface of the skin and penetrates into the tissue under the thermal effects of the blood carried in large superficial veins. In this case, a plane interface commences at the free surface and moves downward into the PCM. Freezing of soil around buried water pipes during winter frost is another example of this situation. The distincly different features of this interface behavior require a new solution approach for the problems treated in this chapter.

The coordinate system used herein (Figure 23) is the same as the two-dimensional problem in chapter II. The important difference in the present problem is that the temperature of the PCM is initially at a constant value T_a and a planar freezing front is generated at the free surface. Because of the complexity of the transient interface shapes expected in the present problem, a numerical solution technique is used.

No previous studies pertaining to this problem have been found in the literature. It will be shown that because of the unbounded solution domain, the behavior of the interface and temperature fields in the far region becomes an important aspect of the solution in the present problem.

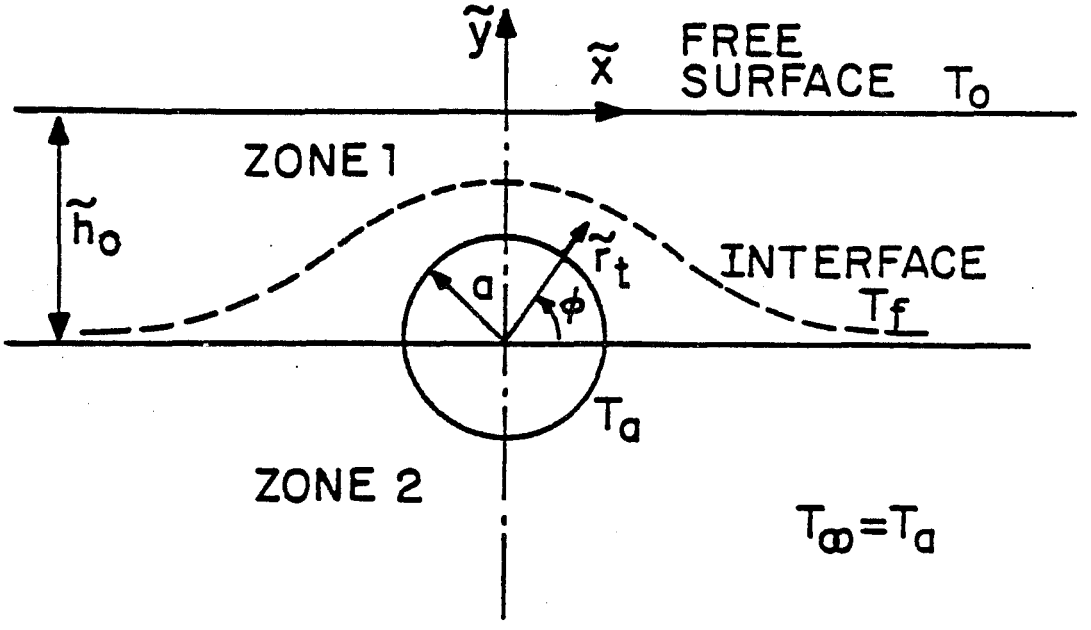

FIGURE 23. CONFIGURATION AND COORDINATE SYSTEM FOR FREEZING COMMENCING AT THE FREE SURFACE

IV.1 ONE-DIMENSIONAL SOLUTIONS

Since the influence of the tube is negligible in the region far from the symmetry line (see Figure 23), it is useful to first review two well-known one-dimensional solutions, the Neumann and the Stefan solutions. As mentioned in the Introduction, the exact solution attributed to Neumann was in terms of a similarity transformation, $\zeta = y/(4\bar{\alpha}_1 t)^{1/2}$, [4] where the penetration depth of the phase front is given by

$$Y_{iN} = 2\lambda\sqrt{\bar{\alpha}_1 t} \qquad \text{(IV.1)}$$

Here, $\bar{\alpha}_1$ is the thermal diffusivity of the frozen region and λ is a constant which satisfies:

$$\frac{e^{-\lambda^2}}{erf\,\lambda} - \theta_a\sqrt{\frac{\bar{\alpha}_1}{\bar{\alpha}_2}}\;\frac{e^{-(\bar{\alpha}_1/\bar{\alpha}_2)\lambda^2}}{erfc\,\sqrt{\bar{\alpha}_1/\bar{\alpha}_2}\,\lambda} = \frac{\pi}{St_1}\lambda \,, \qquad \text{(IV.1-a)}$$

where $\theta_a = K_2(T_a - T_f)/K_1(T_f - T_o)$ is the dimensionless temperature as defined previously. The Stefan number here is given by $St_1 = C_1(T_f - T_o)/L$, which is different from the previous definition, $St_2 = C_2(T_a - T_f)/L$, for freezing starting at the tube surface. For a given PCM, λ is a function of both St_1 and θ_a.

The same problem was solved by Stefan using the quasi-steady approximation when the PCM is initially at the freezing temperature, T_f [4]. The approximate solution for the phase change depth is given by

$$Y_{iS} = \sqrt{2\,St_1\,\bar{\alpha}_1 t} \qquad \text{(IV.2)}$$

Note y_{iN} and y_{is} are dimensional distances. Compared with the exact solution (IV.1), equation (IV.2) is limited to the $St_1 << 1$ and $\theta_a = 0$ and is not a good approximation, even for small Stefan number, when the dimensionless initial temperature θ_a is not sufficiently small. Note that the case $T_a = T_f$ is actually of no interest for the present problem. By combining equations (IV.1,2), one may calculate the relative error of the Stefan solution by

$$\Delta y_i = \frac{\Delta y_i}{y_{iN}} = \frac{y_{is} - y_{iN}}{y_{iN}} = \sqrt{\frac{St_1}{2}} \Big/ \lambda - 1 \qquad \text{(IV.3)}$$

The value of $\overline{\Delta y_i}$ for water for different θ_a and St_1 is given in Table 1. It is noted that the error $\overline{\Delta y_i}$ always increases as θ_a increases. At large θ_a, the error could be large even if the Stefan number is small. For instance, when $\theta_a = 2$ and $St_1 = 0.02$, $\overline{\Delta y_i}$ approaches 50% as seen in the Table. For other phase change materials, such as soil or biological tissue, the smaller the water content the larger the difference $\overline{\Delta y_i}$ if θ_a remains the same. This is because the specific heats for mineral and organic solids are all about the same as that of ice (~ 0.5 cal/g°C) and that the decrease of water content leads to a smaller effective latent heat and thus larger Stefan number.

The two solutions shown here will be used in subsection IV.7 as part of the solutions for the full two-dimensional problem.

TABLE 1. VALUES OF λ, $\overline{\Delta y_i}$, $\overline{\Delta \ell_c}$ FOR SELECTED St_1 AND θ_a

PCM: WATER $\overline{\alpha_1} = 0.0115$, $\overline{\alpha_2} = 0.00144$

	θ_a	λ	$\overline{\Delta y_i}$	$\overline{\Delta \ell_c}$
$St_1 = .01$	.0	.0706	.0017	-.0017
	.2	.0687	.0296	-.0288
	.4	.0668	.0580	-.0548
	.6	.0651	.0868	-.0799
	.8	.0634	.1161	-.1041
	1.0	.0617	.1458	-.1273
	2.0	.0544	.3006	-.2311
	3.0	.0483	.4649	-.3173
	θ_a	λ	$\overline{\Delta y_i}$	$\overline{\Delta \ell_c}$
$St_1 = .02$	.0	.0997	.0033	-.0033
	.2	.0956	.0462	-.0441
	.4	.0918	.0898	-.0824
	.6	.0882	.1343	-.1184
	.8	.0848	.1795	-.1522
	1.0	.0816	.2255	-.1840
	2.0	.0682	.4655	-.3176
	θ_a	λ	$\overline{\Delta y_i}$	$\overline{\Delta \ell_c}$
$St_1 = .04$	.0	.1405	.0066	-.0066
	.2	.1317	.0739	-.0688
	.4	.1238	.1425	-.1247
	.6	.1167	.2123	-.1751
	.8	.1102	.2832	-.2207
	1.0	.1044	.3552	-.2621

	θ_a	λ	$\overline{\Delta y_i}$	$\overline{\Delta \ell_c}$
$St_1 = .06$	.0	.1715	.0099	-.0098
	.2	.1577	.0986	-.0898
	.4	.1457	.1887	-.1588
	.6	.1353	.2802	-.2188
	.8	.1262	.3728	-.2716
	1.0	.1181	.4666	-.3182
	θ_a	λ	Δy_i	$\Delta \ell_c$
$St_1 = .08$	.0	.1974	.0131	-.0129
	.2	.1783	.1217	-.1085
	.4	.1624	.2314	-.1879
	.6	.1490	.3423	-.2550
	.8	.1375	.4543	-.3124
	θ_a	λ	$\overline{\Delta y_i}$	$\overline{\Delta \ell_c}$
$St_1 = .1$	.0	.2200	.0163	-.0161
	.2	.1955	.1436	-.1256
	.4	.1758	.2716	-.2136
	.6	.1597	.4004	-.2859

IV.2 BOUNDARY INTEGRAL METHOD

A boundary integral method is applied for determining the instantaneous position of the interface. The conceptual development of the method derives from classical Green's function and potential theory [23]. The prominent feature of the method is that one is able to reduce the calculation domain by one dimension. This should lead to a significantly more efficient numerical calculation. In contrast to the boundary immobilization technique, in which the nonlinearity is also introduced into the governing equations for each phase, to obtain a constant coordinate interface boundary, the boundary integral method allows one to directly determine either the unknown temperatures or the heat fluxes at the boundaries without requiring a solution for the temperature field. For many boundary value problems where the details of solution away from the boundaries are of little interest, the advantage of this technique is apparent, especially when a moving boundary is involved.

According to potential theory, Green's formula of the second kind can be applied to evaluate a potential function along the boundaries in the form of the boundary integral:

$$\theta(x,y)_{|s} = \frac{1}{2\pi}\oint_S \left[\theta(x,y,\xi,\eta)\frac{\partial U(x,y,\xi,\eta)}{\partial n} - U(x,y,\xi,\eta)\frac{\partial \theta(x,y,\xi,\eta)}{\partial n}\right] ds \qquad \text{(VI.4)}$$

where θ is a harmonic function in domain Ω which is surrounded by its closed boundary S; and ξ,η are both dummy variables. In equation (IV.4), n is the normal coordinate

on the boundaries. Point (x,y) is fixed on S while the integration is carried out as point (ξ,η) moves along the closed boundary. The function $U(x,y,\xi,\eta)$ is the fundamental singular solution given by

$$U(x,y,\xi,\eta) = \ln\left[(x-\xi)^2+(y-\eta)^2\right] \quad \text{(IV.5)}$$

Equation (IV.4) is the Fredholm equation of either the first kind or The second kind depending on whether θ or $\partial\theta/\partial n$ is unknown.

From equation (IV.4), one can see that this method is particularly convenient for the present problem since the unknown temperature field has an unknown discontinuity in the normal derivative along the phase interface, whereas the temperature itself is known to be T_f. In association with the boundary collocation technique, in which a trial solution is fitted at selected points along the boundaries, the method is capable of determining the unknown and highly irregular shape of the phase front. The technique is especially suited for time dependent problems in which the governing field equations are linear and only the moving interface condition is nonlinear.

IV.3 FLOATING BOTTOM TECHNIQUE

Because the solution domain extends to infinity, two artificial boundaries, the right edge and the bottom, are introduced. These boundaries, together with the free surface

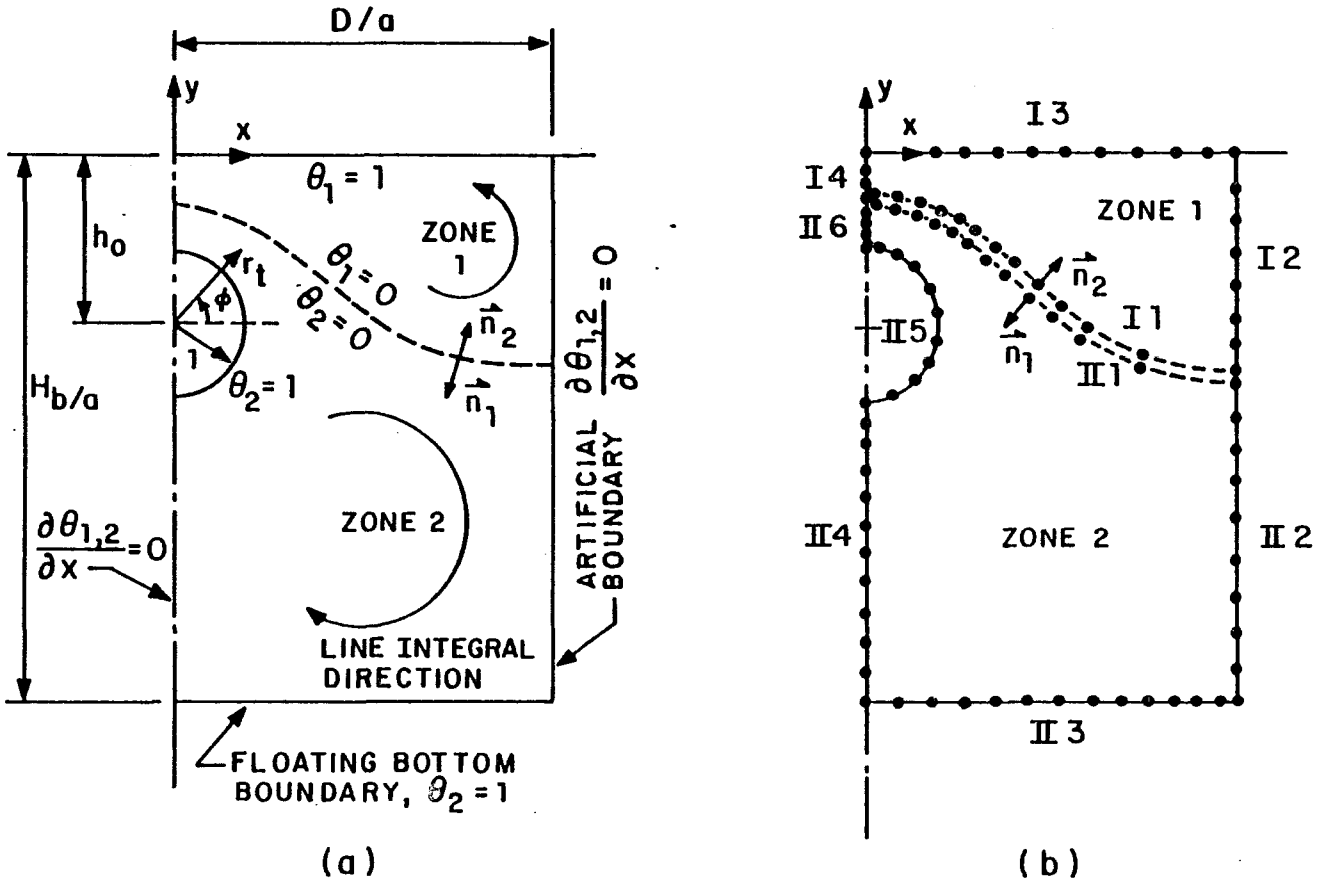

FIGURE 24. SCHEMATIC DIAGRAM SHOWING (a) ARTIFICIAL DOMAINS FOR LINE INTEGRAL (VI.4), AND (b) NODE DISTRIBUTION IN BOUNDARY ELEMENT METHOD

and symmetry axis, form a confined domain (Figure 24(a)). The right edge is set at a position far enough from the tube where the temperature field is nearly one-dimensional and an adiabatic condition can be applied with good approximation along this boundary. On the other hand, the movable bottom boundary is assumed to have a constant temperature, the same as the initial temperature of the PCM. This so-called floating bottom technique is used to take into account the sensible heat in both frozen and thawed zones, which is neglected in the quasi-steady approximation. The instantaneous position of the bottom boundary is determined by neglecting the presence of the tube and equating the heat flux difference across the interface to the Neumann exact solution (IV.1). Using a quasi-steady one-dimensional approximation, a simple algebraic derivation (Appendix E) leads to the following formula for the depth of the bottom boundary,

$$H_b(t) = \left[1 + \theta_a \Big/ \left(1 + \frac{2\lambda^2}{St_1} \right) \right] y_{iN} \qquad \text{(IV.6)}$$

where $y_{iN} = 2\lambda(\bar{\alpha}_1 t)^{1/2}$ is the Neumann solution and λ is a constant determined by equation (IV.1a). By an artificial compensation of the sensible heat, the floating bottom boundary gives the present quasi-steady approximate solution a high accuracy in the far region (as good as the Neumann solution). On the other hand, in the area near the symmetry line between the tube and free surface, the temperature field is dominated by the surface temperatures and is hardly influenced by the artificial bottom boundary. By virtue of

this technique, the approximation may no longer be limited to small Stefan number, even though the primary formulation is based on the quasi-steady assumptions.

As mentioned earlier, the idea of the effective latent heat [4] is commonly used to account for the sensible heat in the quasi-steady approximation. Instead of the real value of the latent heat, a larger value is used which is determined by comparison with exact solutions in simple geometries. For most practical problems, it is difficult to determine an effective latent heat for other than a one-dimensional geometry. In the present problem, the use of the effective latent heat would improve the accuracy of the solution for early times, but for large times, its effects are hard to predict owing to the complex interface geometry. Instead of using an effective latent heat in the energy equation at the interface, the floating bottom technique is applied to the line integration to determine the heat flux at the interface. The advantages are : (i) The behavior of the interface in the far region agrees exactly with Neumann's solution. (ii) In the region near the central line $\phi = \pi/2$ between the tube and planar surfaces, the bottom boundary has almost no influence. Since the heat conduction in front of the interface is significantly larger than that in the far region, the interface moves much more slowly. Therefore, the temperature fields are dominated by the free surface and tube temperatures and are well described by the quasi-steady approximation. In fact, in this region, the

much shorter time for the interface to approach the steady state position greatly reduces the effects of the sensible heat on the entire interface geometry. (iii) In the intermediate region between the two extreme cases, the effects of the bottom boundary vary gradually depending on the distances of the interface to the tube and the bottom boundary. This is reflected in the contour integral (IV.4).

IV.4 FORMULATION

The frozen and thaw zones are described by the same dimensionless temperatures, θ_1 and θ_2, and governed by the same equations as in Chapter I except for the boundary conditions, which are:

$$\theta_1(X, 0, t^{**}) = 1 , \tag{IV.7}$$

$$\frac{\partial\theta_1(0, Y, t^{**})}{\partial X} = \frac{\partial\theta_1(D, Y, t^{**})}{\partial X} = 0 , \tag{IV.8}$$

$$\theta_1(X, Y_i) = \theta_2(X, Y_i) = 0 . \tag{IV.9}$$

$$\theta_2(X, -H_b) = 1 , \tag{IV.10}$$

$$\frac{\partial\theta_2(0, Y, t^{**})}{\partial X} = \frac{\partial\theta_2(D, Y, t^{**})}{\partial X} = 0 , \tag{IV.11}$$

$$\theta_2(1, \Phi, t^{**}) = 1 \tag{IV.12}$$

and

$$\frac{\partial \theta_1(x, y_i, t^{**})}{\partial n_1} - \theta_a \frac{\partial \theta_2(x, y_i, t^{**})}{\partial n_2} = \frac{dn_1}{dt^{**}} \qquad \text{(IV.13)}$$

where y_i, a function of x and t**, describes the interface position and $n_{1,2}$ are the normal coordinates at the interface, which have been made dimensionless using the tube radius. Note that vectors $\vec{n}_1$ and $\vec{n}_2$ point outward from regions 1 and 2, respectively (Figure 24(a)), and t** in equation (IV.13) is a new dimensionless time, $t^{**} = K_1 (T_f - T_0) t / \rho L a^2$, for freezing starting at the free surface. Following the definition of t* in equation (I.1), one can define $t^{**} = t/t_{c1}$ where $t_{c1} = a^2/\bar{\alpha}_1 St_1$ is the characteristic time and $St_1 = C_1 (T_f - T_0)/L$ is the Stefan number. The difference in the definitions of the two characteristic times represents the difference in the phase change processes. Equation (IV.13) describes the motion of the interface with the initial condition written as

$$y_i(x, 0) = 0 \qquad \text{(IV.13-a)}$$

Substituting the fundamental singularity solution (IV.5) and boundary conditions (IV.7-12) into equation (IV.4) for regions 1 and 2, respectively, one obtains the following two boundary integral equations:

$$\begin{aligned} 2\pi \theta_1(x, y)_{|s} &= \oint \left[\theta_1 \frac{\partial U}{\partial n_1} - U \frac{\partial \theta_1}{\partial n_1} \right] dS \\ &= -\int_{S_i} U \frac{\partial \theta_1}{\partial n_1} dS + \int_{y_i(0, t^{**})}^{0} \theta_1 \frac{\partial U}{\partial \xi} d\eta \\ &\quad - \int_0^0 \left(\frac{\partial U}{\partial \eta} - U \frac{\partial \theta_1}{\partial \eta} \right) d\xi + \int_0^{y_i(0, t^{**})} \theta_1 \frac{\partial U}{\partial \xi} d\eta \end{aligned} \qquad \text{(IV.14)}$$

and

$$2\pi\theta_2(x,y)_{|S} = \oint \left[\theta_2 \frac{\partial U}{\partial n_2} - U \frac{\partial \theta_2}{\partial n_2}\right] dS$$

$$= -\int_{S_i} U \frac{\partial \theta_2}{\partial n_2} dS - \int_{Y_i(0,t^{**})}^{-H_b} \theta_2 \frac{\partial U}{\partial \xi} d\eta - \int_{\beta}^{0} \left(\frac{\partial U}{\partial \eta} - U \frac{\partial \theta_2}{\partial \eta}\right) d\xi$$

$$- \int_{-H_b}^{-h_0-1} \theta_2 \frac{\partial U}{\partial \xi} d\eta - \int_{-\frac{\pi}{2}}^{\frac{\pi}{2}} \left(\frac{\partial U}{\partial r_t} - U \frac{\partial \theta_2}{\partial r_t}\right) d\phi$$

$$- \int_{-h_0+1}^{Y_i(0,t^{**})} \theta_2 \frac{\partial U}{\partial \xi} d\eta \qquad \text{(IV.15)}$$

Equations (IV.14,15) represent unique solutions for θ_1 and θ_2 on the boundaries in terms of either the unknown dimensionless temperature, θ, or the unknown normal derivative, $d\theta/dn$, along each boundary. These equations can be solved using the boundary element technigue by subdividing the boundaries into small line elements, along each of which the unknown function assumes some average value to be determined. The integral equations (IV.14,15) are consequently expressed as the finite summations of unknown values which can be written as

$$2\pi(\theta_1)_j = \sum_{k=1}^{N_1} \left[I_{A_{jk}} (\theta_1)_k + I_{B_{jk}} \left(\frac{\partial \theta_1}{\partial n_1}\right)_k \right], \quad (j = 1,2 \ldots N_1) \qquad \text{(IV.16)}$$

and

$$2\pi(\theta_2)_j = \sum_{k=1}^{N_2} \left[A_{jk} (\theta_2)_k + B_{jk} \left(\frac{\partial \theta_2}{\partial n_2}\right)_k \right], \quad (j = 1,2 \ldots N_2) \qquad \text{(IV.17)}$$

where subscript k denotes the kth element on the boundaries, j represents the center of the jth element, and N_1 and N_2

are the number of boundary elements of regions 1 and 2, respectively. The coefficients A^{I}_{jk}, A^{II}_{jk}, B^{I}_{jk} and B^{II}_{jk} are all constants evaluated from the integral on the right hand side of equation (IV.4) along the kth boundary element. The superscripts I and II denote the regions 1 and 2, respectively. Since the elements are all line segments, the integration along each element can be carried out analytically. The derivation of equations (IV.16,17) and the formulae for A_{jk} and B_{jk} are given in Appendix F. Equations (IV.16) and (IV.17) are two sets of linear algebraic equations and can be solved for the N_1 and N_2 unknown $(\theta)_j$ and $(\partial\theta/\partial n)_j$ on the boundaries of each region.

Note that the dimensionless formulation merely provides convenience for programming and the final solution must be dimensional anyway since the instantaneous depth of the floating bottom boundary (IV.6) is related to the Neumann solution which has no characteristic length.

IV.5 NUMERICAL PROCEDURE

The width of the calculation domain, D, is taken to be 15 times the tube radius. For larger times, it is extended to 20 tube-radii. The depth of the floating bottom boundary is given by condition (IV.6) except for early times when the position is set at a small distance below the bottom-most point of the tube. For early times, the motion of the interface is controlled by the free surface temperature and thus

the depth of the bottom boundary has little effect on the solution. The number of elements along boundaries I1, I2, I3 and I4 of region 1 is chosen to be 30, 5, 20 and 10 respectively, whereas for region 2 the numbers are 30, 20, 20, 20, 20 and 10 corresponding to boundaries II1, II2, II3, II4, II5 and II6 (Figure 24(b)). Equal length for the elements along each boundary, except the interface boundary, is automatically guaranteed by the program as the floating bottom boundary and phase surface progress downward. Along the interface, the nodes are arranged to be relatively dense near the tube.

The numerical calculation includes the following major steps:

(1) Since the behavior of the interface is primarily controlled by the free surface at early times, the Neumann solution is used as the starting step.

(2) Equation (IV.6) is used to determine the position of the bottom boundary for a given time t.

(3) Equations (IV.16,17) are used to find the gradients $\partial\theta_1/\partial n_1$ and $\partial\theta_2/\partial n_2$, at the selected nodes on the interface in terms of the interface location at time t determined from the previous time step. This implies that the temperature fields are assumed to be quasi-stationary.

(4) Equation (IV.13) is invoked to determine the interface location after a small time interval Δt while the temperature fields and the bottom boundary are temporarily

held fixed.

(5) A smooth interface is obtained by connecting the new node points with cubic spline curves.

IV.6 RESULTS

Table 2 presents two sets of parameters which were used to perform the numerical calculations. Some additional calculated items are also given for reference. Both cases have the same tube radius and burial depth.

The interface shapes are plotted at selected times in Figures 25(a,b) and the Neumann solution is tabulated for comparison with the solutions in the far region. The results are in a very good agreement with the Neumann solution for each case at the right edge of the finite domain as long as the interface is perpendicular to the artificial boundary. A slight difference at very early times is due to the initial position of the floating bottom, which sits beneath the tube and is deeper than it should be according to equation (IV.6). For larger times, the consistency can only be expected at some distance beyond the artificial boundary because the thermal disturbance from the tube actually extends to infinity. In the region near the symmetry line and the plane surface, the interface approaches a steady state position much more quickly than any other place. The portion of the interface above the tube gradually becomes nearly stationary, and the stationary part

TABLE 2. DATA FOR THE TWO CASES SHOWN IN FIGURES 25(a,b,c)

		I	II
a	(cm)	1.0	1.0
$\tilde{h}_o$		3.0	3.0
PCM		WATER	WATER
K_1	(cal/cm °C s)	0.00530	0.00530
K_2		0.00144	0.00144
ρ	(g/cm^3)	1.0	1.0
C_1	(cal/g°C)	0.465	0.465
C_2		1.0	1.0
L	(cal/g)	73.6	73.6
T_o	(°C)	-5.0	-20.0
T_a		18.4	18.4
T_f		0.0	0.0
$\bar{\alpha}_1$	(cm^2/s)	0.0114	0.0114
$\bar{\alpha}_2$		0.00144	0.00144
θ_a		1.0	0.25
St_1		0.032	0.126
λ		0.097	0.208
$\overline{\Delta y}_i$		0.31	0.21
$\overline{\Delta \ell}_c$		-0.24	-0.17
$\tilde{r}_{is}$	(cm)	2.828	1.468
$\tilde{h}_{is}$	(cm)	4.000	3.187
$y_{iN}/\sqrt{t}$	(cm/$min^{1/2}$)	.160	.384
$y_{is}/\sqrt{t}$		.208	.434
$H_b/\sqrt{t}$		.496	.790

* $\tilde{r}_{is}$ and $\tilde{h}_{is}$ are calculated from equations (I.18,12,13)

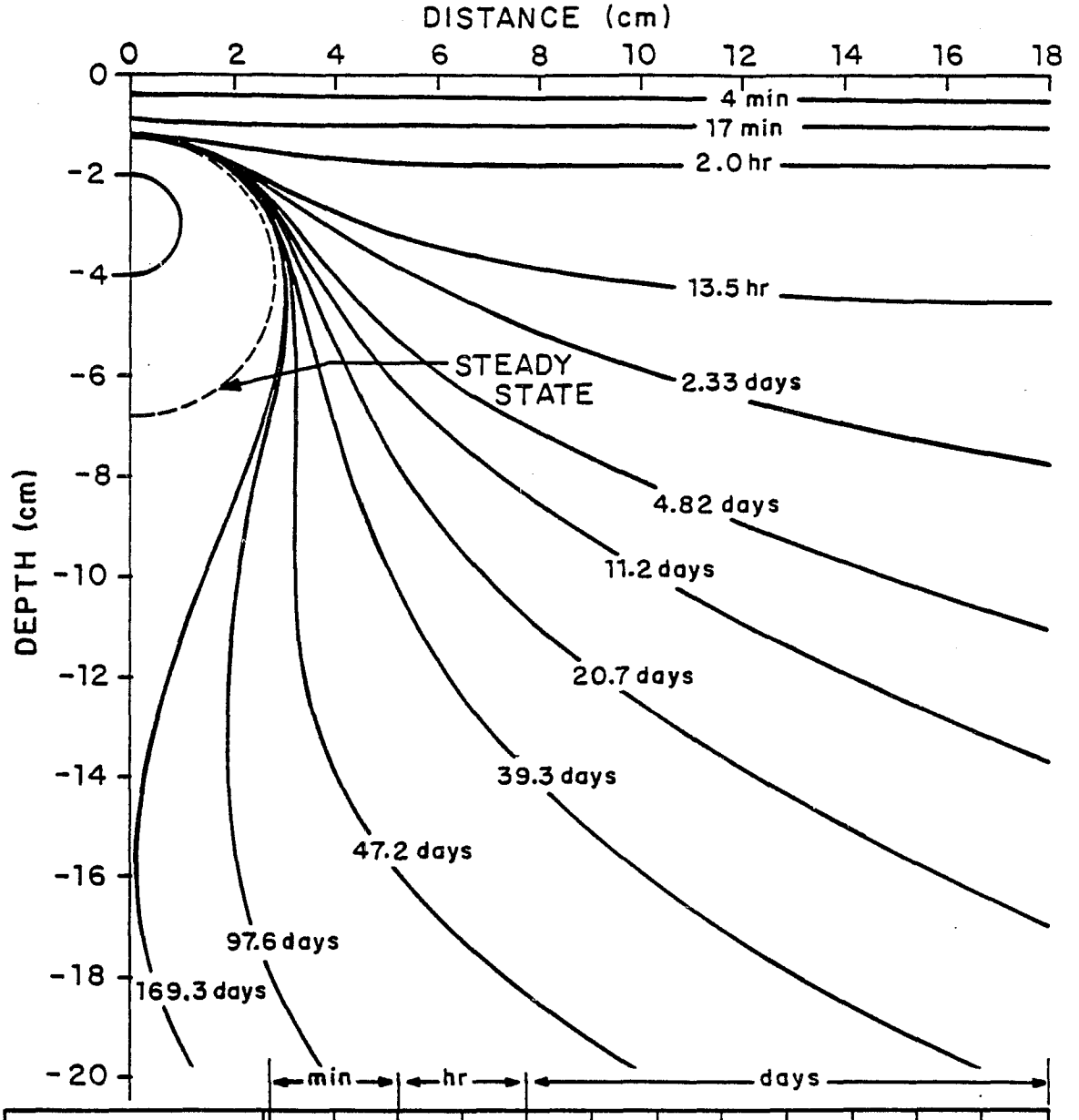

t	4	17	2.0	13.5	2.33	4.82	11.2	20.7	39.3	47.2	97.6	169.3
Neumann Solution (Eq. VI.1) (cm)	0.3	0.7	1.7	4.6	9.3	13.3	20.3	27.6	38.1	41.7	60.0	79.0

FIGURE 25(a). INTERFACE PROFILE AT SELECTED TIMES FOR CASE 1 IN TABLE 2

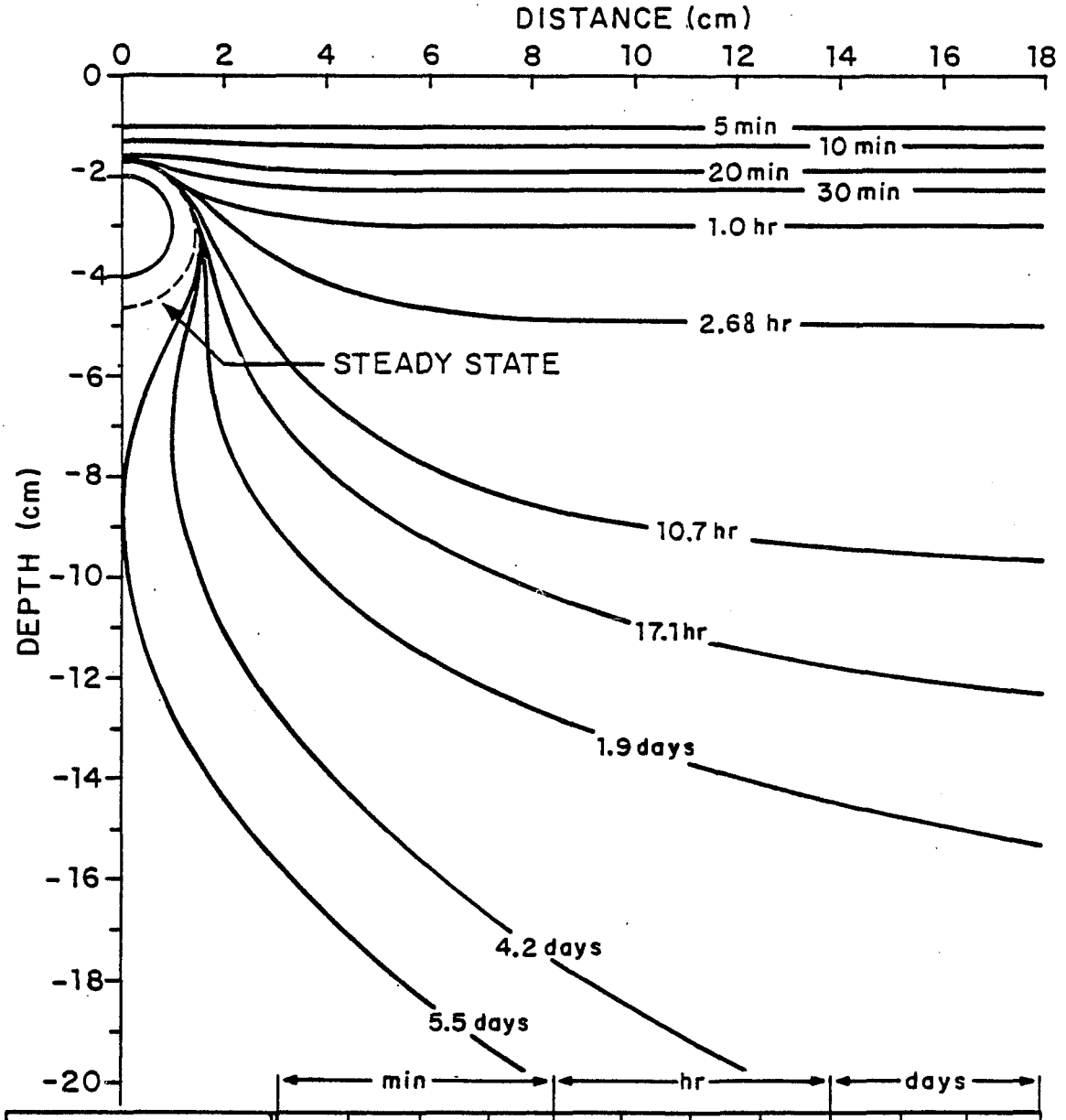

t	5	10	20	30	1	2.68	10.7	17.1	1.9	4.2	5.5
Neumann Solution (Eq. VI.1) (cm)	0.9	1.2	1.7	2.7	3.0	4.9	9.7	12.3	20.0	29.8	34.1

FIGURE 25(b). INTERFACE PROFILE AT SELECTED TIMES FOR CASE 2 IN TABLE 2

expands with time. This stationary arc is part of the steady state circle with radius $\tilde{r}_{is}$ and center $\tilde{y} = -\tilde{h}_{is}$ determined by equations (I.18) and (I.12,13) in subsection I.2.2. The values of $\tilde{r}_{is}$ and $\tilde{h}_{is}$ for each case are also shown in Table 2. Comparison of the two solutions shows that the larger θ_a in case 1 not only produces a larger final equilibrium thaw bulb around the tube but also necessitates a much longer time for the interface to envelop the tube. The slower motion in the far region allows the thermal disturbance to propagate over a larger area during the phase change process.

It is interesting to examine the effects of the moving bottom boundary by comparing the solution with the case where the bottom edge is located very far from the free surface. For this purpose, the interface position in case 2 is recalculated by fixing the bottom at the distance, $H_b = 100a$. The results are shown by the dashed curves in Figure 25(c), where the corresponding solutions using the floating bottom technique are also presented (solid curves). Because the bottom boundary is set at a relatively large distance, good agreement with the Stefan solution can be anticipated in the far rigion for all times (up to 2.68 hours as can be seen in the Figure). In fact, using the one-dimensional quasi-steady model, one can show that the interface penetration distance after 1.16 days differs by only 1.6% from the Stefan soluton corresponding to $H_b = \infty$. Thus, fixing the bottom boundary at $H_b = 100a$ is almost

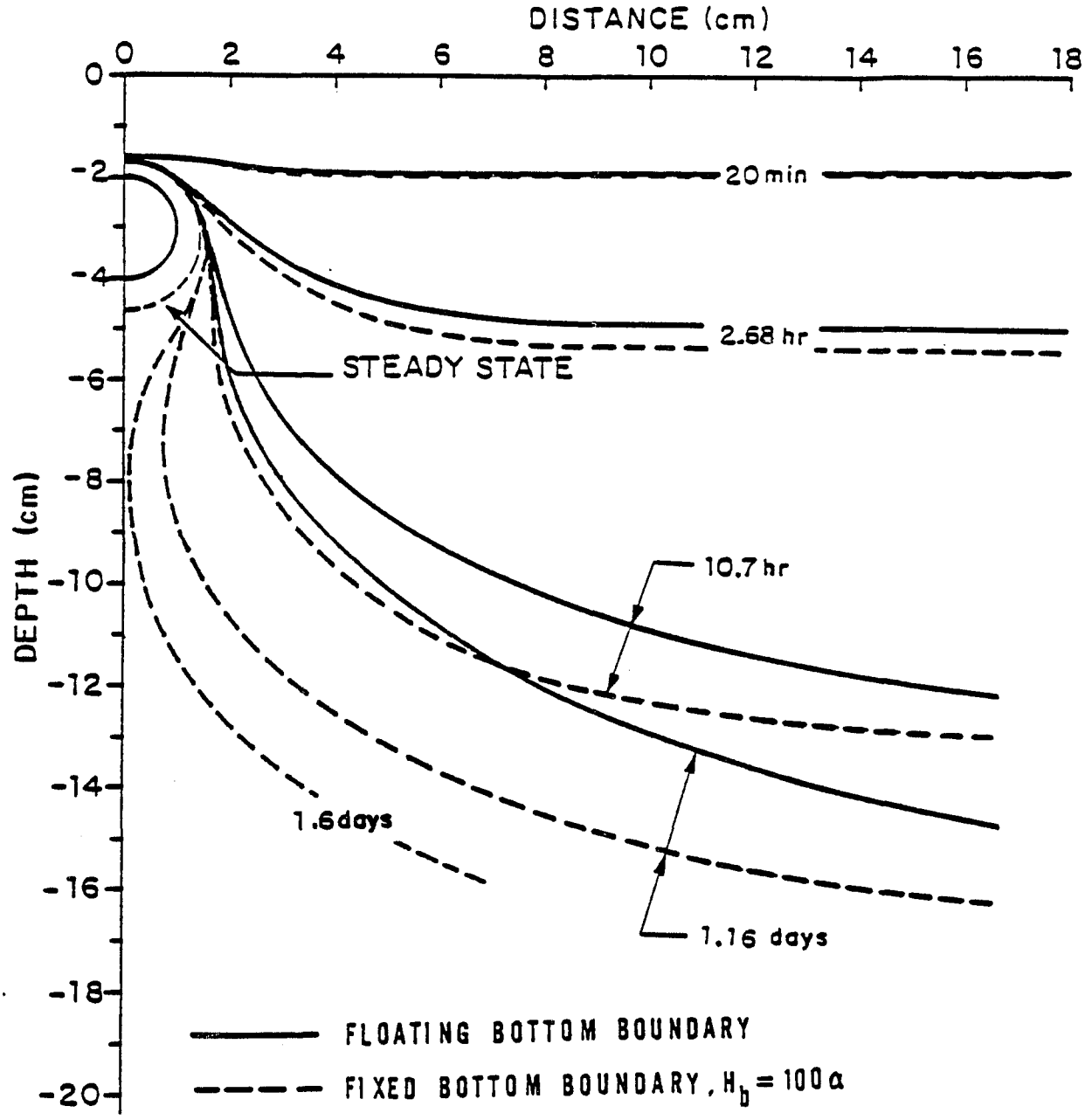

FIGURE 25(c). COMPARISON OF INTERFACE PROFILES USING THE FLOATING BOTTOM TECHNIQUE AND A FIXED BOTTOM, $H_b = 100a$, FOR CASE 2 IN TABLE 2

equivalent to setting $H_b = \infty$. In Figure 25(c), significant difference is observed between the two solutions, particularly at large times. As was indicated in subsection (IV.3), in the far region the the two solutions differ from each other in the same manner as Neumann's solution differs from Stefan's solution. However, they are indistinquishable in the region above the tube near the centerline $\phi = \pi/2$. On the other hand, the fixed bottom solution vastly underestimates the time required for the interface to envelope the tube. Figure 25(c) shows that this time to be 1.6 days as compared to 5.5 days predicted by the moving bottom solution shown in Figure 25(b). The difference in the interface behavior predicted by the two solutions will be further discussed in the next subsection.

All calculations are terminated when the interface envelopes the tube. The interface will then separate into two parts. The part surrounding the tube approaches the equilibrium circle, whilst the other keeps moving further downward and becomes more planar. The latter will behave as in the Neumann problem when time approaches infinity.

The Neumann solution, y_{iN}, and the Stefan solution, y_{iS}, corresponding to the far region for cases 1 and 2 are shown for comparison in Figure 26. Note that the one-dimensional quasi-steady approximate solution with floating bottom boundary must be identical to the Neumann solution as was anticipated. Since the penetration depth is proportional to

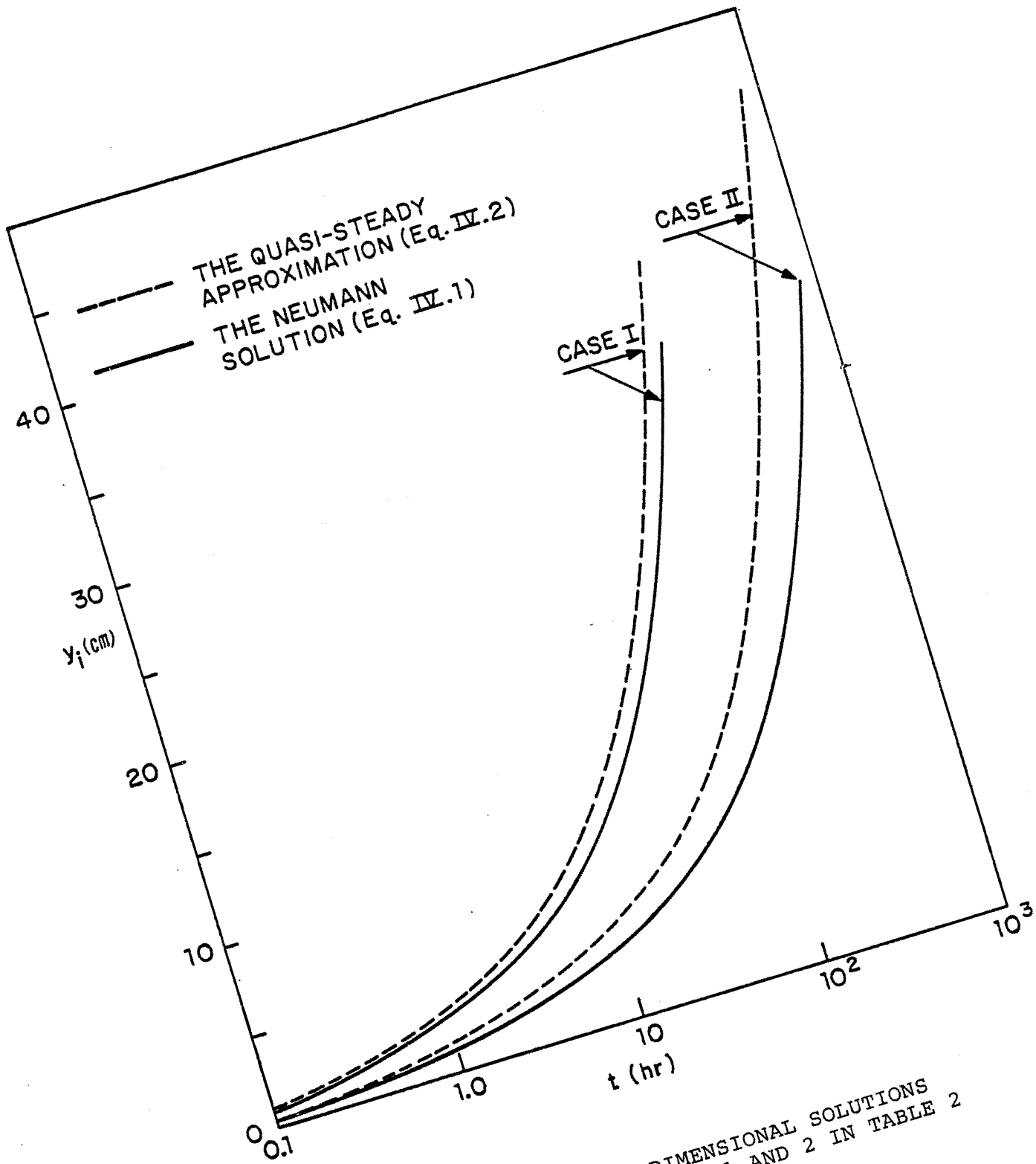

FIGURE 26. COMPARISON OF ONE-DIMENSIONAL SOLUTIONS CORRESPONDING TO CASES 1 AND 2 IN TABLE 2

the square root of time, $\sqrt{t}$, these curves will be straight lines in $\tilde{y}$-$\sqrt{t}$ plane. The constant slopes, $y_{iN}/\sqrt{t}$ and $y_{iS}/\sqrt{t}$, for each case are listed in Table 2, where the values of $H_b/\sqrt{t}$, from equation (IV.6) for the motion of the floating bottom boundary are also presented. One can see the importance of the parameter θ_a independently from the Stefan number.

IV.7 DISCUSSION

(1) Because of the complexity of the two-dimensional motion of the interface, it is instructive to examine the interface behavior in the far region and its effects on the interface shape near the tube. If the quasi-steady approximation is used without the floating bottom, the far region solution will be simply the Stefan solution. As can be seen in Figure 26, this solution always overestimates the penetration distance of the phase front. The comparison between the two classical one-dimensional solutions was briefly discussed before, equation (IV.3). However, in the present problem, neglecting the sensible heat not only overestimates the frozon depth in the far region but also significantly influences the instantaneous shape of the interface. This phenominon is clearly observed in Figure 25(c) as was indicated previously.

In Figures 25(a,b), one sees that the distortion of the interface from a planar surface first occurs near the cen-

tral line of the tube and then gradually extends outward. The active area of such a disturbance up to a certain time depends on the position and intensity of the heat sources at the tube wall and also the surface temperature of the free surface. In fact, the latter determines the interface behavior in the far region. It is important to note that the one-dimensional solution provides not only the instantaneous position of the interface in the far region but also an important reference time scale for the thermal disturbance from the tube surface to take effect. Since the travel distance of the thermal disturbance from the tube wall is characterized by the time scale of the diffusion, $t_d = 1/\bar{\alpha}_2 St_2$, the scale of the disturbance is associated with the vertical velocity of the interface in the far region. In terms of the characteristic depth, $(\tilde{h}_{is}+\tilde{r}_{is})$, the time scale for this motion may be written as $(\tilde{h}_{is}+\tilde{r}_{is})^2/4\bar{\alpha}_1\lambda^2$ using the Neumann solution (IV.1) and $(\tilde{h}_{is}+\tilde{r}_{is})^2/2\bar{\alpha}_1 St$, for the quasi-steady approximation and the Stefan solution (IV.2). The lateral scale of the distortion of the interface thus is characterized by ℓ_c, which satisfies $(\ell_c^2/\bar{\alpha}_2 St_2) \approx (\tilde{h}_{is}+\tilde{r}_{is})^2/4\bar{\alpha}_1\lambda^2$ or

$$\ell_c = (\tilde{h}_{is} + \tilde{r}_{is})\left(\frac{\bar{\alpha}_2}{\bar{\alpha}_1}\frac{St_2}{4\lambda^2}\right)^{1/2}$$

For the quasi-steady approximation, this scale is expressed as

$$\ell_c' = (\tilde{h}_{is} + \tilde{r}_{is})\left(\frac{\bar{\alpha}_2}{\bar{\alpha}_1}\frac{St_2}{4\lambda^2}\right)^{1/2}$$

The difference can be estimated by

$$\overline{\Delta \ell_c} = \frac{\Delta \ell_c}{\ell_c} = \frac{\ell_c' - \ell_c}{\ell_c} = \left(\frac{\lambda}{St_1/2} - 1 \right), \qquad \text{(IV.18)}$$

which is independent of the defined characteristic length. Note that $\overline{\Delta \ell_c}$ is always less than zero and represents the extent of the underestimation of the lateral scale of the interface distortion in the quasi-steady approximation as sketched in Figure 27(a). The values of $\overline{\Delta \ell_c}$ are listed in Table 2 for each case and in Table 1 as a function of St_1 and θ_a for general reference. From Table 2, the largest $|\overline{\Delta \ell_c}| = 0.24$ in case 1 indicates that for $\theta_a = 1$, the thermal disturbance scale due to the tube prediced by the quasi-steady approximation is up to 25% smaller than in the real situation, even though the Stefan number is small ($St_1 = 0.032$). For larger Stefan numbers, the situation will be worse (refer to Table 1). It should be pointed out that because of the transient behavior of the interface, the quasi-steady approximation may result in a severe displacement the interface rather than simply an overestimation of the penetration depth in the far region or an underestimation of the lateral scale of distortion of the interface. Figure 27(b) is a schematic diagram showing the transient effects on the interface geometry due to the neglect of the sensible heat which is similar to that in Figure 25(c) as was noted previously. The situation is obviously worse for large times which are usually needed in the quasi-steady approximation when small Stefan number is required and the interface moves very slowly.

The foregoing discussion indicates that the quasi-steady

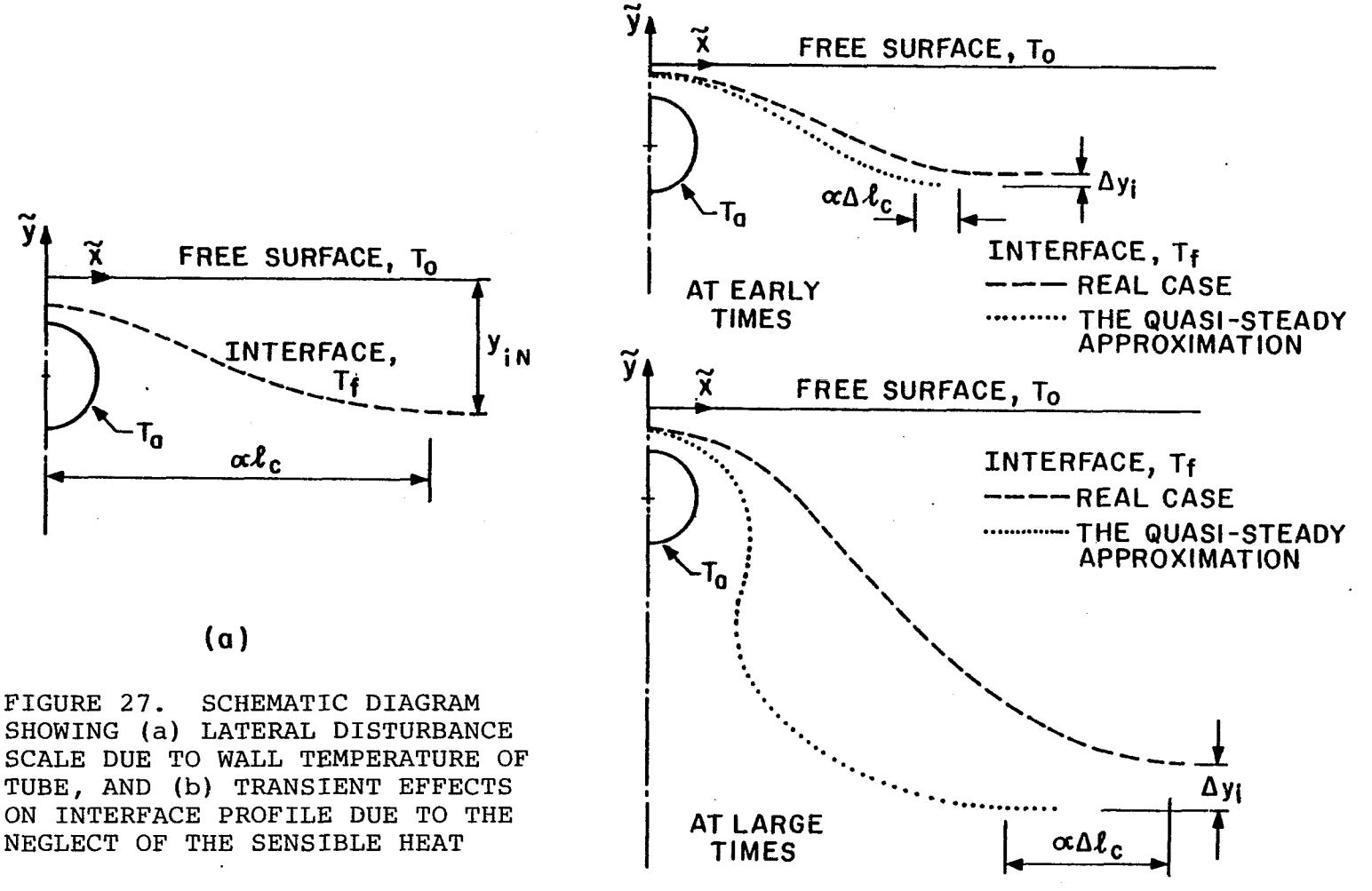

FIGURE 27. SCHEMATIC DIAGRAM SHOWING (a) LATERAL DISTURBANCE SCALE DUE TO WALL TEMPERATURE OF TUBE, AND (b) TRANSIENT EFFECTS ON INTERFACE PROFILE DUE TO THE NEGLECT OF THE SENSIBLE HEAT

approximation should be used with great caution except in cases with very small dimensionless temperature θ_a and small Stefan number (conditions that are not satisfied for many practical problems involving buried tubes) and when the water content of the PCM is small. The fact is that the important part of the solution, i.e. the far region solution, becomes independent of the initial as well as the tube surface temperature, T_a, in the quasi-steady approximation.

Since a reliable prediction of the instantaneous interface contour is related to the Neumann solution, calculation with dimensionless quantities is not recommended. From the above discussion and equation (IV.3), one can recognize that the similarity constant λ determined by equation (IV.1-a) in the Neumann solution is an important parameter independent of the Stefan number, St_1, which alone is considered in the quasi-steady approximation.

(2) Because the thermal disturbance from the tube is actually unbounded, the adiabatic boundary conditions, on the artificial boundary are not satisfied at all times, particularly at large times. Although one may eliminate the effects of the artificial boundary by moving it outward, it is not economical to keep enlarging the calculation domain and then devote much of the computation to a region which has little interest for the analysis. Nevertheless, it is believed that the interface shape in the neighborhood of the tube will not be affected significantly at large times if the artificial boundary is selected far enough from the

tube. Several numerical tests have been executed by changing the width from 15a to 20a and 30a and the results show only a little difference in the solutions in the neighborhood of the tube. However, for the floating bottom boundary, this is true only if it moves to a great depth where there is no significant influence on the region near the tube. One can see from Figures 25(a,b) and Table 2, that a surprisingly large depth of the artificial bottom boundary is needed before the interface starts bending around the tube sides.

From present experience, the width of the calculation domain should be $D \sim 10(\tilde{h}_{is}+\tilde{r}_{is})$. It is more reasonable to use $(\tilde{h}_{is}+\tilde{r}_{is})$ rather than the tube radius as the reference scale.

(3) The accuracy of the finite difference procedure cannot be analyzed due to the nonlinearity of the problem. It is noted that in the numerical computation, larger time intervals might lead to an early closing of the interface since the velocity components in two dimensions, which vary from point to point along the interface as well as with time, will be unrealistically exaggerated by too large time steps. For the same reason, the standard treatments to achieve the numerical stability of a differential equation cannot go into effect. The reliability of the solution is tested by checking it with different time steps by trial and error and comparing the result in the far region with the Neumann solution if possible.

REMARKS

The numerical calculations were performed for the freezing case. Although the formulation is basically the same for freezing and melting, the solution may be different because the thermal diffusivity of the thaw region is considerably less than that of the frozen and thus the heat flow will be reduced even with the same temperature gradient. Nevertheless, the melting problem can be analyzed in the same manner as for freezing case in association with the new values of $\bar{\alpha}_{1,2}$, St_1 and θ_a.

The boundary integral method and floating bottom technique proposed herein can also be used for the three-dimensional situation. With the quasi-three dimensional assumption, as was done in Chapter III, the extention of the present problem is straightforward. In fact, the heat flux at the tube surface is available simultaneously with that at the interface from equations (IV.4) or (IV.16,17) and therefore the energy equation in the fluid inside the tube, equation (III.3), can be integrated with a finite difference procedure as was done in Chapter III.

CONCLUDING REMARKS

A closed-form analytical solution is obtained for steady state three-dimensional freezing and melting around a tube embedded in the vicinity of a free surface. While the solution takes into account the axial thermal interaction between the PCM and the fluid flowing in the tube, the axial heat conduction is neglected in the formulation. This model represents most practical problems in which the axial temperature variation in the PCM is minor compared to that in the radial direction and the heat convection is much more important than conduction in the fluid inside the tube.

All previous quasi-steady approaches to two-dimensional melting or freezing around a buried tube were concerned only with the prediction of the depth of the thaw region. In attempting to provide a representation of the instantaneous interface configuration as well as the isotherms, a careful analysis of the transient behavior of the interface was presented. Based on this analysis, the new solution method separates the solution domain into parts above and below the tube. The motion of the upper portion of the interface is determined by applying the energy equation at the top-most point of the interface. This method is not used to predict the instantaneous position of the lower portion since it has been shown that the Porkhayev solution (II.9) is not a good approximation except when the final equilibrium state is reached. In order to describe the actual motion of the interface which gradually changes from the early time behavior governed by the infinite burial solution (II.1) to the

very large time behavior when the Porkhayev solution becomes a suitable approximation, the apparent free surface was introduced and the Porkhayev approximation was then applied with respect to the appropriately determined fictitious free surface instead of the real free surface. Although different formulae are used for the upper and lower portions, the relationship between them is included in the determination of the position of the apparent free surface and the polynomial shape approximation (II.15). The comparison between the present solution and numerical results shows excellent agreement and confirms the basic correctness of the analysis.

The so-called apparent free surface method has been extended to the three-dimensional situation where the temperature field in the PCM is thermally coupled with the fluid flowing in the tube. The solution exposes an important new feature that has not been described in previous two-dimensional mathematical models using either an analytical approximation or a numerical approach. The thermal interaction between the PCM and the fluid in the tube may cause the local temperature of the fluid to be far from the equilibrium value. The assumption of a constant surface temperature at the tube which uncouples the axial thermal interaction might lead to a large overestimation of the thaw region.

While the analytical solution method is developed for the particular case where the phase change commences at the tube

surface, a more general numerical technique is used to solve the problem when the freezing starts at the planar surface. The boundary integral method reduces the calculation domain by one dimension and leads to a high efficiency in computation. This method can also be applied to the first type of problem where the phase change starts at the tube wall.

It is noticed that although the mapping (I.11) provides for a bounded calculation domain, it is not recommended when the numerical method is used. As shown in subsection II.2, the scale factor $|Z'(W)|$ of the transformation (I.11) is much larger in the region below the tube than the upper region. The energy equation at the interface (II.4) in the complex W-plane shows that the velocity of the interface is inversely proportional to the second power of the local scale factor which varies dramatically along the interface from the bottom-most point to the top-most point. The large difference in magnitude of the scale factor along the interface requires a higher degree of accuracy in the prediction of the heat flux along the interface in the complex W-plane than in the physical Z-plane. The situation would be much worse in the second type of problem where freezing starts at the planar surface. The interface, which extends to infinity in the physical plane, intersects the outer circular boundary, $R = R_o$ in the complex W-plane at the singularity of the transformation with $\alpha = -\pi/2$ (Figure 3). The boundary element technique will give very poor accuracy because of the singular point where the interface and the outer

boundary are very close to each other at all times. The extreme heat flux at the bottom portion of the interface, which results from the boundary integral of the outer frozen region, severely affects the accuracy in the upper portion. Consequently, a great deal of computer time would be spent on the lower region, which corresponds to the far region in the physical plane and is of little interest, and the poor accuracy would destroy the reliability of the solution.

The present studies are based on the quasi-steady approximation. The effect of neglecting the sensible heat in both liquid and solid regions can not be rigorously analyzed. The parameter θ_a, which can be expressed in terms of the ratio of the Stefan numbers, $\theta_a = \bar{\alpha}_2 St_2 / \bar{\alpha}_1 St_1$, represents the relative importance of the sensible heat in the two regions. θ_a is relatively unimportant in applying the quasi-steady approximation in the first type of problem, but is a really important factor in the second problem. For the problem described in Chapters II and III, where the interface is a closed surface and hence limited to a region near the tube surface bounded by the steady state circle, the neglect of the sensible heat may lead to overestimation of the penetration distance in all directions but will not significantly affect the interface shape. However, for phase change starting at the planar surface, the phase front extends to infinity and the omission of the sensible heat becomes questionable because of the very different geometrical surroundings in the neighborhood of the tube and the far

region. In general, one must be cautious in using the quasi-steady approximation to deal with a moving interface problem in a complex geometry.

The present solutions can be improved using the quasi-stationary approximation to include the effects of the sensible heat for small Stefan number problems. The governing equations (I.1,2) are replaced by the transient heat conduction equations, but the energy equation at the interface remains the same as in the present case. The available boundary integral techniques for pure diffusion without phase change [24] can first be applied to each region separately. The solid-liquid surface can then be determined for each time-step. The main difficulty which may arise is numerical instability. Two separate finite difference procedures are involved and the trial and error method used to determine the time step in the present work may be inapplicable because of the large amount of computer time needed.

Once this problem has been treated, the extension of the quasi-stationary solution to three dimensions is similar to that described for the quasi-steady approximation.

APPENDIX A

GEOMETRICAL RELATIONSHIP BETWEEN Z AND W PLANES

The coordinates (x_e, y_e) of point e in Figure 12 is the intersection of the two circles with radius r_{ia} and r_{ib}, respectively. From Figure 28, a sketch simplified from Figure 12, one may easily determine the following geometrical relation:

$$r_{ia}^2 - (d^2 + \Delta h_i)^2 = x_e^2 \tag{A1}$$

and

$$r_{ib}^2 - x_e^2 = d^2 \tag{A2}$$

where $\Delta h_i = h_{ia} - h_{ib}$, and d is the distance shown in Figure 28. x_e and d are then given by

$$d = \frac{r_{ia}^2 - \Delta h_i^2 - r_{ib}^2}{2\Delta h_i} \tag{A3}$$

and

$$x_e = (r_{ib}^2 - d^2)^{1/2} \tag{A4}$$

The coordinates of point e are given by

$$x_e = \left\{ r_{ib}^2 - \left[\frac{r_{ia}^2 - (h_{ia} - h_{ib})^2 - r_{ib}^2}{2(h_{ia} - h_{ib})} \right]^2 \right\}^{1/2} \tag{II.15-e}$$

and

$$y_e = d - h_{ib} = -h_{ib} + \frac{r_{ia}^2 - (h_{ia} - h_{ib})^2 - r_{ib}^2}{2(h_{ia} - h_{ib})} \tag{II.15-f}$$

The angle Φ_e thus is:

$$\Phi_e = \tan^{-1} \frac{y_e + h_o}{x_e} \qquad \text{(II.15-h)}$$

With a complex notation $Z_e = x_e + iy_e$ for point e in the physical Z-plane, the corresponding point e' in the complex W-plane can be written as

$$W_{e'} = u_{e'} + i v_{e'} = \frac{R_o Z_e + (R_o h_o - 1) i}{R_o - h_o - Z_e i} \qquad \text{(A5)}$$

Separating Z_e into real and imaginary parts in equation (A5), one can expresses $u_{e'}$ and $v_{e'}$ respectively in terms of x_e and y_e, and the angle $\alpha_{e'}$ can be written as a function of x and y ,

$$\alpha_e = \tan^{-1} \frac{V_{e'}}{u_{e'}} = \frac{-x_e^2 R_o + [R_o - (h_o + y_e)][R_o(h_o + y_e) - 1]}{x_e (R_o^2 - 1)} \qquad \text{(III.4-a)}$$

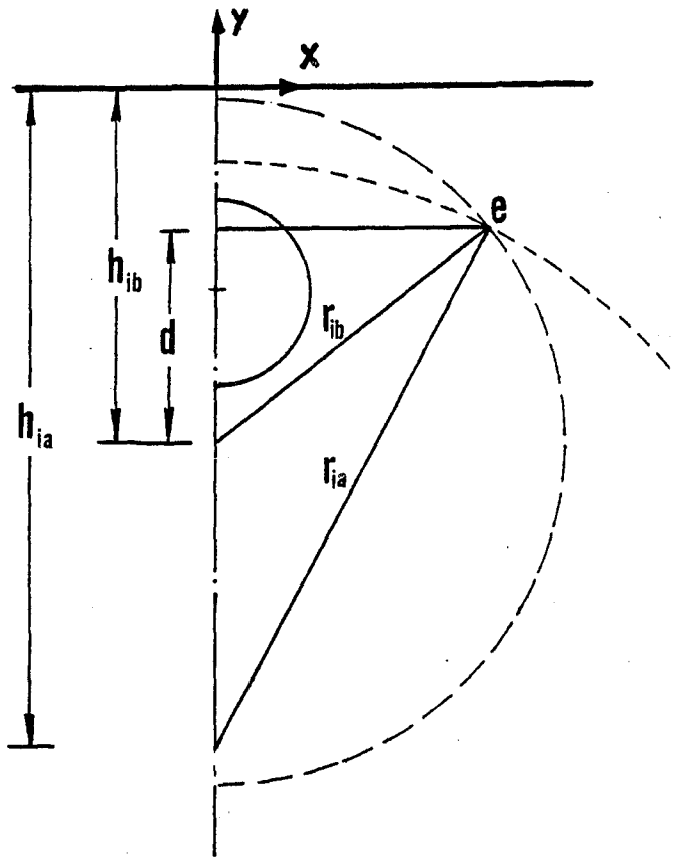

FIGURE 28. GEOMETRICAL SKETCH OF POINT e
(REFER TO FIGURE 18(a))

APPENDIX B

EVALUATION OF $\delta(t^*)$ - METHOD (I)

We wish δ to approach infinity as t^* approaches zero (or r_{ib} approaches unity) and exponentially decay to zero as r_{ib} approaches its steady state value r_{is}. An approximation for δ that satisfies these conditions is:

$$\delta = -\gamma \ln \frac{r_{ib} - 1}{r_{is} - 1} , \tag{B1}$$

where the final steady state value of r_{is} is from equations (I.12,18) and given by

$$r_{is} = \frac{(R_o^2 - 1)\, R_o^{\theta_a/(1+\theta_a)}}{R_o^2 - R_o^{2\theta_a/(1+\theta_a)}} \tag{B2}$$

Constant γ in equation (B1) is determined by matching with simpler solution $\delta^{(o)}$, which is valid only at very short time. For small time t^*, equation (II.13-a) can be written in the form:

$$\delta = \frac{h_o^2 - 1 - y_{ia} y_{ib}}{2(h_{ib} - h_o)} , \tag{B3}$$

where $y_{ia} = (h_{ia} - r_{ia})$ and $y_{ib} = (h_{ib} + r_{ib})$ are the distances of the top and bottom points of the thaw front measured from the free surface. For very early times, the interface can be approximated by a slightly eccentric circle passing through both points a and b in Figure 12. The motion of point a is given by

$$-\frac{dy_{ia}}{dt^*} = \frac{(R_o^2 - 1)}{(R_o + R_i)^2}\frac{dR_{ia}}{dt^*} \qquad \text{(B4)}$$

where the dR_{ia}/dt^* is obtained from equation (II.8). The motion of point b is determined by the Carslaw and Jaeger solution (II.1). Equations (II.8) and (B4) are integrated over some small but finite time t^*. It is obvious that the circle passing through points a and b will be nearly concentric about the tube provided that δ is large compared to the burial depth of the tube. The principal difference between the Carslaw and Jaeger solution and the present solution at these short times is that there is a slight difference in penetration depths d_{ia} and d_{ib} of the top and bottom points due to the small non-uniform flux in the outer region when θ_a is finite. The result is that the center of the circle through a and b is shifted down a distance $(d_{ia}+d_{ib})/2$ and has its center at $h_{ib} = h_o + (d_{ib} - d_{ia})/2$ while the radius of the thaw cylinder r_i is slightly smaller than the Carslaw and Jaeger solution and has the value, $r'_{ib} = r_{ib} - (d_{ib} - d_{ia})/2$, where r_{ib} here is the Carslaw and Jaeger value. The value of δ, which is much greater than h_o, does not significantly affect the prediction of the position of point b, since this is well approximated by the infinite burial solution, but it does reflect the slight eccentricity that develops due to the small differences between d_{ia} and d_{ib}. One can show in the limit as both d and d approach zero that equation (II.13-a) or (B3) reduces to

$$\delta^{(o)} = \frac{d_{ia} + d_{ib}}{d_{ib} - d_{ia}} \qquad \text{(B5)}$$

This follows from the approximation, $h_{ib} - h_o \approx (d_{ib} - d_{ia})/2$, and the geometrical definitions of y_{ia} and y_{ib}.

To determine the value of the constant, γ, and the location of the match point r_{ibo} where one shifts from equation (B5) to (B1), one requires that

$$\delta = \delta^{(o)} \tag{B6}$$

and

$$\frac{dy_{ib}}{dt^*} = \frac{dy_{ib}^{(o)}}{dt^*} \tag{B7}$$

The right hand side of equation (B6) is given by (B5) while the right hand side of (B7) is obtained from the differential form of the Carslaw and Jaeger solution. The left hand side of equation (B7) is given by

$$\frac{dy_{ib}}{dt^*} = \frac{(R_{ob}'^2 - 1)}{(R_{ob}' - R_{ib}')^2} \frac{dR_{ib}'}{dt^*} \tag{B8}$$

where dR_{ib}'/dt^* is obtained from equation (II.14).

The value of dy_{ib}/dt^*, therefore, is a function of δ and r_{ib} (or γ and r_{ib}). A numerical procedure is required to satisfy the matching conditions (B6) and (B7). For values of r_{ib} greater than r_{ibo}, one uses equation (B1) to determine δ.

APPENDIX C

EVALUATION OF $\delta(z,\bar{t}^*)$ - METHOD (II)

The polynomial given by equation (II.15) and boundary conditions (II.15a-d) takes into account the influence of the upper portion of the interface on the lower portion and gives a reasonable approximation of the interface shape. However, it is still not sufficiently accurate to describe the local curvature of the interface at the bottom-most point for the determination of δ. The difficulty is that the intersection of the upper and lower circles does not adequately represent the actual joining point of the interface in the upper and lower regions. This is due to the large variation in curvature in the vicinity of point e, Figure 12. The following procedure based on Figure 26 was developed to overcome this difficulty:

(1) At early times, the Carslaw and Jaeger solution [6] is used to calculate the position of point b. The polynomial equation (II.15) is first applied to link points b and a (see Figure 26) by replacing conditions (II.15-c-d) with $r_p(\pi/2) = h_o - (h_{ia} - r_{ia})$ and $dr_p(\pi/2)/d\Phi = 0$, respectively, and thus gives the radius of the local curvature, r'_{ib}, by equation (II.16). Using r'_{ib} and h'_{ib} given by equations (II.16,17), the value of δ is then readily obtained from equation (II.18).

(2) A relatively large value δ_o is assigned (say $\delta_o = 10h_o$ or larger) such that when δ is larger than this

assigned limit, $\delta > \delta_o$, the apparent free surface will hardly affect the motion of the interface around its bottom-most point. The Carslaw and Jaeger solution in fact can be employed until δ is equal to or less than δ_o.

(3) For large times, equation (II.14) is used. To determine $\delta(\bar{t}^*)$ at any instant in time $\bar{t}^*$, one first divides the abscissa distance of point e, $x_e(\bar{t}^*)$, into M_o divisions (see Figure 26). Each division has the same size, $\Delta x_e = x_e/M_o$ and all nodes are numbered in order by M, where $M_o \geq M \geq 0$, such that $x(0) = x_e$, $x(M_o) = 0$ and $x(M) = x_e - M\Delta x_e$. To determine r'_{ib}, the polynomial, equation (II.15), is applied between point b and an appropriately chosen point e_1 along curve $\widehat{ae}$ to calculate a_1 and a_2 for equation (II.16). Point e_1 is identified by number M^* by a simple relation $x_{e1} = x_e - M^*\Delta x_e$ where x_{e1} is the abscissa distance of point e_1 and M^* is remained to be determined. Substituting r'_{ib} into equation (II.17). and then into equation (II.18), one obtaines $\delta(\bar{t}^*)$. Since point e is indicated by M^*, it is obvious that r'_{ib} or δ is a function of M^*. The conditions to determine M^* are that $r'_{ib}(M^*) < r_{ib}(\bar{t}^* - \Delta\bar{t}^*) < r'_{ib}(M^*-1)$, where $r_{ib}(\bar{t}^* - \Delta\bar{t}^*)$ is obtained from the solution of equation (II.14) in the preceding time step if one notes that $r_{ib}(\bar{t}^*) = r'_{ib}(M^*)$.

To describe the shape of the interface, a new joining point is defined at the position (x_{eo}, y_{eo}) along curve $\widehat{ae}$, where $x_{eo} = (x_e + x_{e1})/2$. The instantaneous shape of the interface is constructed using the circular curve $\widehat{ae}$ as its

upper portion and curve $\widehat{e_o b}$, the polynomial linking points b and e_o, as its lower portion.

One can show that both $M^*(\bar{t}^*)$ and $\delta(\bar{t}^*)$ converge to zero as $\bar{t}^*$ goes to infinity if $\Delta\bar{t}^*$ and $\Delta x_e(\bar{t}^*) = x_e(\bar{t}^*)/M_o$ are both small enough. For practical purposes, one may take $\delta_o = 10h_o$ and choose M_o such that $M^*(\bar{t}^*)$ satisfies the following conditions: (i) M^* must monotonically approach zero until the steady state is reached, (ii) as predicated by the analysis of the apparent free surface method, the solution should not be sensitive to the assigned value of δ_o when $\delta_o > 10h_o$.

In the present paper, $M_o = 50$ is chosen for both cases. In general, one may with little difficulty determine a suitable value of M_o by trial and error by satisfying the aforementioned conditions. Although the value of M_o satisfying the above conditions may be located in a certain range of numbers, e.g. $M_o = 20$ to 150 for case 1 and $M_o = 10$ to 60 for case 2, it is found that the relative errors of the solutions for the penetration depth under the tube, d_{ib}, until 10 years were less than 1.8% for both situations.

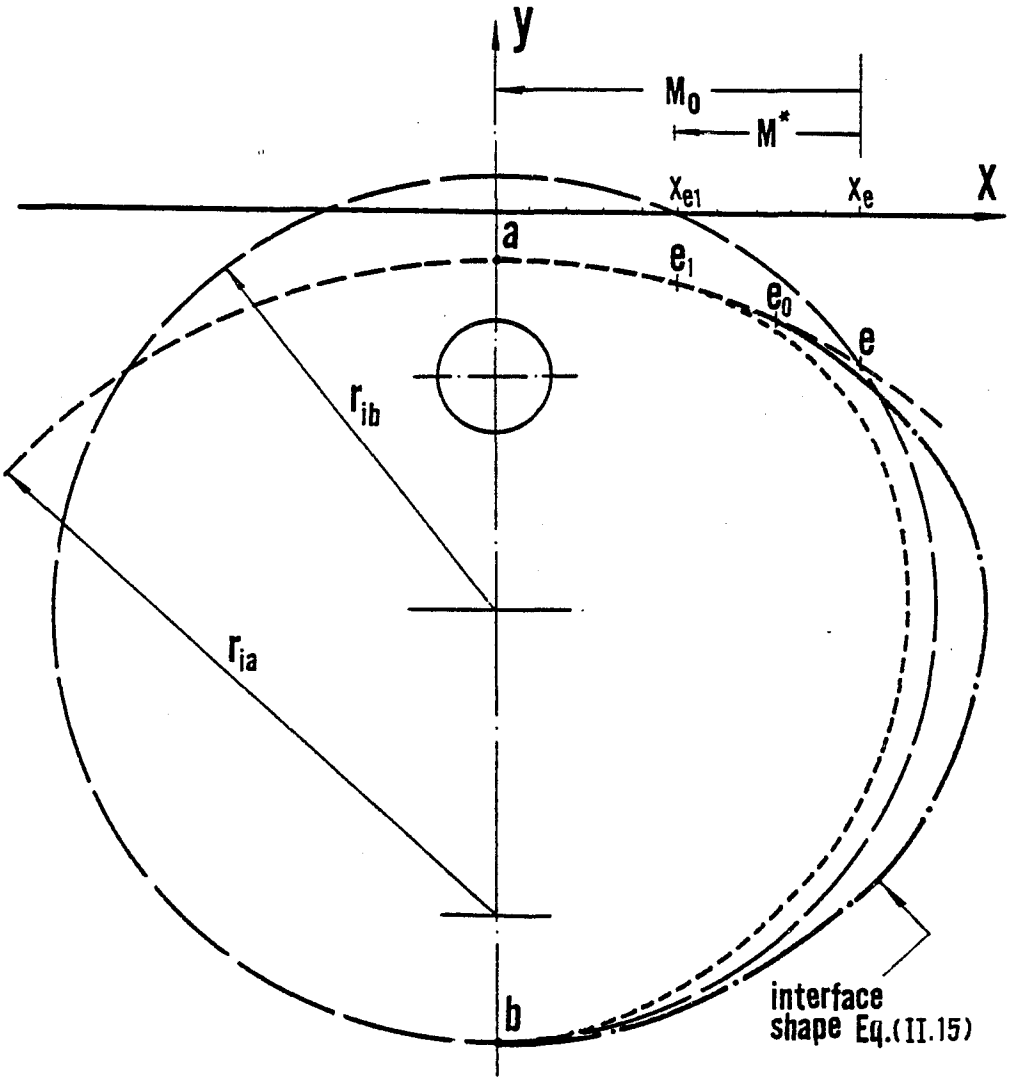

FIGURE 29. SCHEMATIC DIAGRAM SHOWING DETERMINATION FOR δ

APPENDIX D

SOLUTION FOR THE REGION NEAR THE TUBE WALL

In subsection III.2.2., we already have the energy equation in the fluid in the tube,

$$\frac{Pe^*}{\bar{\theta}_a}\frac{\partial \bar{\theta}_a}{\partial z} = -\frac{4}{\ell n\, S_p} \qquad \text{(III.16-a)}$$

and at the interface,

$$\frac{1}{\bar{\theta}_a}\frac{\partial S_p}{\partial \bar{t}^*} = \frac{4}{\ell n\, S_p} \qquad \text{(III.17-a)}$$

where $S_p = r_p^2$, represents the cross-sectional area of the thaw region around tube. By assuming a new differential variable with respect to time, $d\tau(z,\bar{t}^*) = \bar{\theta}_a(z,\bar{t}^*)\,d\bar{t}^*$, one can integrate equation (II.17-a) to yield:

$$4\tau = S_p \ell n\, S_p - S_p + 1 \qquad \text{(D1)}$$

or

$$\tau = \frac{1}{4}\left\{\left[r_p^2(2\ell n\, r_p - 1)\right] + 1\right\} \qquad \text{(D2)}$$

This is of the same form of the Carslaw and Jaeger solution (II.1) but τ and r_p here are functions of z as well as $\bar{t}^*$. Equation (D1) shows that the S_p is a function of the new variable τ only. Thus, equating the right hand sides of equations (16-a,17-a) leads to:

$$Pe\,\frac{\partial \ell n\, \bar{\theta}_a}{\partial z} = -\frac{dS_p}{d\tau} \qquad \text{(D3)}$$

and

$$Pe^{*}\,\frac{\partial \bar{\theta}_a}{\partial z} = -\frac{\partial S_p}{\partial \bar{t}^{*}} \qquad \text{(D4)}$$

Note that the complete derivative $dS_p/d\tau$ can be written as

$$\frac{dS_p(z,\bar{t}^{*})}{d\tau} = \frac{\partial S_p(z,\bar{t}^{*})}{\partial z} \Big/ \frac{\partial \tau(z,\bar{t}^{*})}{\partial z} \qquad \text{(D5)}$$

where $\partial\tau(z,t^{*})/\partial z$ is given by

$$\frac{\partial \tau}{\partial z} = \frac{\partial}{\partial z}\int_0^{\bar{t}^{*}} \bar{\theta}_a\, d\bar{t}^{*} = \int_0^{\bar{t}^{*}} \frac{\partial \theta_a}{\partial z}\, d\bar{t}^{*} \qquad \text{(D6)}$$

according to the definition of τ. Using equation (D3), equation (D5) becomes:

$$\frac{\partial \tau}{\partial z} = -\int_0^{\bar{t}^{*}} \frac{1}{Pe^{*}}\,\frac{\partial S_p}{\partial \bar{t}^{*}}\, d\bar{t}^{*} = -\frac{(S_p-1)}{Pe^{*}} \qquad \text{(D7)}$$

Substituting (D7) into (D5) and (D4), one obtaines an equation with only one partial derivative,

$$\frac{\partial \ln \bar{\theta}_a}{\partial z} = \frac{1}{(S_p-1)}\,\frac{\partial S_p}{\partial z} \qquad \text{(III.19)}$$

The integration of equation (III.12) is straightforward and gives:

$$\frac{\theta_a}{S_p-1} = e^{c(\bar{t}^{*})} \qquad \text{(III.19-a)}$$

and

$$c(\bar{t}^{*}) = -\ln(r_{po}^{2}-1) \qquad \text{(III.19-b)}$$

where $r_{po} = r_p(0,\bar{t}^*)$ at the entrance of the tube is simply determined by the Carslaw and Jaeger solution (II.1). Combination of equations (III.19-a,b) gives a simple algebraic relation between $\bar{\theta}_a(z,\bar{t}^*)$ and $r_p(z,\bar{t}^*)$:

$$\bar{\theta}_a(z,\bar{t}^*) = \frac{r_p^2(z,\bar{t}^*)-1}{r_{po}^2(\bar{t}^*)-1} \qquad \text{(D8)}$$

Equation (D8) shows that the dimensionless temperature of the fluid decreases linearly with the decrease of the cross-sectional area of the thaw cylinder along the tube axis. Since the interface always remains partially in the region near the tube wall until it entirely departs from the tube surface, this solution is actually applied to a thin layer around of the tube to match the non-circular solution determined by equations (II.8,14) in the outer region. If at time $\bar{t}^*$, the fluid temperature $\bar{\theta}_a$ and local radii r_{ia} and r_{ib} (note $r_{ib} \approx r_{ia}$ here) at the axial position $z = z_o$ is obtained from the outer region solution, one can then calculate the axial temperature distribution in the fluid by the linear relation:

$$\frac{\bar{\theta}_a(z,\bar{t}^*)}{\bar{\theta}_a(z_o,\bar{t}^*)} = \frac{r_p^2(z,\bar{t}^*)-1}{r_p^2(z_o,\bar{t}^*)-1} \qquad \text{(D9)}$$

for the region in the vicinity of the tube. Note that equations (D8,9) provide a solution for $\bar{\theta}_a$ in terms of r_p only. By combining equations (III.16-a) and (III.19), the relation between r_p and z is determined as

$$\frac{1}{Pe^*}\frac{dz}{dS_p} = -\frac{\ln S_p}{4(S_p-1)} \qquad \text{(D10)}$$

The integral form is

$$\frac{z}{Pe^*} = -\frac{1}{4}\int_{S_{po}}^{S_p}\frac{\ln S_p}{S_p-1}\,dS_p \qquad \text{(D11)}$$

where $S_{po} = r_p^2(0,t^*)$ at $z = 0$, or

$$\frac{z-z_o}{Pe^*} = -\frac{1}{4}\int_{S_{po}}^{S_p}\frac{\ln S_p}{S_p-1}\,dS_p \qquad \text{(D12)}$$

with known S_{pzo} at position $z = z_o$ matching with the outer region solution. Using Talor expansion of $\ln S_p$ around $S_p = 1$:

$$\ln S_p = \sum_{n=1}^{\infty}\frac{(-1)^{n+1}(S_p-1)^n}{n} \qquad \text{for } |S_p| < 2 \qquad \text{(D13)}$$

one can integrate equation (D12) analytically. In the present calculation, the analytical axisymmetric solution was used for region $r_p \lesssim 1.2$.

APPENDIX E

DETERMINATION OF THE POSITION OF THE FLOATING BOTTOM BOUNDARY

The energy equation at the interface, equation (II.2-a), can be written as the following dimensional form (refer to Figure 29):

$$K_1 \frac{\partial T_1}{\partial n} - K_2 \frac{\partial T_2}{\partial n} = \rho L \frac{d\tilde{n}}{dt} \quad . \tag{E1}$$

In the far region, equations (I.1,2) become one-dimensional and result in linear temperature fields in both regions. The normal derivatives are then given by

$$\frac{\partial T_1}{\partial \tilde{n}} = \frac{T_f - T_o}{Y_i(t)} \tag{E2}$$

and

$$\frac{\partial T_2}{\partial \tilde{n}} = \frac{T_a - T_f}{H_b(t) - Y_i(t)} \tag{E3}$$

Substituting with (E2) and (E3), equation (E1) becomes:

$$K_1 \frac{T_f - T_o}{Y_i(t)} - K_2 \frac{T_a - T_f}{H_b(t) - Y_i(t)} = \rho L \frac{dY_i(t)}{dt} \tag{E4}$$

or

$$\frac{1}{Y_i(t)} - \frac{\theta_a}{H_b(t) - Y_i(t)} = \frac{\rho L}{K_1 (T_f - T_o)} \frac{dY_i(t)}{dt} \tag{E5}$$

Solving it for $H_b(t)$, one obtains:

$$H_b(t) = \frac{\theta_a}{\frac{1}{Y_i(t)} - \frac{\rho L}{K_1 (T_f - T_o)} \frac{dY_i(t)}{dt}} Y_i(t) \quad . \tag{E6}$$

By assuming the heat flux difference across the interface to be equal to the exact Neumann solution, $y_i(t)$ and $dy_i(t)/dt$ in equation (E6) can be replaced by y_{iN} and dy_{iN}/dt given by equation (VI.1)

$$y_i(t) = y_{iN} = 2\lambda\sqrt{\bar{\alpha}_i t}$$

and

$$\frac{dy_i(t)}{dt} = \frac{dy_{iN}}{dt} = \lambda\sqrt{\frac{\bar{\alpha}_i}{t}}$$

Thus, equation (E6) becomes:

$$H_b(t) = \left(1 + \frac{\theta_a}{1 - 2\lambda^2/St_1}\right) \cdot 2\lambda\sqrt{\bar{\alpha}_i t} \qquad \text{(VI.6)}$$

where $St_1 = C_1(T_f - T_o)/L$ is the Stefen number.

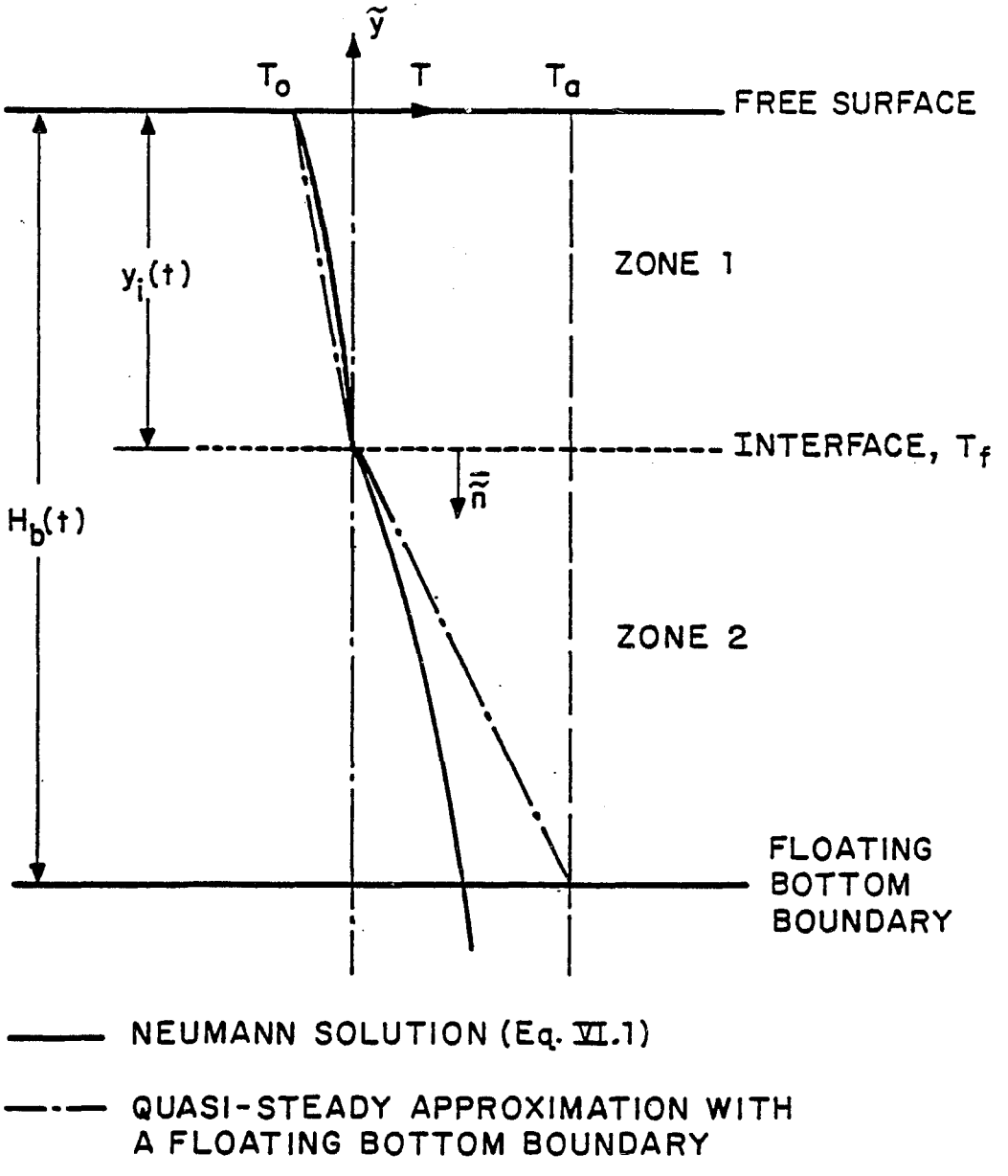

FIGURE 30. SCHEMATIC DIAGRAM SHOWING DETERMINATION OF POSITION OF FLOATING BOTTOM BOUNDARY

APPENDIX F

DERIVATION OF EQUATIONS (VI.16,17)

As shown in Figures 24(a,b), the boundaries of each zone in the calculation domain are subdivided into small segments s_k (k = 1,2,...,N) and the unknown function θ or $\partial\theta/\partial n$ along s_k is approximated by some mean value θ_k or $(\partial\theta/\partial n)_k$. The integral equation (VI.4) then can be written as

$$\theta(x_j, y_j) = \frac{1}{2\pi}\sum_{k=1}^{N}\int_{s_k}\left[\theta_k\frac{\partial U(x_j, y_j, \xi, \eta)}{\partial n} - \left(\frac{\partial\theta}{\partial n}\right)_k U(x_j, y_j, \xi, \eta)\right] ds$$

$$= \frac{1}{2\pi}\sum_{k=1}^{N}\left[\theta_k\int_{s_k}\frac{\partial U(x_j, y_j, \xi, \eta)}{\partial n} ds - \left(\frac{\partial\theta}{\partial n}\right)_k\int_{s_k} U(x_j, y_j, \xi, \eta)\, ds\right] \qquad (F1)$$

$(j = 1, 2 \ldots N)$

where point (x_j, y_j) locates at the center of the jth segment. Expression (F1) can be used for both regions. The line integral in equation (VI.4) is carried out anticlockwise for region 1, and thus the normal coordinate n in equation (F1) points outward from the frozen region according to Green's formula (VI.4). In order to keep both integrals for regions 1 and 2 in the same direction along the interface, the integral in equation (F1) is performed clockwise for zone 2 and thus n directs inward in this region. The number of equations N, which is equal to element number, may also be different for the two regions. Equation (F1) can be written in another form:

$$\theta_j = \frac{1}{2\pi}\sum_{k=1}^{N}\left[A_{jk}\,\theta_k + B_{jk}\left(\frac{\partial\theta}{\partial n}\right)_k\right] \qquad (j = 1, 2 \ldots N) \qquad (F2)$$

where

$$A_{jk} = \int_{S_k} \frac{\partial U(x_j, y_j, \xi, \eta)}{\partial n} dS \qquad \text{(F3a)}$$

and

$$B_{jk} = - \int_{S_k} U(x_j, y_j, \xi, \eta)\, dS \qquad \text{(F3b)}$$

With the boundary condition (VI.9), i.e. $\theta_{1,2} = 0$ along the interface, one recognizes that A_{jk} along boundary I1 or II1 as indicated in Figure 24(b) will not be involved in equation (F1). Similarly, B_{jk} along the boundaries I2, I4, II2, II4 and II6 will not appear either due to the adiabatic boundary conditions (VI.8,11). The remaining coefficients A_{jk} and B_{jk} are determined by evaluating the integral (F3a) or (F3b) along each segment s_k.

For region 1, one first substitutes the singular solution (VI.5) into equation (F3a) on boundary I1,

$$B_{jk}^{(I_1)} = \int_{x_k}^{x_{k+1}} - \ln\left[(x_j-\xi)^2 + (y_j-\eta)^2\right]\left[1+\left(\frac{d\eta_i}{d\xi}\right)^2\right]^{1/2} d\xi \qquad \text{(F4)}$$

Here, $\eta_i(\xi) = y_k + (\xi - x_k)(y_{k+1}-y_k)/(x_{k+1}-x_k)$ is the linear expression of the element s_k of the interface. The derivative, $d\eta_i(\xi)/d\xi = (y_{k+1}-y_k)/(x_{k+1}-x_k) \equiv e_k$. Since x_k, y_k, x_{k+1}, y_{k+1} and e_k are all known constants, equation (F2) can be integrated as follows:

$$B_{jk}^{(I_1)} = - \int_{x_k}^{x_{k+1}} \ln\left\{(x_j-\xi)^2 + [y_j - (y_k + \xi - x_k e_k)]^2\right\}(1+e_k)^{1/2} d\xi$$

$$= -(1+e_k)^{1/2}\left\{(x_{k+1}-x_k)\ln(1+e_k^2) + (x_{k+1}-b_{jk})\ln\left[(x_{k+1}-b_{jk})^2 + d_{jk}^2\right]\right.$$

$$- (X_{k+1} - b_{jk}) \ln [(X_{k+1} - b_{jk})^2 + d_{jk}^2] - 2(X_{k+1} - X_k) +$$

$$2 d_{jk} \left(\tan^{-1} \frac{X_{k+1} - b_{jk}}{d_{jk}} - \tan^{-1} \frac{X_k - b_{jk}}{d_{jk}} \right) \Bigg\}, \qquad \text{(F4a)}$$

where $$b_{jk} = \frac{X_j + d_{jk} e_k}{1 + e_k^2},$$

$$d_{jk} = \frac{\alpha_{jk} + X_j e_k}{1 + e_k^2},$$

$$\alpha_{jk} = Y_j - Y_k + X_k e_k .$$

For boundary I2, one obtains:

$$A_{jk}^{(I_2)} = \int_{Y_k}^{Y_{k+1}} \frac{\partial \ln [(X_j - D)^2 + (Y_j - \eta)^2]}{\partial \xi} \, d\eta$$

$$= 2 \left(\tan^{-1} \frac{Y_j - Y_{k+1}}{X_j - D} - \tan^{-1} \frac{Y_j - Y_k}{X_j - D} \right). \qquad \text{(F5)}$$

Due to $\theta_i = 1$ along boundary I3, all A_{jk} on boundary I3 can be summed up and expressed by the sub-summation:

$$\sum_k A_{jk}^{(I_3)} = \int_D^0 \frac{\partial \ln [(X_j - \xi)^2 + (Y_j - 0)^2]}{\partial \eta} \, d(-\xi)$$

$$= 2 \left(\tan^{-1} \frac{X_j - D}{Y_j} - \tan^{-1} \frac{X_j}{Y_j} \right). \qquad \text{(F6a)}$$

B_{jk} on I3 is given by

$$B_{jk}^{(I_3)} = \int_{X_k}^{X_{k+1}} - \ln [(X_j - \xi)^2 + Y_j^2] \, d(-\xi)$$

$$= \Big\{ (X_j - X_{k+1}) \ln [(X_j - X_{k+1})^2 + Y_j^2] - (X_j - X_k) \ln [(X_j - X_k)^2 + Y_j^2]$$

$$-2(X_{k+1}-X_k)+2Y_j\left(\tan^{-1}\frac{X_j-X_{k+1}}{Y_j}-\tan^{-1}\frac{X_j-X_k}{Y_j}\right)\Big\}. \qquad \text{(F6b)}$$

On boundary I4, only A_{jk} appears and is obtained as

$$A_{jk}^{(I_4)}=\int_{Y_k}^{Y_{k+1}}\frac{\partial \ln[X_j^2+(Y_j-\eta)^2]}{\partial(-\xi)}\,d(-\eta)$$

$$=2\left(\tan^{-1}\frac{Y_j-Y_{k+1}}{X_j}-\tan^{-1}\frac{Y_j-Y_k}{X_j}\right). \qquad \text{(F7)}$$

It is easy to show that all formulae above involving anti-tangent function should disappear when the denominator of its argument vanishs. Note that integrals (F3a,b) involving the singularity at the center on the segment of k = j are convergent and thus have the same analytic expressions.

Following the same procedure as shown above, one can integrate equations (F3a,b) on each boundary of region 2. Note that the line integration is carried out clockwise and the normal coordinate n in equation (VI.4) points from outward of this region. The formulae are listed as follows,

$$A_{jk}^{(II_2)}=A_{jk}^{(I_1)}, \qquad \text{(F8)}$$

$$B_{jk}^{(II_2)}=B_{jk}^{(I_1)}, \qquad \text{(F9)}$$

$$B_{jk}^{(II_3)}=\Big\{(X_k-X_{k+1})\ln\left[(X_j-X_{k+1})^2+(Y_j+H_b)^2\right]-$$

$$(X_j-X_k)\ln\left[(X_j-X_k)^2+(Y_j+H_b)^2\right]-2(X_{k+1}-X_k)+$$

$$(y_j + H_b)\left(\tan^{-1}\frac{x_j - x_{k+1}}{y_j + H_b} - \tan^{-1}\frac{x_j - x_k}{y_j + H_b}\right)\Bigg\} \qquad \text{(F10)}$$

and

$$\sum_k A_{jk}^{(II_3)} = 2\left(\tan^{-1}\frac{x_j - D}{y_j + H_b} - \tan^{-1}\frac{x_j}{y_j + H_b}\right) . \qquad \text{(F11)}$$

For the integrals along the tube surface, one may use the polar coordinates given by

$$r_t = [x^2 + (y + h_0)^2]^{1/2}$$

and

$$\phi = \tan^{-1}\frac{y + h_0}{x} .$$

The fundamental singular solution (VI.5) in the polar coordinates is given by

$$U(r_{t_j}, \phi_j, r_t, \phi) = \ln[r_{t_j}^2 + r_t^2 - 2 r_t r_{t_j}\cos(\phi - \phi_j)] ,$$

where r_{t_j} and ϕ_j denote point j. The coefficients can then be expressed by

$$\sum_k A_{jk}^{(II_5)} = \int_{-\frac{\pi}{2}}^{\frac{\pi}{2}} \frac{\partial \ln[r_{t_j}^2 + r_t^2 - 2 r_t r_{t_j}\cos(\phi - \phi_j)]}{\partial r_t}\Bigg/_{r_t = 1} d\phi$$

$$= 2\int_{-\frac{\pi}{2}}^{\frac{\pi}{2}} \frac{r_{t_j}\cos(\phi - \phi_j) - 1}{r_{t_j}^2 + 1 - 2 r_{t_j}\cos(\phi - \phi_j)} d\phi \qquad \text{(F12)}$$

Integrating (F12), one can obtain:

for $r_{t_j} = 1$,

$$\sum_k A_{jk}^{(II_5)} = \pi \quad ; \qquad \text{(F12a)}$$

for $r_{t_j} > 1$,

$$\sum_k A_{jk}^{(II_5)} = 2\pi \qquad (\phi_j = -\pi/2) \qquad \text{(F12b)}$$

$$\sum_k A_{jk}^{(II_5)} = 0 \qquad (\phi_j = \pi/2) \qquad \text{(F12c)}$$

$$\sum_k A_{jk}^{(II_5)} = \pi - 2\left\{\tan^{-1}\left[\frac{r_{t_j}+1}{r_{t_j}-1}\tan\left(\frac{\pi}{4}-\frac{\phi_j}{2}\right)\right] + \tan^{-1}\left[\frac{r_{t_j}+1}{r_{t_j}-1}\tan\left(\frac{\pi}{4}+\frac{\phi_j}{2}\right)\right]\right\} \qquad \text{(F12d)}$$

and $B_{jk}^{(II_5)}$ can be calculated using the same formula for the interface.

$$B_{jk}^{(II_5)} = B_{jk}^{(I_1)} = B_{jk}^{(II_1)} \qquad \text{(F12e)}$$

On boundary II6, A_{jk} is same as on boundary I4,

$$A_{jk}^{(II_6)} = A_{jk}^{(II_4)} \qquad \text{(F13)}$$

NOTES

1. Lunardini, V. J., Thawing of Permafrost Beneath a Buried Pipe, Journal of Canadian Petroleum Technology, Vol.16.pp,34-37, 1977.

2. Lunardini, V. J., Phase Change Around Insulated Buried Pipes: Quasi-Steady Method, J.Energy Resources Tech., Vol.103(3), pp.201-207, 1981.

3. Wheeler, J. A., Simulation of Heat Transfer from a warm Pipeline Buried in Permafrost, Paper presented at the 74th National Meeting, Am.Inst. Chem. Engr., New Orleans, La., 1973.

4. Lunardini, V. J., Heat Transfer in Cold Climates, Van Nostrand Reinhold, New York, 1981.

5. Caratheodory, C., Conformal Representation, New York, Cambridge University Press, 1958.

6. Carslaw, H. S. and Jaeger, J. C., Conduction of Heat in Solids, 2nd ed., Oxford at the Clarendon Press, 1959.

7. Porkhayev, G. V., Temperature Fields in Foundations, in Proc. 1st Int. Conf. On Permafrost, Lafayette, Indiana, pp.285-291, 1963.

8. Thornton, D. E., Steady State and Quasi-Static Thermal Results for Bare and Insulated Pipes in Permafrost, Canadian Geotechnical Journal, Vol.13, pp.161-170, 1976.

9. Hwang, C. T., On Quasi-Static Solutions for Buried Pipes in Permafrost, Canadian Geotechnical Journal, Vol.14,pp.180-192, 1977.

10. Lunardini, V. J., Approximate Phase Change Solutions for Insulated Buried Cylinders, Journal of Heat Transfer, ASME, Vol.105, pp.25-32, 1983.

11. Hwang, C. T., Seshadri, R. and Krishnayya, A. V. G., Thermal Design for Insulated pipes, Canadian Geotechnical Journal, Vol.17, pp.613-622, 1980.

12. Seshadri, R. and Krishnayya, A. V. G., Quasi-Steady Approach for Thermal Analysis of Insulated Structures, International Journal of Heat and Mass Transfer, Vol.23, pp.111-121, 1980.

13. Lachenbruch, A. H., Some Estimate of the Thermal Effects of a Heated Pipeline in Permafrost, U.S.Geological Survey, Circular 632, 1970.

14. Gold, L. W., Johnston, G. H., Slusarchuk, W. A. and Goodrich, L. E., Thermal Effects in Permafrost, Proc. Canadian Northern Pipeline Research Conference, pp.25-45, 1972.

15. Hwang, C. T., Murray, D. W. and Brooker, E. W., A Thermal Analysis for Structures on Permafrost, Canadian Geotechnical Journal, Vol.9, pp. 33-46, 1972.

16. Hwang, C. T., Predictions and Observations on the Behavior of a Warm Gas Pipeline on Permafrost, Canadian Geotechnical Journal, Vol.13, pp.452-480, 1976.

17. Weinbaum, S., Zhang, G-P. and JiJI, L. M., An Apparent Free Surface Method for Determining the Transient Freezing Around a Buried Pipe in a Semi-Infinite Region, in Proceedings of the Third International Offshore Mechanics and Arctic Engineering Symposium, ed, V. J. Lunardini, Vol.III, pp.1-10, 1984, ASME.

18. Asgarpour, S. and Bayazitoglu, Y., Heat Transfer to Laminar Flow with Phase Change Boundary, Journal of Heat Transfer, ASME, Vol.104, pp.678-682, 1982.

19. Sparrow, E. M. and Hsu, C. F., Analysis of Two-Dimensional Freezing on the Outside of a Coolant-Carrying Tube, International Journal of Heat and Mass Transfer, Vol.24, pp.1345-1357, 1981.

20. Grossman, G. and Pesotchinski, D., A Two-Dimensional Model for Thermal Energy Storage in a Phase Changing Material Interacting with a Heat-Carrying Fluid, Presented at the ASME Winter Annual Meeting, November 15-20, 1981. Paper No. 81-WA/HT-35.

21. Shamsunder, N., Formulae for Freezing Outside a Circular Tube with Axial Variation of Coolant Temperature, International Journal of Heat and Mass Transfer, Vol.25, pp.1614-1616, 1982.

22. Shamsunder, N. and Srinivasan, R., Effectiveness-NTU Charts for Heat Recovery from Latent Heat Storage Units, Journal of Solar Energy Engng., Vol.102, pp.263-271, 1980.

23. Banerjee, P. K. and Butterfield, R., Boundary Element Method, Mcgraw-Hill, 1981.

24. Liggett, J. A. and Liu, Philip L-F., The Boundary Integral Equation Method for Porous Medis Flow, George Allen & Unwin, 1983.

BIBLIOGRAPHY

Asgarpour, S. and Bayazitoglu, Y., Heat Transfer to Laminar Flow with Phase Change Boundary, Journal of Heat Transfer, ASME, Vol.104, pp.678-682, 1982.

Banerjee, P. K. and Butterfield, R., Boundary Element Method, Mcgraw-Hill, 1981.

Caratheodory, C., Conformal Representation, New York, Cambridge University Press, 1958.

Carslaw, H. S. and Jaeger, J. C., Conduction of Heat in Solids, 2nd ed., Oxford at the Clarendon Press, 1959.

Gold, L. W., Johnston, G. H., Slusarchuk, W. A. and Goodrich, L. E., Thermal Effects in Permafrost, Proc. Canadian Northern Pipeline Research Conference, pp.25-45, 1972.

Grossman, G. and Pesotchinski, D., A Two-Dimensional Model for Thermal Energy Storage in a Phase Changing Material Interacting with a Heat-Carrying Fluid, Presented at the ASME Winter Annual Meeting, November 15-20, 1981. Paper No. 81-WA/HT-35. Hwang, C. T., Murray, D. W. and Brooker, E. W., A Thermal Analysis for Structures on Permafrost, Canadian Geotechnical Journal, Vol.9, pp. 33-46, 1972.

Hwang, C. T., Predictions and Observations on the Behavior of a Warm Gas Pipeline on Permafrost, Canadian Geotechnical Journal, Vol.13, pp.452-480, 1976.

Hwang, C. T., On Quasi-Static Solutions for Buried Pipes in Permafrost, Canadian Geotechnical Journal, Vol.14,pp.180-192, 1977.

Hwang, C. T., Seshadri, R. and Krishnayya, A. V. G., Thermal Design for Insulated pipes, Canadian Geotechnical Journal, Vol.17, pp.613-622, 1980.

Lachenbruch, A. H., Some Estimate of the Thermal Effects of a Heated Pipeline in Permafrost, U.S.Geological Survey, Circular 632, 1970.

Liggett, J. A. and Liu, Philip L-F., The Boundary Integral Equation Method for Porous Medis Flow, George Allen & Unwin, 1983.

Lunardini, V. J., Thawing of Permafrost Beneath a Buried Pipe, Journal of Canadian Petroleum Technology, Vol.16.pp,34-37, 1977.

Lunardini, V. J., Phase Change Around Insulated Buried

Pipes: Quasi-Steady Method, J.Energy Resources Tech., Vol.103(3), pp.201-207, 1981.

Lunardini, V. J., Heat Transfer in Cold Climates, Van Nostrand Reinhold, New York, 1981.

Lunardini, V. J., Approximate Phase Change Solutions for Insulated Buried Cylinders, Journal of Heat Transfer, ASME, Vol.105, pp.25-32, 1983.

Porkhayev, G. V., Temperature Fields in Foundations, in Proc. 1st Int. Conf. On Permafrost, Lafayette, Indiana, pp.285-291, 1963.

Seshadri, R. and Krishnayya, A. V. G., Quasi-Steady Approach for Thermal Analysis of Insulated Structures, International Journal of Heat and Mass Transfer, Vol.23, pp.111-121, 1980.

Shamsunder, N. and Srinivasan, R., Effectiveness-NTU Charts for Heat Recovery from Latent Heat Storage Units, Journal of Solar Energy Engng., Vol.102, pp.263-271, 1980.

Shamsunder, N., Formulae for Freezing Outside a Circular Tube with Axial Variation of Coolant Temperature, International Journal of Heat and Mass Transfer, Vol.25, pp.1614-1616, 1982.

Sparrow, E. M. and Hsu, C. F., Analysis of Two-Dimensional Freezing on the Outside of a Coolant-Carrying Tube, International Journal of Heat and Mass Transfer, Vol.24, pp.1345-1357, 1981.

Thornton, D. E., Steady State and Quasi-Static Thermal Results for Bare and Insulated Pipes in Permafrost, Canadian Geotechnical Journal, Vol.13, pp.161-170, 1976.

Weinbaum, S., Zhang, G-P. and Jiji, L. M., An Apparent Free Surface Method for Determining the Transient Freezing Around a Buried Pipe in a Semi-Infinite Region, in Proceedings of the Third International Offshore Mechanics and Arctic Engineering Symposium, ed, V. J. Lunardini, Vol.III, pp.1-10, 1984, ASME.

Wheeler, J. A., Simulation of Heat Transfer from a warm Pipeline Buried in Permafrost, Paper presented at the 74th National Meeting, Am.Inst. Chem. Engr., New Orleans, La., 1973.